TESIS DE PREGRADO

Evaluación electroquímica de nanocompositos plata-fullereno como catalizadores para electrodos en baterías flexibles de zinc-aire

Chipoco Haro, Danae A.

Award date:
2020

UNIVERSIDAD DE INGENIERÍA Y TECNOLOGÍA UTEC

Energy Engineering

ELECTROCHEMICAL EVALUATION OF SILVER - FULLERENES NANOCOMPOSITES AS CATALYSTS FOR ELECTRODES IN FLEXIBLE ZINC - AIR BATTERIES

Thesis for the Professional Engineering Degree in Energy Engineering

Danae Ariana Chipoco Haro

Student ID: 201510107

Advisor

Juan Carlos Rodríguez Reyes

Lima – Peru

April 2020

Dedication:

To God, my Lord, my strength and rest.

To my father, for being an example of prudence. To my mother, for the wisdom and confidence she has always transmitted me. To them both, for their care, for supporting my dreams even though they did not understand them, for the guidance, and for their unconditional love. To my grandmother, for being a silent companion, a unique support, a withstanding professional and, overall, a model. To my brother, with whom I shared many thoughts and thought me through silence. To my family, for their kindness and for always backing me.

To my Master, who showed me the Jedi path.

To all my friends. To the loyal ones which stayed by my side even though life took as through different paths. To my project partner, with whom a shared dream took us through many adventures and taught me many lessons. To the ones with whom I shared deep conversations and fandom analysis. To my classmate since school, for her kindness and complicity. To my little sister, for all the things she taught me without knowing, for all the friendly games, happy memories and her support on the most difficult moments of my journey.

To my teachers and administrative staff at UTEC, who supported me during these years, who believed in me long before I did, and went beyond from what their duty dictated.

To the land witness of my birth, my growth and the society that forged my personality. Because, despite all the troubling times we may be going through, I believe in our strength to overcome the differences and join together to build a dreamed Peru.

Acknowledgments:

First, I would like to thank Ph.D. Juan Carlos Rodriguez-Reyes, who guided me throughout the development of the thesis as an advisor and mentor, for introducing me to his research group and colleagues who helped me in many ways in this work, for his commitment in my professional and personal growth, for his support and comprehension in difficult times, for being a model of a researcher, professor, and ethic person, for the kindness he has always shown to me, and for being my Master.

I would also like to thank Dr. Adolfo de la Rosa Toro for allowing me to work with his research group, facilitating equipment and materials for the different electroanalytical tests, and Dr. Angélica Baena, for allowing me to work in the facilities under her supervision.

Specially, I would like to thank Ph.D. Julio Valdivia for his support by allowing me to use the facilities under his supervision and Ph.D. Julien Noel, for the economic support for the study and his guidance during these five years of undergraduate studies.

A very special gratitude goes to Luis Palomino, for his guidance in the use of equipment and techniques for nanoparticles synthesis and life lessons he gave me. Also, to Antony Bazán, Rey Fernández, Yuri Ccallocunto and Ana Luz Tupa for their guidance in the use of equipment for electroanalytical tests, the help in the interpretation of the obtained data and the support during the study.

With a special mention and affection to Karinna Visurraga, Luz Pérez, Giuliana Travi and Jesenia Zapata, for their administrative and logistical support, and the kind guidance throughout the project. Also, to Sheyla Chero and Carsten Benndorf, for the useful discussions and help in the XPS measurements and Mario Carbajal, Flor Granda and Andrea Aranda for their logistical help in the laboratory. Also to Ximena Guardia, for her help in the writing of the thesis and comprehension.

I am also grateful to José Ruiz, Rocío Hoyos and Vanessa Quispe for the useful discussions and lessons on electrochemistry.

And finally, last but by no means least, also to everyone in the Research Group of Juan Carlos Rodriguez-Reyes (UTEC) and the Research Group from Applied Electrochemistry (UNI) for welcoming me at their research groups. The Harvard - UTEC partnership for research is acknowledged for providing financial support.

TABLE OF CONTENTS

Pág.

ABSTRACT ..... **xiv**

RESUMEN ..... **xv**

INTRODUCTION ..... **xvi**

1 CHAPTER I THEORETICAL FRAMEWORK **1**

1.1 Working principles of batteries 1

1.1.1 Cell potentials 2

1.1.2 Classification of batteries 3

1.2 Metal-air batteries 5

1.2.1 Working principle 6

1.2.2 Advantages and disadvantages 8

1.2.3 Zn-air batteries 10

1.3 Synthesis of silver nanoparticles 20

1.4 Characterization methods for cathode materials 22

1.4.1 Ultraviolet and visible absorption spectrometry 23

1.4.2 X-ray photoelectron spectroscopy 24

1.5 Electroanalytical methods 27

1.5.1 Open circuit potential 27

1.5.2 Cyclic voltammetry 27

1.5.3 Galvanostatic charge-discharge test 32

2 CHAPTER II METHODOLOGY **35**

2.1 Preparation of the air cathode 36
2.1.1 Silver nanoparticles synthesis 36
2.1.2 Impregnation of silver nanoparticles over buckypapers through the ink evaporation method 39
2.1.3 Execution of electroanalytical tests 41
2.2 Methods for characterization 45
2.2.1 Ultraviolet and visible spectroscopy 45
2.2.2 X-ray photoelectron spectroscopy 46
3 CHAPTER III RESULTS AND DISCUSSION 47
3.1 Preparation of the air cathode 48
3.1.1 Silver nanoparticles synthesis 48
3.1.2 Impregnation of silver nanoparticles over buckypapers through ink evaporation 54
3.2 Electroanalytical tests 59
3.2.1 Open circuit potential 59
3.2.2 Cyclic voltammetry 59
3.2.3 Galvanostatic charge-discharge test 69
3.3 Flexibility test 75
CONCLUSIONS 76
BIBLIOGRAPHY 79
ANNEXES 87

ABBREVIATION INDEX

CNT	carbon nanotubes
CV	cyclic voltammetry
GDL	gas diffusion layer
NP	nanoparticle
OCP	open circuit potential
OER	oxygen evolution reaction
ORR	oxygen reduction reaction
PHF	hydroxyl fullerene
SPR	surface plasmon resonance
UV-vis	ultraviolet and visible absorption spectroscopy
XPS	X-ray photoelectron spectroscopy

TABLE INDEX

Pág.

Table 1.1. Differences between primary and secondary cells 3
Table 1.2. Types of batteries. 4
Table 1.3. Advantages and disadvantages of metal-air batteries 8
Table 1.4. Examples of flexible batteries configurations in academia. 16
Table 1.5. Summary of electroanalytical tests. 27
Table 3.1. UV-vis characterization of silver nanoparticles synthesized using Frens method. 50
Table 3.2. OCP results of all samples 59
Table 3.3. Peaks attributed to silver reactions in this work and other references using as reference SHE. 65
Table 3.4. Peaks attributed to ORR in this work and other references using as reference the SHE 65
Table 6.1. Zn-air batteries with Ag-based catalysts and their performances. 87

FIGURE INDEX

Pág.

Figure 1.1. Designs for metal-air batteries 5
Figure 1.2. Working principle of Zn-air batteries. (a) Charge of the battery. (b) Discharge of the battery. 11
Figure 1.3. Cutaway view of typical Zn/Ag_2O button type battery. (a) Transversal view. (b) Upper view. 13
Figure 1.4. Schematics of prismatic primary Zn-air battery 14
Figure 1.5. Schematic representation of Zn-air flow battery configuration 15
Figure 1.6. General schematic of flexible Zn-air battery 16
Figure 1.7. Schematic representation of performance-limiting phenomena in Zinc anode. (a) dendrite growth, (b) shape change, (c) passivation, and (d) hydrogen evolution..... 18
Figure 1.8. Chemical structure of polydroxy fullerene molecule. 22
Figure 1.9. Schematic representation of an electrochemical cell for voltammetry 29
Figure 1.10. Voltage vs. Time excitation signals in cyclic voltammetry 29
Figure 1.11. (a) Potential vs. time waveform. (b) Cyclic voltammogram..... 30
Figure 1.12. Voltage vs. capacitance graph example. 33
Figure 1.13. Voltage vs. time graph example. 34
Figure 2.1. Methodology flow diagram. 36
Figure 2.2. Schematic of the Frens method for silver nanoparticles synthesis. (a) Place of 50 mL of silver nitrate in Erlenmeyer flask covered with aluminum foil. (b) Heat the solution until boiling point. (c) Add 500 µL of sodium citrate. (d) Stir for 20 minutes. (e) Microcentrifugate to obtain the silver nanoparticles. 37
Figure 2.3. Erlenmeyer flask with a magnetic pill totally covered with aluminum foil being heated. 38

Figure 2.4. Schematic of silver nanoparticles impregnation through ink evaporation. (a) Deposition of colloids over the buckypaper. (b) Irradiation of light over the drop to dry the water and IPA. (c) Schematic of resultant electrode. 39
Figure 2.5. Silver nanoparticles ink drying by IR light over buckypaper pasted over glassy carbonGlassy carbon work electrode..... 40
Figure 2.6. Set-up for the cyclic voltammetry..... 42
Figure 2.7. Settings for an electrochemical cleaning..... 43
Figure 2.8. General settings for a cyclic voltammetry in neutral medium. 44
Figure 2.9. Schematic of step-by-step measurement procedure. (a) Resuspension of silver nanoparticles in distillated water at two different concentrations. (b) Place 2µL of sample into the NanoDrop. (c) Typical graph obtained for measurement. The wavelength at which the spectrum shows a maximum is related to the nanoparticle size, assuming spherical nanoparticles. ..... **¡Error! Marcador no definido.**
Figure 2.10. Schematic representation of an XPS system .... **¡Error! Marcador no definido.**
Figure 3.1. UV-vis spectrum of silver nanoparticles synthesized using Frens method. (a) shows the spectrum of a solutions from 33 mM of this work and referenced work. (b) shows the spectrum of solutions from 33 mM and 66 mM multiplied by 0.5 for comparison. 49
Figure 3.2. UV-vis spectrum of silver nanoparticles synthesized using Frens method in colloids of DI and DI with IPA. 51
Figure 3.3. Silver particles with PHF after centrifugation. 53
Figure 3.4. UV-vis spectrum of silver particles synthesized using PHF as reducing agent. 54
Figure 3.5. XPS spectrum from silver nanoparticles synthesized using the Frens method impregnated using ink evaporation method using a colloid at 66 mM. (a) Shows the whole spectrum of not impregnated and impregnated CNT buckypapers. (b) Shows a shorter range for the silver peak of silver nanoparticles after impregnation and after washing with distillated water. 56
Figure 3.6. XPS spectrum from CNT buckypaper and silver nanoparticles synthesized using the Frens method impregnated over CNT buckypaper using ink evaporation method by a colloid at 66 mM before and after cyclic voltammetry in alkaline medium. (a) Shows the spectrum of CNT and CNT-66mM before and after cyclic voltammetry in alkaline medium.

(b) Shows a shorter range for the lector to appreciate the silver peaks before and after cyclic voltammetry. 58
Figure 3.7. Cyclic voltammetry results in neutral medium for silver nanoparticles synthesized using the Frens method. 61
Figure 3.8. Cyclic voltammetry in neutral medium for silver nanoparticles along the different cycles. 62
Figure 3.9. Cyclic voltammetry results in alkaline medium for (a) CNT buckypaper and silver nanoparticles synthesized using the Frens method at a width window, (b) CNT buckypaper impregnated with silver nanoparticles showing Ag peaks, and (c) CNT buckypaper impregnated with silver nanoparticles showing OER and ORR peaks. 64
Figure 3.10. Cyclic voltammetry results in alkaline medium for the three different samples of silver particles synthesized using PHF as reducing agent. 66
Figure 3.11. Cyclic voltammetry results in alkaline medium for (a) CNT cathode, CNT buckypaper impregnated with silver nanoparticles synthesized by Frens method, silver particles synthesized using PHF as reducing agent, and only PHF; and (b) CNT impregnated with only PHF. 67
Figure 3.12. Second cycle of the galvanostatic charge-discharge test for CNT, CNT with silver nanoparticles and CNT with PHF. 70
Figure 3.13. Galvanostatic charge-discharge test of CNT at 0.64 mA cm^{-2}, 0.8 mA cm^{-2}, 0.96 mA cm^{-2} and 1.12 mA cm^{-2}. 71
Figure 3.14. Galvanostatic charge-discharge test of CNT and silver nanoparticles synthesized using Frens method at 0.2 mA cm^{-2}, 0.25 mA cm^{-2}, 0.30 mA cm^{-2} and 0.35 mA cm^{-2}..... 72
Figure 3.15. Galvanostatic charge-discharge test of CNT impregnated with silver nanoparticles synthesized using Frens method and PHF at 0.64 mA cm^{-2}, 0.8 mA cm^{-2}, 0.96 mA cm^{-2} and 0.1.12 mA cm^{-2}. 73

ANNEX INDEX

Pág.

ANNEX 1: Zn-air batteries with Ag-based catalysts 87

ABSTRACT

Metal-air batteries are characterized by a high energy density with relatively simple and safe chemistry which makes them suitable for many applications, especially the ones requiring flexibility. These energy storage devices consist of one metal electrode, an air electrode, which enhance the oxygen evolution and oxygen reduction reactions (OER and ORR, respectively), and an electrolyte. The air electrode is lighter than most metal electrodes present in batteries; therefore, these batteries have a high energy density. However, the most critical problem this technology faces involves the air electrode design, especially because of the requirement of a bifunctional catalyst for both OER and ORR.

Here, the enhancement of the catalytic activity of silver nanoparticles impregnated on carbon nanotubes (CNT) for OER and ORR using polyhydroxy fullerene (PHF) is discussed, as well as the methodology needed for an experimental demonstration of this hypothesis. The electrochemical tests demonstrated that silver nanoparticles from 60 nm to 70 nm were successfully impregnated over the CNT buckypapers and the electrode was stable over several cycles. The nanocomposite Ag-PHF was also successfully impregnated, but the electrode was not as stable as the electrode with only Ag nanoparticles. However, the higher current achieved by the Ag-PHF electrode confirmed the hypothesis that the presence of PHF enhances the catalytic activity of silver nanoparticles. The implications of our findings in the improvement of materials for Zn-air batteries is discussed. This study contributes to the worldwide efforts of the scientific community to develop flexible, small and light batteries and may be a starting point in the use of PHF for this application.

KEYWORDS:

Flexible air electrode; Zn-air batteries; silver nanoparticles synthesis; PHF; cyclic voltammetry; XPS; galvanostatic charge-discharge; UV-vis.

RESUMEN

Las baterías de metal-aire se caracterizan por su alta densidad energética y una composición química segura y sencilla. Estas características las hacen apropiadas para diversas aplicaciones, especialmente aquellas que demandan flexibilidad. Estos dispositivos de almacenamiento de energía consisten en un electrodo de metal, un electrodo de aire que permite la reducción y evolución de oxígeno (ORR y OER, respectivamente), y un electrolito. El electrodo de aire es más liviano que la mayoría de electrodos metálicos usados en baterías convencionales, lo cual resulta en una alta densidad energética. Sin embargo, el problema más importante que enfrenta esta tecnología es el diseño de este electrodo, especialmente porque se requiere un catalizador que pueda favorecer ambas reacciones (ORR y OER).

En el presente estudio, se discute la mejora de la actividad catalítica de nanopartículas de plata impregnadas sobre nanotubos de carbono (CNT) para OER y ORR mediante el uso de fullerenos hidroxilos (PHF). También, se presenta la metodología requerida para la demostración experimental de esta hipótesis. Las pruebas electroquímicas demostraron que las nanopartículas de plata (60 nm - 70 nm) fueron impregnadas satisfactoriamente sobre CNT y el electrodo fue estable a través de varios ciclos. El nanocomposito Ag-PHF también fue impregnado satisfactoriamente, pero la estabilidad de este electrodo no se equiparó con el Ag-PHF. Sin embargo, la corriente que alcanzó fue mayor. Esto confirma que la presencia de PHF mejora la actividad catalítica de las nanopartículas de plata. Adicionalmente, se discuten las implicancias de nuestros descubrimientos en la mejora de los materiales para las baterías de Zn-aire. Este estudio contribuye a los esfuerzos de la comunidad científica para desarrollar baterías flexibles, pequeñas y livianas. Además, es el inicio del uso de PHF para esta aplicación

PALABRAS CLAVE:

Electrodo de aire flexible; baterías de Zn-aire1; síntesis de nanopartículas de plata; PHF; voltametría cíclica; XPS; carga-descarga galvanostatica; UV-visible.

INTRODUCTION

"The important thing is not to stop questioning."

- *Albert Einstein*

Up to 2020, an increase in more than 50% in wearable devices acquisitions in comparison to 2016 is expected [1]. This market trend shows the interest of big industries in the development of flexible components for these devices, including energy storage devices such as batteries. Even though there has been a great advance in this field, a continuous improvement in the design and efficiency of batteries is sought.

Among the many types of energy-storage devices evaluated as candidates to achieve the flexibility needed, metal-air batteries have become very promising due to their high energy density with a relatively simple and safe chemistry [2]. There are plenty of metals suitable for this application, being the most common lithium, magnesium, aluminum and zinc [3].

This study focuses on zinc-air batteries because of their high energy density [2], low price [4], [5], and abundance in the continental crust [6], especially in Peru as the third zinc exporter worldwide [4]. Even though the scientific work on the field is considerable, there are still some challenges to overcome. One of the most critical problem this technology faces involves the air electrode design, especially because of the requirement of a bifunctional catalyst for oxygen reduction reaction (ORR) and oxygen evolution reaction (OER) [7]. Therefore, this thesis explores the theory behind the use of different materials as flexible air cathodes to evaluate their catalytic activity and the resulting impact they may have on the performance of flexible Zn-air batteries. Moreover, it discusses the suitability of the tested materials for this application. Specifically, the materials explored are carbon buckypaper impregnated with a) silver nanoparticles, and b) silver nanoparticles with PHF. The methods evaluated for synthesizing silver nanoparticles were the Frens method and one developed by

the groups of Juan Carlos Rodriguez-Reyes at UTEC and Vijay Krishna at Cleveland Clinic, using PHF as reducing agent, which size determination could be estimated using UV visible light spectroscopy. The air cathode was built by impregnating these nanomaterials over a carbon nanotube (CNT) paper, which acts as current collector and support. The characterization is carried out via X-ray photoelectron spectroscopy, while the catalytic activity towards OER and ORR was determined by cyclic voltammetry. The stability over time was tested through galvanostatic charge-discharge tests. The literature review showed PHF as a stabilizer for noble-metal nanoparticles, moreover, it is hypothesized and proved that PHF can also be used as reducing agent in the synthesis of noble-metal nanoparticles, more specifically, silver nanoparticles, thus, enhancing its catalytic activity towards ORR and OER.

Scope

The present work involves the experimental comparison of the performance of different nanoparticles-based materials as flexible cathodes for Zn-air batteries, for which a previous establishment of a suitable method for the experimental evaluation of these flexible cathodes is presented.

The proposed methodology includes the specifications of the synthesis of silver nanoparticles and its impregnation over CNT buckypapers for the flexible cathode building, as well as the characterization techniques and the electrochemical tests for the performance evaluation of the cathodes in terms of catalytic activity and stability over time. The selected characterization techniques were X-ray spectroscopy (XPS) for the characterization of the air cathode and UV-visible absorption spectroscopy (UV-vis) for determining the size of the silver nanoparticles synthesized. The electrochemical tests proposed for the performance evaluation are open circuit potential, cyclic voltammetry and galvanostatic charge-discharge test. Other electrochemical methods, such as polarization curves and rotating disk electrodes, are excluded for the analysis of this work. Moreover, the test of these electrodes in a battery

prototype as well as an economic evaluation and market comparison are out of the scope of this study.

The presented work is done in the Research Group of Juan Carlos Rodriguez-Reyes at the Universidad de Ingeniería y Tecnología (UTEC), with the support of the Research Group from Applied Electrochemistry of the Universidad Nacional de Ingeniería (UNI) in charge of Adolfo de la Rosa Toro Gómez.

Background information

There are plenty of synthesis and assembly methods for flexible air electrodes found in the literature [3]. However, the most direct and simplest method is to grow a gas diffusion and catalytic layer over a current collector [8]. The materials most widely used have been carbon-based current collectors due to the stability of their structures, high conductivity and light-weight. However, other materials like nano-silver ink for printing [9], titanium [10] and stainless steel mesh [11], have also been used with good battery performances. For example, the stainless steel mesh used showed more binding capability to the catalysts than carbon-based materials due to its mechanical strength [12]. The advantages and disadvantages that each current collector gives have been an important part of some studies. In this work, carbon nanotubes (CNT) in the form of buckypaper are employed as current collectors.

One of the limiting factors in the development of Zn-air batteries is the lack of efficient bifunctional catalysts for oxygen evolution and reduction reactions in the air cathode [13]. Therefore, the scientific community has been working on the synthesis of new stable catalysts. Noble-metal oxides are highly active for OER and have a good metallic conductivity, however, they are expensive in comparison to other materials. There have been also considered transition metals oxides, which are not as expensive as the noble-metal oxides and possess semiconducting properties [2]. Many of these materials are combined along with different synthesis methods in the search of more efficient materials for the air cathode of Zn-air batteries.

Silver is a noble metal which has been reported to be an effective catalyst for ORR due to the reduction reaction involving four electrons (as will be described below), similar to platinum catalysts. However, silver presents difficulties in the adsorption of oxygen molecules, therefore, scientists usually combine this noble metal with other materials to improve the catalytic activity of silver [14]. There are many synthesis methods available for preparing silver particles and impregnating them over the conductor layer and gas diffusion layer (GDL), like the hydrothermal method, pulsed layer deposition method, reduction/adsorption, among others. A summary of the performances of some Zn-air batteries developed using Ag-based catalysts in the air cathode synthesized with different methods, can be found on ANNEX 1.

Some studies used sodium borohydride and sodium citrate for the synthesis of catalysts containing silver for reduction activity in alkaline media with notable results. An Ag/C catalyst was developed using a citrate-protecting method; its ORR activity was found to proceed through a four-electron pathway [15]. Then, a Co-based phthalocyanines on silver nanoparticles supported on carbon which ORR activity was higher than Ag catalysts and Co-based phthalocyanines on carbon [16]. Furthermore, a Ag-Cu alloy was synthesized using sodium citrate as complexing agent [17].

This study used the synthesis protocols developed by Research Group of Juan Carlos Rodriguez-Reyes [18], [19], which used sodium citrate as reducing agents for silver nanoparticles synthesis. Moreover, this study used polyhydroxy fullerene (PHF) as surfactant and to enhance the catalytic activity of the silver nanoparticles for OER and ORR, which synthesis method is going to be the subject for another publication. These synthesis methods, to the best of the author's understanding, have not been used for this application before.

Moreover, this study proposes the use of carbon nanotubes buckypaper as current collector and support for the catalyst, due to its light density and conducting properties. Other outstanding characteristics from this material are its conductivity and hydrophobicity. These makes it suitable as base for the air cathode. On the other hand, its porous structure has proved to be a good base for the catalyst deposition and for avoiding the agglomeration of nanoparticles.

Justification

Modern electronics is a developing field that has reached a point in which the competition on low cost and improved performance is ever-increasing. Therefore, nowadays companies are focusing on other attributes to increase the value of their products, with flexibility standing out among others due to the variety of fields requiring this property [20]. These fields include, but are not limited to, wearables for commercial and biomedical applications [21], [22], optoelectronic devices [23], and soft robotics [24]. Among the devices needed for the development of these fields are batteries for energy storage.

One overlooked aspect of flexible electronic devices is that the batteries powering them must also have this bending attribute. Among the many types of energy-storage devices evaluated as candidates to achieve the flexibility needed, metal-air batteries have become very promising due to their high energy density with a relatively simple, safe chemistry. These devices differentiate themselves by having the cathode outside the battery, because they use oxygen from air as agent for electrochemical reactions [2]. The need for flexible batteries and the impact of novel battery materials and architectures is then the motivation of the present project.

Despite the fact that the energy-storage devices market is dominated by lithium-ion batteries, it seems that this technology has reached its maximum development peak, and further improvement could bring only an additional 30% increase in energy density [25]. Thus, metal-air batteries are a promising replacement for Li-ion batteries in applications where high energy density is needed. The main parameters evaluated for efficient batteries are high open-circuit voltage (OCV), operating voltage, energy efficiency, specific capacity, energy density, power density, and cyclic stability [2]. Commercial devices feature different values depending on the type of cell. $LiCoO_2$ / graphite pouch cell values, for example, are reported around 140 mA h g^{-1} and 3.85 V vs. Li/Li^+ [26]. In this lithium-predominant context, this alkaline metal as anode material for metal-air batteries was evaluated because of his high

specific energy of 5928 W h kg^{-1} and high cell voltage of 2.96 V [2]. However, Li-air batteries had many drawbacks and limitations like cost and scarcity. The trend in lithium prices seems to be stabilized between 4000 and 5000 USD/ton from 2009 to 2015, with a drop in 2011 to 3879 USD/ton [5]. Just to mention a few examples, lithium prices in October, 2017 were more than twice the zinc prices, as well as 9% more than cupper prices [4].

Lithium supply has been an important topic of discussion because of its importance for technological development and the fear caused by its scarcity. There is almost 10 ppm of lithium in the continental crust, while there are some other rare metals which are ten times more easily found [6]. Moreover, the demand of lithium is predicted to rise annually 16% in the following five years, mainly because of the increase in demand of batteries for transportation [27], but without a productive capacity able to sustain this demand growth, despite the possibility of matching the need in terms of extraction of raw material [28], the price of lithium will increase even more.

For the further development of metal-air batteries and their establishment in the industry, the fabrication cost is important; therefore, predictions of lithium costs are not favorable [5]. Moreover, the lack of production capability and scarcity in the Earth's crust [6] have pushed scientists to look into alternative metals for this technology. More specifically, in Peru the extraction of lithium presents many difficulties in the current sociopolitical framework for the exploitation of the huge deposits of lithium that were found in Puno in 2018. Therefore, other materials should be considered and zinc seems promising due to its high specific energy and volumetric energy density. Moreover, it represents a good opportunity for the development of technology in Peru using proper natural resources, since it is the first exporter of this metal in the region and third in the world. Zinc deposits are estimated to contribute with 60.1 million of fine metric tons of production for 2050 in Peru, which would mean 170 thousands of millions of USD in sales [4]. Zn-air batteries have a notable performance, but in order to compete with the Li-based batteries, a further development must be done. This type of energy-storage devices has different improvement possibilities in each of their parts, nonetheless, the most critical problem this technology faces

is regarding the air electrode design, especially because of the need of a bifunctional catalyst for ORR and OER [7], reactions that will be explained in following chapters.

In this sense, the present thesis will be focused on the advantages and opportunities regarding the design of air electrodes, making emphasis in the performance of certain materials in order to help the worldwide efforts of scientists in the development of Zn-air batteries technology. Specifically, this thesis tests previous developed synthesis methods of silver nanoparticles as catalysts for Zn-air batteries and will explore the potential of other silver-based nanoparticles. This work is framed in the need for doing research using the metals and minerals abundant in our soil as a demonstration of the possibility to produce high technology in Peru, not only the exportation of metals or mineral concentrates.

General objective

Evaluate the performance of nanoparticles supported on carbon papers as novel flexible air-cathodes for Zn-air batteries through the use of electroanalytical methods for studying the oxidation-reduction cycles and of characterization techniques for confirming the stability of cathodes throughout these cycles.

Specific objectives

- Prepare different nanoparticles-based materials to be used as air cathodes for Zn-air batteries.
- Conduct open circuit voltage, cyclic voltammetry and galvanostatic charge-discharge tests to evaluate the performance of the materials as air cathodes.
- Use X-ray photoelectron spectroscopy and UV-visible light spectroscopy to understand the behavior of materials during their preparation and use as cathodes.

1 CHAPTER I
THEORETICAL FRAMEWORK

1st UNCONFERENCE RULE

"Whoever shows up are the right people."

- Tim O'Reilly

This chapter presents a literature review on Zn-air batteries and the main challenges this technology presents with a focus on materials for the air cathode. Also, an analysis of the approaches for improving the performance of flexible air cathodes by changing its materials is presented. Furthermore, it describes the theoretical basis which allows the establishment of a methodology for the experimental analysis of the proposed materials for air cathodes.

In this sense, the structure of this chapter starts with a general description of batteries, with emphasis on metal-air batteries, which is the focus of this work. Afterwards, a general description of silver nanoparticles as catalysts for ORR and OER and its potential in air cathodes is given. Finally, general information about the characterization techniques and electroanalytical methods widely used for the evaluation of cathodes is presented.

1.1 Working principles of batteries

Batteries are electrochemical cells which use reduction-oxidation (redox) reactions to generate electricity. Among them, galvanic or voltaic cells produce an electric current with the transfer of electrons from spontaneous reactions [29]. These cells or group of cells are commonly named batteries. This defer from electrolytic cells, which need external electric energy in order to produce these reactions in the opposite direction of spontaneous reaction [30].

The redox reaction taking place in the battery involves a reductive agent and an oxidizing agent, which are contained within the battery structure, whether as an electrode or as an electrolyte. The electrodes are a cathode (positive electrode) and an anode (negative electrode), which undergo the redox reactions and generate ions in the process. Electrolytes a medium for containing this ions, which also help as a pathway for balancing ionic charges [29].

1.1.1 Cell potentials

The spontaneous flow of electrons in an external circuit from the anode to the cathode is caused by the higher potential energy of electrons in the anode. The difference in the energy per electric charge is denominated potential energy and is measured in volts (V). Then, the cell potential will be the difference of the potentials from the electrodes in the cell. Therefore, this cell potential will depend on the redox reactions within its electrodes, the concentrations of the reactants and products, and the temperature at which these reactions take place [31].

To standardize these values, the reactions at 25°C with 1M of reactants concentrations or 1 atm of partial pressure (in case of gases) are considered with respect to the standard hydrogen electrode (SHE), which has been given an arbitrary value of 0.0 V. In this sense, the reduction reactions of different electrodes against the SHE at standard conditions are evaluated and the cathode-anode cell potential is then made equal to that of the novel electrode. Based on the previous explanation, the potential of galvanic cells will always have a positive value of cell potential, whereas in an electrolytic cell the potential is negative. [31]. In this sense, rechargeable batteries work as galvanic cells during discharge and as electrolytic cells during charge. The different types of batteries are explained in the following subsection.

To evaluate the performance of a battery there are several parameters to take into consideration. These are high open-circuit voltage (OCV), operating voltage, energy efficiency, specific capacity, energy density, power density, and cyclic stability [2]. The first one refers to the potential differences between electrodes, adding to the analysis the effects of the liquid-junction potential resulting from the interaction between electrodes and the

electrolyte [32]. The subsequent parameters are a normalization of capacity, energy and power using the weight of a battery, thus, allowing a comparison among batteries from different materials and sizes. Finally, cyclic stability refers to the stability a battery has upon many charge and discharge cycles and after how many of them, the battery starts to decay.

1.1.2 Classification of batteries

Batteries are classified in two main groups: primary and secondary. The main difference between them is that the primary batteries can only be used once since they act only as galvanic cells, which means that they are nor rechargeable devices, while the secondary batteries are rechargeable devices as they at as galvanic and electrolytic cells [33]. Other characteristics of these types of cells are described in Table 1.1.

Primary batteries	**Secondary batteries**
Lower cost	Higher cost
It is not rechargeable.	Allows savings because it can be use more than once.
Disposable	Recharge and maintenance needed.
Commercial ones are smaller and lighter.	Research is being done on the improvement of energy density and size of batteries.
Commercial ones present longer life time and capacity.	Research is being done in longer life time and better capacity of secondary batteries.

Table 1.1. Differences between primary and secondary cells.
Source: T. Stobe. Classification of Cells and Batteries [34].

Nowadays, the market is dominated by primary batteries. The Battery Association of Japan shows that, from January to September of 2018, 59.32% of the sales from batteries have been from primary batteries, while 40.68% form secondary batteries [35]. However, due to the advantages that secondary batteries represent and the advances in science, the demand on secondary batteries is increasing.

Furthermore, considering the multiple characteristics of batteries and the difference among them, a more specific classification is needed. Amid the many types of batteries seen in the market and on research, there are the ones listed in Table 1.2.

The focus of this work is metal-air batteries; therefore, the next sections will deepen into their working principle, and into the advantages and disadvantages of this type of battery.

Type		**Half reactions**	**Cell voltage [V]**	**Energy density [MJ/kg]**	**Comments**	**Ongoing research**
Primary cells	Zn-carbon dry cell	Zn/Zn^{2+} Mn^{3+}/Mn^{4+}	1.5	0.13	Tends to leak out	Recovery of metals
	Alkaline	Zn/Zn^{2+} Mn^{3+}/Mn^{4+}	1.5	0.5	Like Zn-C cells, but with alkaline electrolytes	Recovery of metals
	Metal-air	M/M^{n+} O_2/OH^-	1.0 – 2.4	4.68 – 4.32	Lighter than many batteries	Rechargeable and performance improvement
Secondary cells	Nickel-cadmium	Ni^{2+}/Ni^{3+} Cd/Cd^{2+}	1.2	0.14	Jelly-roll design for reducing size	Increase stability
	Lead-acid	Pb/Pb^{2+} Pb^{2+}/Pb^{4+}	2.2	0.14	Caution with disposal	Increase stability
	Lithium-ion	$LiMO_2/Li_{1-x}MO_2+xLi^+$	3.6	0.46	Most common in the market	Improve performance and reduce costs

Table 1.2. Examples of primary and secondary batteries, including some characteristics of their working principle and performance.
Source: Own elaboration based on data from [33], [36], [37].

1.2 Metal-air batteries

Metal-air batteries have the potential of having high specific energy and energy density, therefore, a great scientific effort is being done on its development [37]. Among the metals tested for this application, zinc has driven the attention of researchers due to its theoretical capacity, relatively high stability in aqueous and non-aqueous alkaline electrolytes and price. There are many metal-air batteries designs, which are summarized in Figure 1.1. The use of liters and kilograms for expressing the energy density is for complementing, while the first one is based on the volume of the device, the latter is based on its mass.

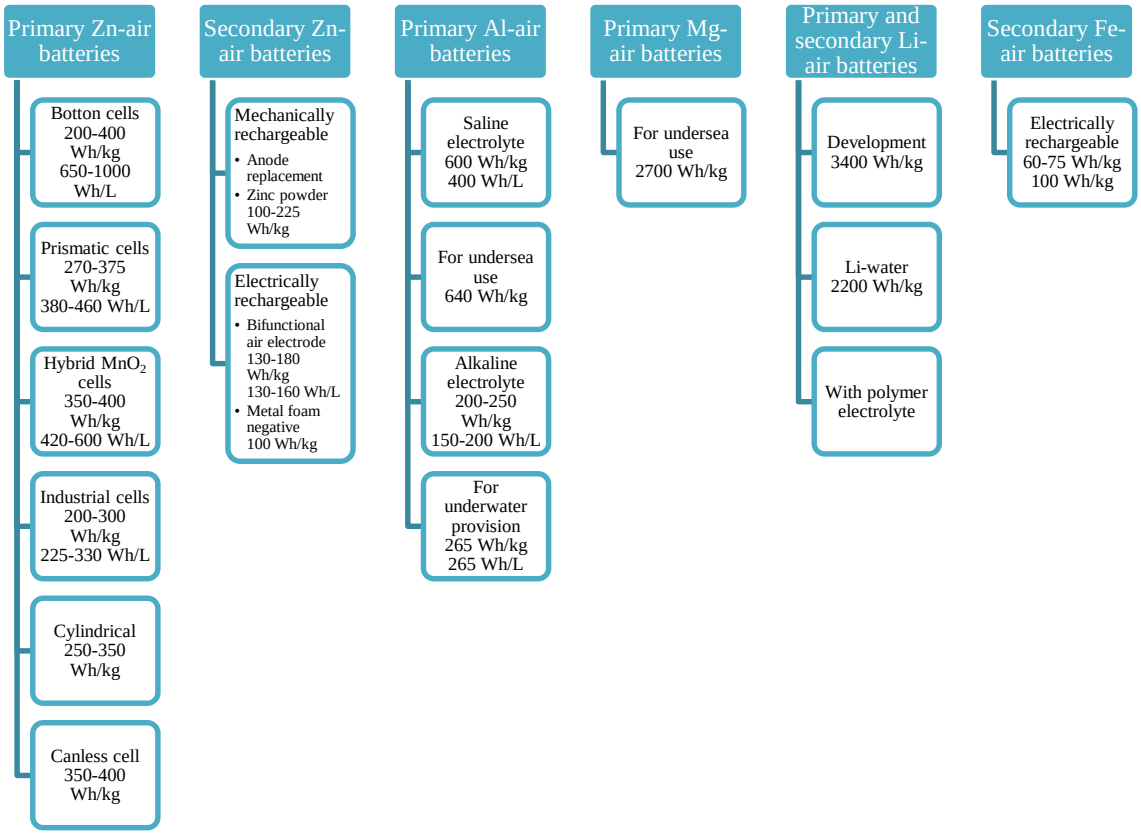

Figure 1.1. Diverse designs for metal-air batteries and its energy density based on their anode material. Source: T.B. Reddy & D. Linden. Linden's Handbook of Batteries [37].

1.2.1 Working principle

Metal-air batteries differ from others since there is no need to store one of the chemicals (oxygen), which comes from the air. This results in a battery with an open cell structure. For this reason, they potentially have a high energy density. Many metals and alloys can act as anode, and depending on them and their reaction mechanisms, the batteries have different architectures and components to satisfy the anode's needs [7].

The air-cathode is different from regular battery cathodes in that it needs to allow the oxygen flow from the outside in, to later facilitate or catalyze the reactions known as oxygen reduction and oxygen evolution reaction (ORR and OER, respectively). Its weight is also important for contributing to the high energy density. The most common configuration consist of a hydrophobic GDL and a moderately hydrophilic catalyst layer for ORR and OER [7]. According to [2], GDL has four important functions:

i. Provides physical support for the catalyst or catalyst layer.
ii. Promotes a uniformly distributed transportation of O_2 to and from the catalyst.
iii. Prevents aqueous electrolyte from leaking out.
iv. Provides a pathway for current collection.

Therefore, GDL should be thin, conductive, highly porous, and hydrophobic. Scientists are focusing their search for air-electrodes in nonprecious alternatives, such as carbon-bases materials [38], in the aim of reducing costs.

In order to achieve a conventional electrical recharge, two materials are needed: one to favor ORR and another for OER. However, this would increase the size and weight of the battery. Therefore, a bifunctional air-cathode is preferred [2]. Regarding the catalytic activity, the kinetics of ORR and OER stunts the scientists due to the unpredictable reactions. The reduction of oxygen may take two different pathways: the four-electron and the two-electron mechanisms, which are shown in Equation (1.1)**¡Error! No se encuentra el origen de la referencia.** and Equation (1.2)**¡Error! No se encuentra el origen de la referencia.** respectively. From both, two-electron mechanism is not preferred due to the poisoning that

the electrolyte of carbon material may cause [2]. On the other hand, the four electron mechanism has a higher energy efficiency due to the higher amount of electrons involved. The latter one is predominant on noble metals [39].

$$O_2 + 2H_2O + 4e^- \Leftrightarrow 4OH^- \quad (1.1)$$

$$O_2 + H_2O + 2e^- \Leftrightarrow HO_2^- \, OH^- \quad (1.2)$$

There are also many ways to arrange these different parts therefore, many configurations have been explored in metal-air batteries, such as primary, reverse, electrically rechargeable, and mechanically rechargeable ones. The principle of a mechanical recharge is the replacement of the discharged anode, this means that it basically acts as a primary battery [37].

Among the main classification that is used for these energy-storage devices, is the one based on electrolyte type. There are two main types or electrolytes: aqueous and solid-state electrolytes. Aqueous electrolytes use many solvents; however, some like the aprotic ones are degraded with moisture[7]. Even though the aqueous electrolytes are currently more common, scientists are working on the development of solid-state electrolytes. There are two methods to build them. The first one is to impregnate basic functional groups into polymer backbones with a single phase. Examples of this are alkaline anion-exchange membranes. The second method consists in the incorporation of alkaline salts into an inter polymer matrix, like gel electrolyte membranes [60]. In further subsections, current challenges in solid-state electrolytes for Zn-air batteries is explained.

1.2.2 Advantages and disadvantages

Even though this battery system has many positive aspects to suit the needs of certain applications, as it was discussed in the INTRODUCTION Chapter, they have also disadvantages. These properties have been summarized in Table 1.3.

Advantages	**Disadvantages**
High energy density	Dependent on environmental conditions
Flat discharge voltage	Limited operating temperature range
Long shelf life	H_2 from anode corrosion
Low cost	Carbonation of alkali electrolyte

Table 1.3. Advantages and disadvantages of metal-air batteries.
Source: T.B. Reddy & D. Linden. Linden's Handbook of Batteries [37].

As it was explained previously, the high energy density is due to the lack of storage of the element needed for the reduction, since this is collected from the air and the use of non-bulk metal electrode which is typically lighter than the ones used in the market; as a result, the weight of the battery is significantly reduced. The low cost is also related to the "lack" of an electrode. Usually, electrodes are pieces of metals or alloys in a bulk phase. In air-electrodes, however, the electrodes are a gas diffusion layer (GDL) with metals or alloys as catalysts impregnated in the form of nanoparticles or particles from smaller size, as explained in the previous subsection. As a result, the price of the battery is usually determined by the price of the anode [37].

Among the disadvantages of this kind of batteries is the strong dependence on environmental conditions, such as temperature and moisture. Even though many batteries are susceptible to these conditions, in the case of metal-air batteries, its effect are felt in a stronger way due to the need of oxygen from the environmental air for its functioning. This is strongly related to the limited operating temperature range [2].

Besides the redox reaction which is the principle of operation for a galvanic cell, there are other reactions that may take place thus reducing the performance of the battery. The hydrogen evolution reaction leads to the production of H_2 gas which results in the corrosion

from anode [40], which is explained in more detail in the following section. This reaction is favored because many standard reduction potential of metals are below the one of hydrogen evolution [2]. The carbonation of alkaline electrolytes results in the presence of carbonate particles on the air-cathode, which decreases its performance by blocking the access of O_2. It takes place due to the presence of carbon dioxide in the air, the carbonation of the electrolyte may change the conditions inside the cell [2]. Nowadays, researchers are working in the overcoming of the disadvantages in order to make this technology suitable for certain applications.

As it was explained in the previous section, there are many metals which were analyzed as anodes for metal-air batteries. The first one was lithium, due to the market domain of Li-ion batteries nowadays. However, this component has certain issues such as high cost, low rate of recycling and scarcity: Even some countries such as Peru have demonstrated reserved of this metal, extraction often involves sociopolitical problems and therefore the availability is not favored.

There are many other materials that can be used for this application, such as aluminum and magnesium. However, they also present some drawbacks like low coulombic efficiency, irreversibility, and high self-discharge rate. In order to present a better behavior, an alloy between these materials and other metals are done, which increases the cost of the battery. Therefore, and due to the high zinc production in the country, zinc was chosen as anode for the battery in the current work.

1.2.3 Zn-air batteries

Zn-air batteries have four main components: An air electrode, which is mainly composed of a GDL with a suitable catalyst, an alkaline electrolyte, a separator and a zinc anode. The atmospheric oxygen diffuses through the air cathode and its reduced to hydroxide ions (ORR), as shown in Equation (1.3). In the case of a battery with a liquid electrolyte, this happens at a three phase reaction site, since molecular oxygen is a gas, electrolyte a liquid, and the catalyst a solid. During charging, the hydroxide ions react with zinc forming zincate ($Zn(OH)_4^{2-}$) ions at the anode. These ions then decompose into insoluble zinc oxide (ZnO). The oxygen evolves (OER) and the zinc deposits in the cathode surface [2]. This process is shown in Equation (1.4).

$$O_2 + 2H_2O + 4e^- \Leftrightarrow 4OH^-,\ E = 0.40\ \text{V vs SHE} \quad (1.3)$$

$$Zn + 2OH^- \Leftrightarrow ZnO + H_2O + 2e^-,\ E = 0.8\ \text{V vs SHE} \quad (1.4)$$

$$2Zn + O_2 \Leftrightarrow 2ZnO,\ E = 1.2\ \text{V vs SHE} \quad (1.5)$$

Where

SHE stands for Standard Hydrogen Electrode;

E potential [V]

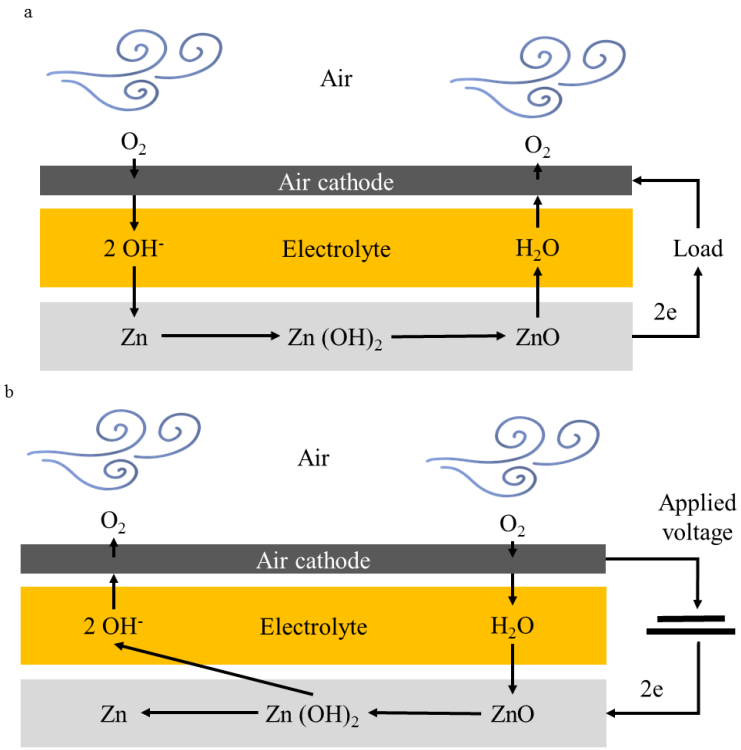

Figure 1.2. Reactions taking place in Zn-air batteries during the (a) charge and(b) the discharge of the battery. Source: Own elaboration based on T. B. Reddy & D. Linden. Linden's Handbook of Batteries [37].

Even though all Zn-air batteries work under the same principle, there are several characteristics that impact in their performance. The two most important are the materials that made up each of their parts, and the different configurations these main parts can be arranged. Since the materials of the cathode is the focus of this work, it is going to be addressed in more details in other sections. The configuration Zn-air batteries may have, is discussed in the following subsection.

1.2.3.1 Design and architecture of batteries

There are three main configurations in which Zn-air batteries can be divided, each of them have been built prioritizing different attributes. For example, conventional planar configurations were designed to prioritize high energy density, while Zn-air flow batteries were designed for a longer operational lifetime compared to the conventional planar configurations [2]. In the case of flexible batteries, they are designed, as their name suggest, for devices where this characteristic is needed like for optoelectronics, soft robotics,

wearables, among other applications that have been previously discussed. Last but not least, multi-cell configuration gives higher voltage than the previous discussed models.

a) Conventional planar batteries

Among the planar configurations, the most common one is the button type battery, which is typically build with zinc metal powder as anode and potassium or sodium hydroxide electrolyte, the silver oxide cathode is used to catalyze the OER and ORR. A cutaway view of this configuration is presented in Figure 1.3, but with silver oxide as cathode instead of a membrane for air collection [37].

a

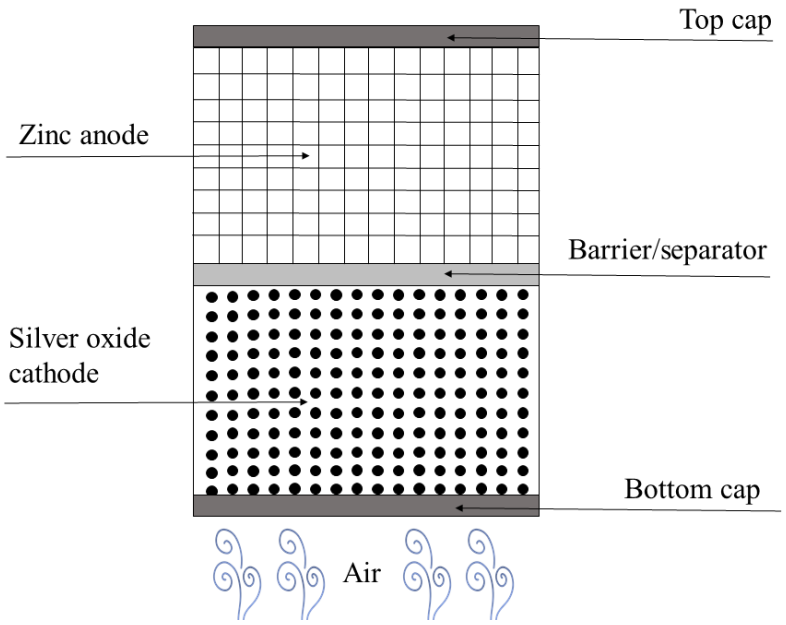

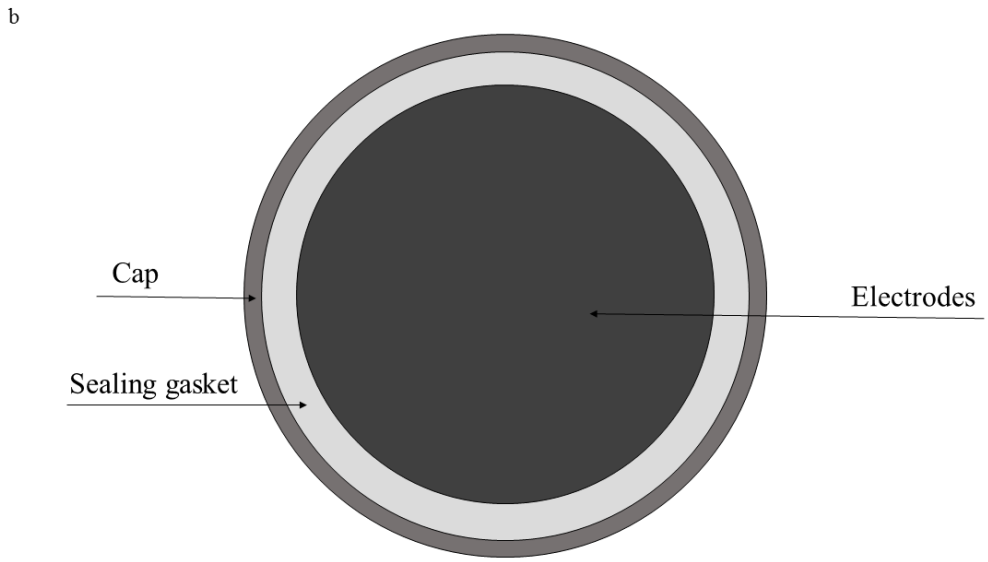

Figure 1.3. Cutaway view of typical Zn/Ag_2O button type battery. (a) Transversal view where it can be seen the air flow to the bottom cap and all the layers up to the top cap, and the electric separation between the electrodes by an ionically conducting layer. (b) Upper view where it can be seen that the electrodes are in the center of the battery, the sealing gasket avoids leakage, and the cap protects the inner layers while acting as current collector.
Source: Own elaboration based on T. B. Reddy & D. Linden. Linden's Handbook of Batteries [37].

The electrodes are placed into caps, which act as current collectors, and they are electrically separated by a disk of cellophane or grafted polymeric membrane, which is also an ionically conductive layer, allowing the redox reactions previously explained to take place [2]. This type of configuration is designed to be anode limited, which means there is more cathode capacity than anode capacity, in order to avoid the formation of zinc-iron or zinc-nickel couples between the anode and the cathode that could later origin hydrogen gas formation [37].

Another typical configuration is the prismatic one, which is shown in Figure 1.4. This configuration differs from the button cell in three aspects: Its shape, the conductive current collectors inside the plastic chasing, and external tabs for the electrodes.

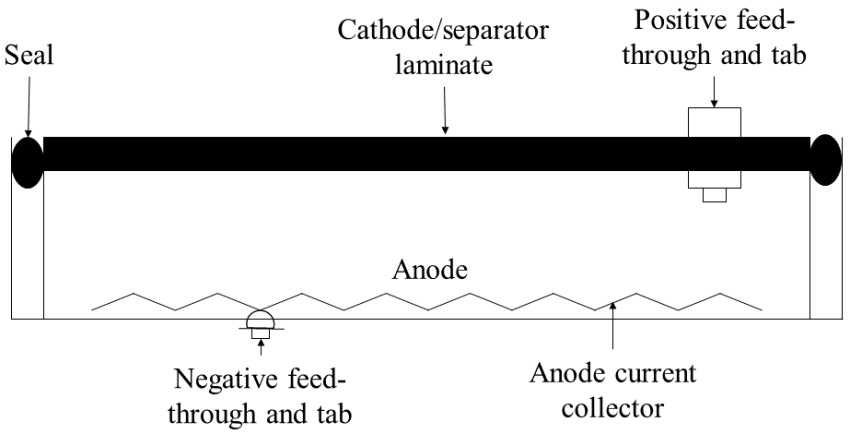

Figure 1.4. Schematics of prismatic primary Zn-air battery
Source: Own elaboration based on R. Putt, *et al.* Advanced Zinc-Air Primary Batteries [41].

The easiest way in which researchers build these cells for tests is by combining plastic plates and gaskets fastened together, for a quick assembly and disassembly [2]. Their configuration can be horizontal or vertical [42]–[44]. The advantages of having a horizontal configuration are the better current distribution in the zinc anode and easier oxygen removal from the air electrode. However, it can be seen that it could generate an electrolyte loss due to evaporation [2].

b) Flow batteries

As its name suggests, this configuration has an electrolyte channel through which it circulates, as shown in Figure 1.5 in order to increase performance and avoid degradation. This configuration brings improvements in the functioning of Zn-air batteries, but it also brings complexities. The flow of the electrolyte removes unwanted solids from the air-electrode and improves the current distribution, as a result, there is a decrease in the dendrite formation, a challenge that is going to explain in the next section. However, this configuration increases the complexity in assembly and disassembly and increases the energy density and specific volume[2].

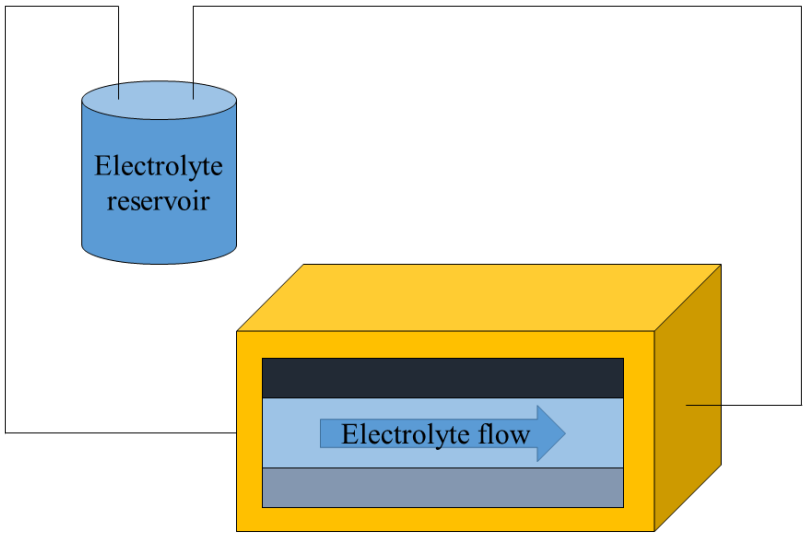

Figure 1.5. Schematic representation of Zn-air flow battery configuration, which is characterized by a channel for electrolyte flow.
Source: Based on J. Fu, *et al*. Electrically Rechargeable Zinc-Air Batteries: Progress, Challenges, and Perspectives [2].

c) Flexible batteries

Research on this configuration of batteries is ongoing due to the needs presented in the wearables market, optoelectronic devices and soft robotics, as explained in the previous chapter. Figure 1.6 presents a general schematic of this flexible configuration, since there are many designs that have been developed, there are summarized in Table 1.4 a summary of different types of configuration found in the academia.

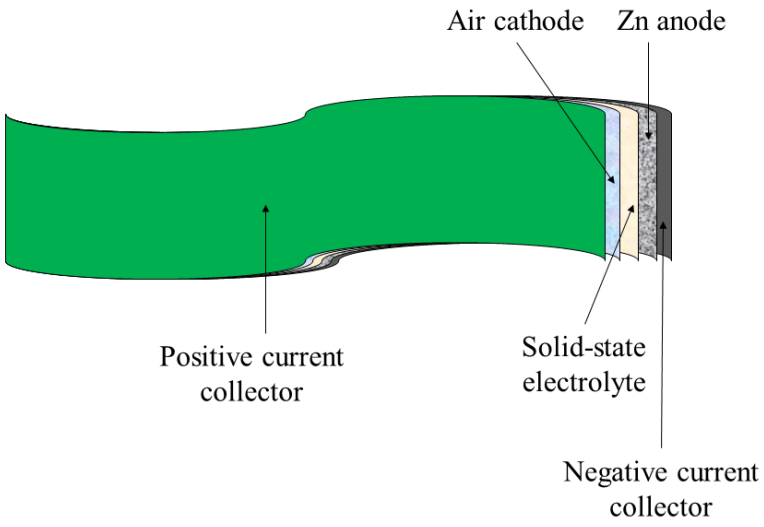

Figure 1.6. General schematic of flexible Zn-air battery
Source: Own elaboration based on J. Fu, *et al*. Electrically Rechargeable Zinc-Air Batteries: Progress, Challenges, and Perspectives [2].

Components	**Design**	**Ref.**
Zn/cellulose film gelled with KOH/Co_3O_4-NCNT	Quasi-solid state	[45]
Zn/KOH with Zn acetate/nanoporous carbon nanofiber films	All-solid state	[46]
Zn/Hydroxide-conductive nanoporus cellulose film/Co_3O_4-NCNT/SS	Hair-like array of air-electrode	[11]
Zn/PPy/MWCNT/BSA	Bio-compatible battery	[47]
Zn/gel polymer electrolyte	All-solid-state cable-type with spiral anode	[48]

Table 1.4. Examples of flexible batteries configurations in academia.
Source: Own elaboration based on data from [45] [46] [11] [47] [48].

d) Multi-cell configuration

This type of configuration is used when a higher voltage is needed, which can be accomplished using two different arrangements. In the monopolar arrangement, the zinc electrode is placed between two air electrodes and the cells are repeated and then connected in series through external connections. The bipolar arrangement connects zinc electrodes of adjacent cells through electrically conductive bipolar plates with air-flow channels.

1.2.3.2 Previous investigations and current challenges

As it was explained before, Zn-air batteries have four different parts and each one of them present opportunities for improvement, which are going to be briefly described in this section.

In the case of the zinc anode, its morphology is the key for a better inter-particle contact and lowering internal electrical resistance [37]. Many shapes such as powders [49], spheres [50], flakes [51], ribbons [52], fibers [53] and foam [54] have been studied. Some efforts are been made to increase the anode's surface area without increasing the corrosion, for which many alloys have been studied [55].

J. Fu and coworkers described four major phenomena which limit its performance, these are summarized in Figure 1.7. One is related to the influence of the shape of the anode on the battery performance. The increase in density of the electrode reduces the capacity. Dendrites are sharp, needle-like metallic lumps that may form during charging due to a gradient in the concentration of $Zn(OH)_4^{2-}$ during reduction. They can fracture and disconnect or break the separator and cause a short-circuit [2]. Several options have been considered for avoiding dendrite growth, including different charging modes and electrolyte management, where flow battery configuration have proven to be effective [56], the use of discharge trapping electrode additives such as Ca and Al to hold the $Zn(OH)_4^{2-}$ close to its original position near the zinc anode [57], [58].

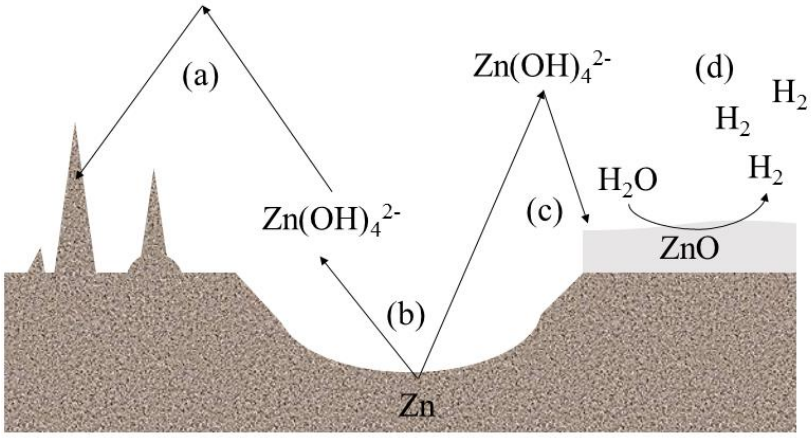

Figure 1.7. Schematic representation of performance-limiting phenomena in zinc anode. (a) Dendrites may form during charging due to a gradient in the concentration of $Zn(OH)_4^{2-}$ during reduction. (b) Shape change. (c) Precipitation of ZnO onto de zinc surface caused by the solubility limit of $Zn(OH)_4^{2-}$. (d) Hydrogen evolution is formed because it is thermodynamically favorable.
Source: J. Fu, *et al.* Eectrically Recheargeable Zinc-Air Batteries: Progress, Challenges, and Perspectives [2].

It is often the case that an insulating film is formed on the surface of the zinc anode due to the precipitation of ZnO onto de zinc surface caused by the solubility limit of $Zn(OH)_4^{2-}$, thus hindering the migration of ions for charge-discharge cycles. This phenomenon is called passivation. In order to avoid this, and to lower the zinc anode resistance, scientists are studying the effects of carbon-based additives such as carbon black [59]. As explain in previous subsections, hydrogen (H_2) formation is thermodynamically favorable in most metal-air batteries because of the difference among the anode reduction potential and hydrogen evolution potential. In this case in specific, the standard reduction potential of Zn/ZnO is-1.26 V SHE, which was explain at the beginning of the section and is shown in Equation (1.5), and the hydrogen evolution reaction potential is -0.83 V SHE, shown in Equation (1.6). Since, H_2 evolution potential is closest to zero, it is thermodynamically favorable [2].

$$Zn + 2H_2O \Rightarrow Zn(OH)_2 + H_2, E = -0.83 \text{ V vs SHE} \quad (1.6)$$

Regarding electrolytes, research efforts are driven towards electrolytes with superior ionic conductivity and reducing their vulnerability to carbon dioxide, in order to prevent the formation of carbonates which may block pores from the air electrode. Recently, solid-state electrolytes have drawn the attention of scientists because of the combination of mechanical

properties from solids and the ion conductivity of liquids [2].One of the challenges when dealing with this type of electrolyte is the interfacial resistance to hydroxide ions transporting over the catalyst surface, which is caused by their their poor wetting properties. In order to solve this problem, the improvement of interfacial properties is sought [2].

Due to the nature of rechargeable Zn-air batteries and the air cathode, the focus of the proposal in this thesis is an electrode which must be bifunctional. This means it must be suitable for both ORR and OER. Furthermore, it must be stable and with a wide potential working range.

Nowadays, there is a need for increasing the stability of cathodes towards oxidation potential and under alkaline electrolytes. On the other hand, metal-based GDL had shown a higher electrical conductivity and better Stability towards electrochemical oxidation [2]. It has been recorded that a uniform distribution of micropores in GDL alleviate the negative influence of the change in porous geometry [60].

Therefore, using silver supported on carbon as catalyst is a promising arrangement for an air cathode.

Carbon materials have shown to be good supports which help increasing the number of active sites at the electrode/electrolyte interface, thus, helping in the reaction. Moreover, they show catalytic activity for ORR. However, it has a low OER catalytic activity and has shown to be susceptible to corrosion in this reaction. There are three breakthroughs that have been made from carbon materials which has shown good catalytic activity: Metal-organic framework, hybridizing graphene with CNT and coupling inorganic nanomaterials with functionalized carbons [2].

1.3 Synthesis of silver nanoparticles

There are numerous catalysts which have been used for ORR and OER, among low-cost metals and non-metallic catalysts. Silver nanoparticles stands out for their ORR activity and excellent corrosion resistance in alkaline electrolytes [61], [62]. Therefore, their synthesis have been extensively studied and various techniques have been developed [63].

There are two approaches for growing nanoparticles: bottom-up and top-down. The first one involves the use of a precursor to form metal atoms which nucleate to form particles in the nanoscale size; this includes methods like chemical synthesis, chemical synthesis assisted by radiation, photochemical synthesis, and electrochemical synthesis [64]. The top-down approach, where metal is broken down by shear forces to form nanoparticles, is mainly based on physical growing [65]. From both chemical reduction, is the most widely used for silver nanoparticles synthesis. Sodium citrate is used for silver- and gold nanoparticles formation [66]. In this case, the reduction of silver takes place as shown in Equation (1.7), the sodium citrate acts not only as a reducing agent but also as a capping to favor the repulsion of nanoparticles in order to avoid agglomeration [18].

$$12AgNO_{3_{(ac)}} + 14C_6H_5O_7Na_{3_{(ac)}} \rightarrow 12Ag^0_{(s)} + 15C_5H_4O_5Na_{2_{(ac)}} + 9CO + 12NaNO_{3_{(ac)}} + 5H_2O \quad (1.7)$$

For this method, reducing- and stabilizing- agents are needed. Generally, sodium borohydride, sodium citrate, hydrazine and ascorbic acid are used as the reducing agents and poly(vinyl alcohol), poly (vinylpurrolidone) cetyltrimethylammonium bromide and sodiumdodecyl sulphate are used as stabilizing agents [67]. In this method, the reduction of silver ions take place in controlled conditions to reduce the probability of nucleation. These conditions include:

i) Use of low concentrations of silver ions and reducing agent.

ii) A correct stirring speed, not too slow for a slow dilution of silver solution and not too fast for clashing silver nuclei.

iii) The use of a stabilizing/capping agent to favor repulsion of nanoparticles.

The stability in nanoparticle formation may occur through two types of mechanisms: Steric and electrostatic repulsion. Steric repulsion occurs when polymers and non-ionic surfactants are adsorbed on the surface of the nanoparticle. In this case the repulsive forces depend on the thickness of the layer formed by the surfactant. In the second mechanism, the nanoparticles are terminated by ions of the same charge, which favors repulsion. A common example is citrate [68] and borohydride [69] surface charge of the disperse phase can be enhanced by ionic surfactant addition providing the electrostatic protection of the nanoparticles from adhering between them [70]. In this sense, sodium citrate is an example of electrostatic repulsion mechanisms and polydroxy fullerene (PHF) is an example of the steric repulsion mechanism, as long as it is in a molecular, not ionic, state.

PHF is a fullerene (C60, an allotrope of carbon) which is terminated with hydroxyl groups after a chemical treatment, which structure representation is shown in Figure 1.8, and has shown to be promising in many applications in the field of medicine [71]. Functionalized fullerenes have been reported to reduce oxidative stress by scavenging reactive oxygen species and to possess antioxidant properties [72]. It has also been used to accelerate photocatalytic degradation of contaminants [73]. K. Kokubo, *et al*. demonstrated that PHF could be used as unimolecular mimic of oxidized carbon materials used as support for gold nanoparticles [74]. These ligands have an effect on the size of the synthesized nanoparticle and their electronic properties could enhance the catalytic activity of the nanoparticle [75]. M. Islam, *et al.* demonstrated that stabilized gold nanoparticles by fullerenes enhanced the photocatalytic degradation of methyl orange and the catalytic reduction of 4-nitrophenol [76]. For these reasons, it is hypothesized that PHF can be used as reducing agent in the synthesis of silver nanoparticles at the same time it acts as stabilizer and enhance its catalytic activity towards ORR and OER.

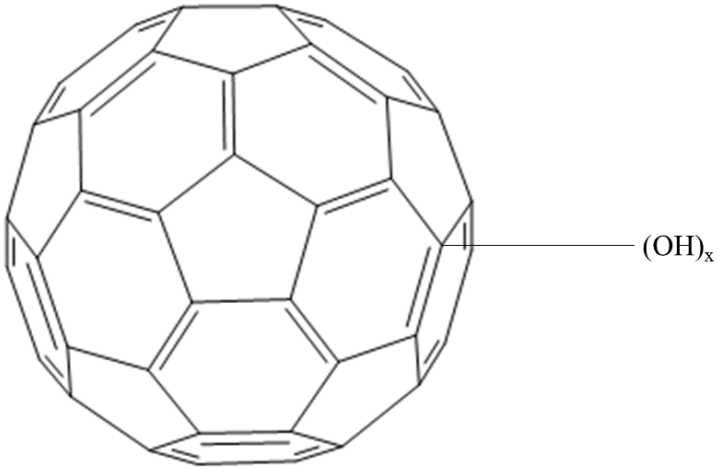

Figure 1.8. Representation of the chemical structure of polydroxy fullerene.

The formation of silver nanoparticles is strongly affected by the concentration of the reducing agent, the pH of the solution, the boiling time, the temperature and the stirring speed of the reactants. The correct pH of the solution depends on the reducing agent and the synthesis method, and has a direct effect on the particle's size and form. The use of sodium citrate results in a slower reduction reaction and the particles are angled towards aggregation; notwithstanding, its use is less toxic in comparison to other reducing agents [66].

1.4 Characterization methods for cathode materials

The focus of the proposed study is the development of materials for the air-cathode; as such, the developed material will need to be characterized in order to make a further analysis for a correlation between their properties and performance. Thus, in the following sections, the main characterization techniques commonly used are described. While ultraviolet - visible absorption spectroscopy (UV-vis) has been used for the determination of nanoparticles size and the distribution of sizes in solution, before the impregnation, X-ray photoelectron spectroscopy (XPS) is a surface analysis technique used to determine the material's composition.

1.4.1 Ultraviolet and visible absorption spectrometry

The absorption of light from different species is unique, therefore, it can be used for qualitative and quantitative analysis of organic and inorganic compounds and materials [77], including nanoparticles. In this technique, samples are illuminated with electromagnetic waves from different wavelengths in the range of visible and ultraviolet spectrum and the transmitted rays are recorded to form a spectrum. Usually, what is plotted in this analysis is the absorbance (A_b), which is defined as the negative logarithm of the transmittance (T_r). Moreover, this technique gives information about the concentration of a sample in accordance of the Lambert-Beer law, which is showed in Equation (1.8):

$$c = \frac{A_b}{\varepsilon d} \tag{1.8}$$

Where

c concentration in a sample given in mol L^{-1};

ε extinction coefficient given in L cm^{-1} mol^{-1}; and

d path length given in cm [78].

Metallic bonds formed on the surface of these materials are compared with plasma because of the free electrons in the conductive band surrounding the nuclei. The collective excitation of the electrons near the surface of the nanoparticles is known as surface plasmon resonance (SPR). These electrons are limited to specific vibrational modes by the size and form of the particle, which means that the colors displayed are usually different from the bulk form of the metal. This means that each metallic nanoparticle presents a unique optical absorption spectrum in the UV-vis range of light [79].

In this sense, a solution containing nanoparticles displays a unique UV-vis spectrum and helps to determine the size, size dispersion and concentration of the nanoparticles in the solution. The peak position is related to the particle size, the full width at half maximum is related to the dispersion of this particle size and the absorption peak indicates the

concentration of nanoparticles of this specific size [18]. Studies have work on relating these characteristics form metallic nanoparticles [80].

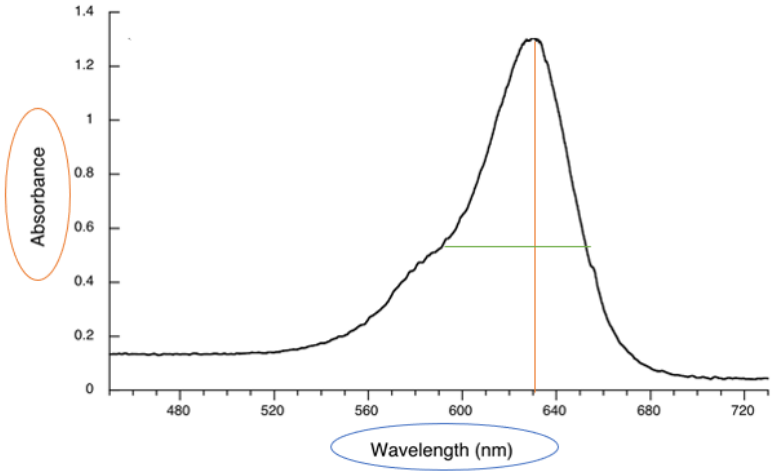

Figure 1.9. Interpretation of UV-vis spectrum for nanoparticles. The wavelength (in blue) gives information about the particle size, absorbance (yellow) gives information about concentration, and width (green) gives information about the dispersion.

1.4.2 X-ray photoelectron spectroscopy

XPS is one of the most often applied techniques in the characterization of solid surfaces [81] because it provides information on the composition of the sample, the chemical environment and oxidation states of the different elements. In this sense, it can determine the presence of silver over the air-cathode, the oxidation state in which it is presented before and after electrochemical tests.

This characterization technique is based on the photoelectric effect by which the energy of a photon is absorbed by an atom and, as a result, an electron is rejected with a specific kinetic energy. This process is described by the Equation (1.9).

$$E_k = h\nu - E_b - \varphi \tag{1.9}$$

Where

E_k the kinetic energy of a photoelectron in eV;

h the Planck's constant 4.14 x 10^{-15} eV s [82];

ν frequency of the incoming radiation in Hz;

E_b binding energy of the photoelectron with respect to the Fermi level of the sample in eV;

φ work function of the spectrometer in eV [83].

Usually, the X-ray sources are Mg Kα and Al Kα, whose energies ($h\nu$) are set to 1 253.6 eV and 1 486.3 eV. Therefore, $h\nu$ in Equation (1.9) is a known, controlled value. The intensity of photoelectrons is measured as a function of their kinetic energy. With this information, the binding energy can be found using Equation (1.9). Usually, the results are plotted in graphs which show the intensity of photoelectrons against E_b [83].

The chemical environment affects the kinetic energy of the rejected electron, therefore, this technique can give information regarding the chemical state of the elements in the sample. For example, previous research in our group demonstrated that a silver nanoparticle attached to a thiol-containing molecules showed a signal of pure silver and Ag-S in XPS [84].

Additional to the peaks obtained due to the photoelectric effect, there are also some peaks observed that are originated by Auger electrons. Even though some peak values from Auger electrons are already reported and well known, one way to differentiate them from those caused by the photoelectric effect, is to perform a measurement in a sample with two different X-ray sources. These electrons have fixed energy, this means they are independent from the X-ray source; therefore, the Auger peaks will appear shifted on the binding energy scale [83].

The equipment used for this test is presented in Figure 1.10. As can be seen, the sample is bombarded with X-rays and the photoelectrons ejected from the sample are colected and directed by the lenses to the analyzer [85].

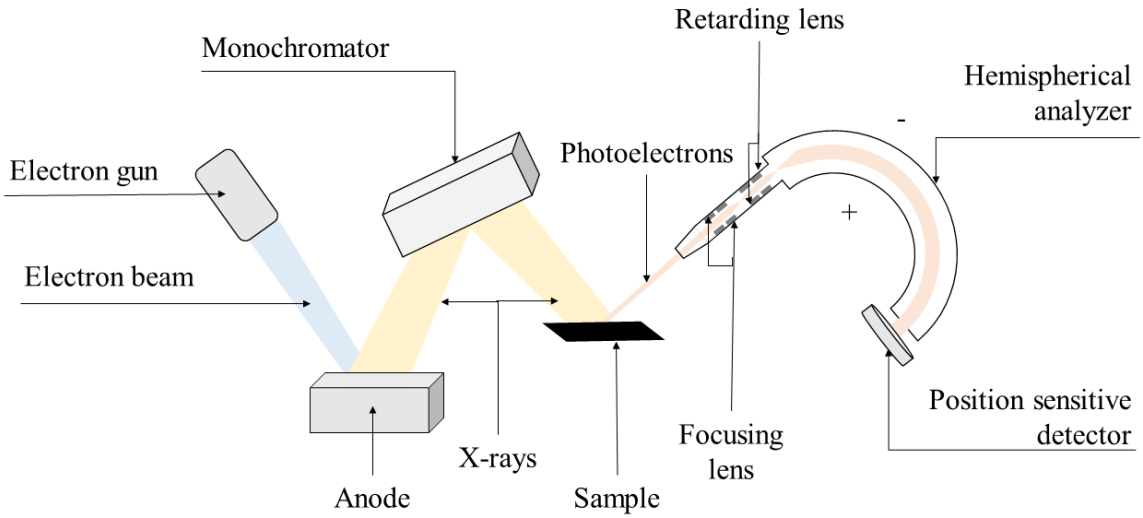

Figure 1.10. Schematic representation of an XPS system
Source: Own elaboration based on C. Cushman, *et al.* Trends in Advanced XPS Instrumentation [85].

1.5 Electroanalytical methods

Electroanalytical methods are the ones used to examine an analyte based on oxidation-reduction reactions, and are commonly used to analyze the behavior of an electrode and test its performance. These methods can be classified into two groups: interfacial methods and solution methods. The first main group focuses on the phenomena that take place between the electrodes and the solution next to it; while the second group isolates the solution from the interfacial effects. The interfacial methods group can be further divided into static and dynamic methods. The main difference between these two subgroups is the possibility of controlling the current in the cell, since the static methods do not use a current for the test, while the dynamic methods do [77]. A summary of the methods presented in this section is found in Table 1.5.

Test	Parameters studied	Variables	Nature
Open circuit potential	Potential [V]	Electrodes and electrolytes	Static
Cyclic voltammetry	Current [A] Redox process	Applied voltage [V]	Dynamic
Galvanostatic charge-discharge	Capacity [Ah]	Current density [$mA\ cm^{-2}$]	Dynamic

Table 1.5. Summary of electroanalytical tests.
Source: Own elaboration based on [2], [37], [77], [86]–[90].

1.5.1 Open circuit potential

The open circuit potential (OCP) is the electrode potential at which there is no current flow [91]. The measured OCP is the sum of the potential differences in the interfaces of a cell [92] at a non-equilibrium state [32]. This value is measured over time to determine the stability of the electrode potential over time. This value is firstly used to determine the start potential of further electroanalytical tests, like cyclic voltammetry. Moreover, its value gives a first sight of the voltage of a battery, since the other electrode has a known potential [32].

1.5.2 Cyclic voltammetry

Voltammetry is a group of electroanalytical methods in which the current is measured as a function of an applied voltage under conditions that promote the polarization of the analyte, for which the electrodes are as small as possible (in the order of a few millimeters)

[77]. Polarization is one of the two phenomena that increase the potentials from the Nernst Equation when exposed to a current, as it can be seen in Equation (1.10).

$$E = E^0 - \frac{RT}{nF} \ln C \tag{1.10}$$

Where

E potential difference in V;

E^0 potential difference under standard conditions in V;

R universal gas constant 8.316 J mol^{-1} K^{-1};

T temperature in K;

n number of mol of electrons transferred in the reaction;

F Faraday constant which is equal to 96 485 C mol^{-1}

C reaction quotient [86].

The type of cell for the voltammetry test varies depending on the analyte and the type of voltammetry. The most common one is the three-electrode configuration, which has four main components that are shown in Figure 1.11:

a) Electrolyte solution: Consists of the analyte and a supporting electrolyte dissolved in a solvent (typically water).
b) Working electrode: Is the electrode to be tested (made of the material under investigation). Its potential is varied respect to the reference electrode.
c) Reference electrode: Electrode with a known, constant potential throughout the whole test. As explain before, the potential of an electrode must be measured against another electrode. Even though potentials are often reported vs. SHE, there are other electrodes which are simpler to handle, such as calomel and platinum.
d) Counter electrode: It is often a coil of platinum wire and is the one which closes de circuit with the working electrode.

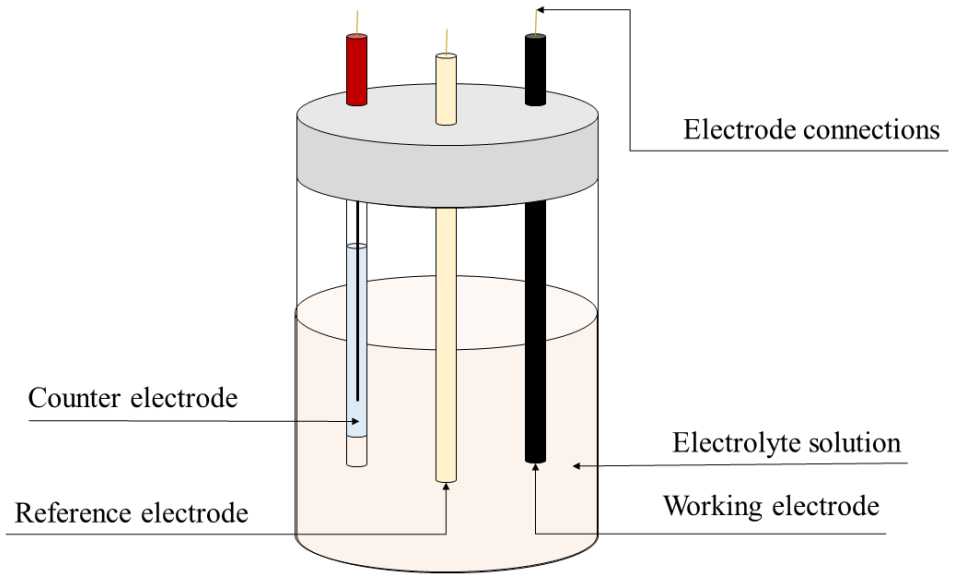

Figure 1.11. Schematic representation of an electrochemical cell for voltammetry
Source: Own elaboration based on N. N. Elgrishi, *et al*, A Practical Beginner's Guide to Cyclic Voltammetry [87].

The input signal for the voltage DC can be either of the four types: linear scan, differential pulse, square wave, or cyclic voltammetry. Only cyclic voltammetry, which pulse is shown in Figure 1.12, is going to be explained in this section, as it is part of the proposed methodology.

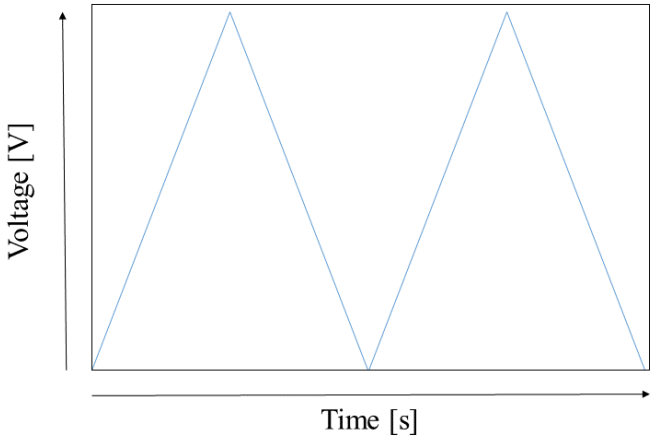

Figure 1.12. Voltage vs. Time excitation signals in cyclic voltammetry
Source: Own elaboration based on D.A. Skoog, *et al*. Fundamentals of Analytical Chemistry [77].

As its own name suggests and can be seen in the excitation signal from Figure 1.13, the cyclic voltammetry allows the study of reduction and oxidation processes, and electron transfer-initiated reactions. Usually, a cyclic voltammogram shows an arrow for the reduction process, the US convention shows the potentials in a decreasing way, while the IUPAC convention shows them in an increasing way [87], in the present work, the IUPAC convention is used.

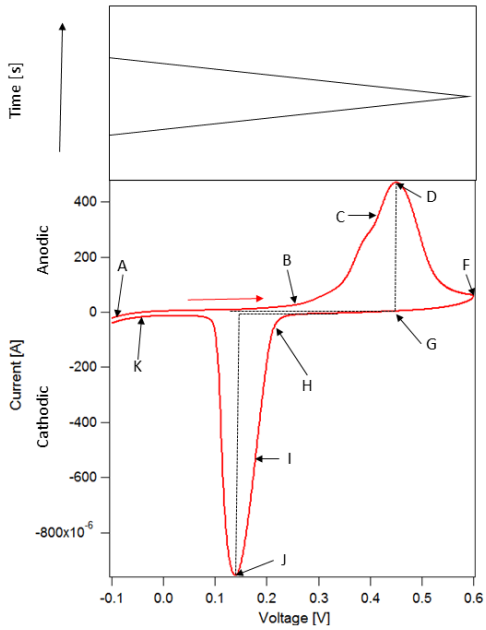

Figure 1.13. (a) Potential vs. time waveform. (b) Cyclic voltammogram
Source: Own elaboration based on [77].

Figure 1.13 shows a cyclic voltammogram, which is taken as a reference to explain the analysis of a voltammogram. The Figure 1.13(a) shows the potential input and Figure 1.13 (b) the system response. At the beginning, a small cathodic (negative) current is seen, but it quickly reaches zero during a broad potential range (approximately from 0 to 0.15 V) until it becomes more positive and an anodic current starts to develop in point B (0.15 to 0.6 V). At D, the maximum current is achieved as a) the potential determined by the Nernst equation is reached and the equilibrium concentration is achieved, and/or b) the normal diffusion-controlled current is delivered [77]. The current starts to decay between D and F

because the diffusion layer grows farther from the electrode. As can be seen in Figure 1.13 (a), the potential starts to increase, but the current stays anodic until it reaches zero and a reduction of the compounds that has been oxidized previously takes place [77]. On points C and I, the concentration of the ions are equal on the surface of the electrode, this means $E = E_{1/2}$. This value is used to solve the Nernst equation for specific reversible reactions. The difference between the anodic and cathodic peak is called peak-to-peak separation when the reaction is chemically and electrochemically reversible [87].

One important parameter of this test is the scan rate, which is the velocity at which the potential is scanned, because faster rates may decrease the size of the diffusion layer and increase the current peaks. The Randles-Sevcik equation, shown in Equation (1.11), describes the increase in current peak and indicates if the analyte is freely diffusing in a solution.

$$i_p = 2.686\ 10^5 n^{3/2} A C^0 D_0^{1/2} v^{1/2} \tag{1.11}$$

Where

i_p peak current in A;

v scan rate in V s^{-1};

A electrode surface area in cm^2;

D_0 diffusion coefficient of the oxidized analyte in $cm^2\ s^{-1}$

C^0 bulk analyte concentration mol cm^{-3} [77].

In cyclic voltammetry, the catalytic activity of a material can be determined by analyzing the onset potential of the peaks of interest and the amount of current this peaks represent. Each peak corresponds to a reduction or oxidation reaction, depending on the polarity of the current (cathodic or anodic). The onset potential is related to the amount of energy required for a reaction to take place. In the case of ORR, the more positive the onset potential is, the better the catalyst. In the case of OER, the lower the onset potential is, the better the catalyst is The amount of current in a peak, is related to the amount of reacting compounds, therefore, a higher peak indicates a higher amount of reacted compounds. In this

sense, better catalysts show onset potentials closest to each other and large amount of current in the peaks of the reactions they are enhancing [93].In the present study, this technique is used to evaluate the catalytic activity of the silver nanoparticles towards OER and ORR, by the identification of the potential in which this peaks are present and their intensity, as it has been done in other studies [13], [46], [94]. When the potential is closest to zero, the energy needed for the reaction is less, then the catalytic activity of the nanoparticles is better. The intensity of the peak, gives information related to the amount of reacted molecules, in this sense, the bigger the peak, the better the catalyst.

1.5.3 Galvanostatic charge-discharge test

As its name suggests, this test charges a battery and discharges it at specific current densities rates, usually measured in mA cm^{-2} [17]. This test shows at which current there is a saturation, the stability of the electrode upon several cycles, as well as the capacitive and faradaic behavior of the electrode and its capacitance [95].

When the voltage is plotted against the capacitance, the slope of the graph indicates the capacitive or faradaic effect. In this sense, a change in the slope as shown in green in Figure 1.14, is attributed to a faradaic effect. On the other hand, a constant and smooth slope is attributed to a capacitive effect, as shown in red [95]. The faradaic effect is common to batteries, while the capacitive effect, as its name suggest, is common to capacitors. The Figure 1.14 only shows one cycle from charge-discharge test for demonstrative purposes, after the charge, the discharge is followed as explain in the CHAPTER II METHODOLOGY chapter, thus the sudden change in current.

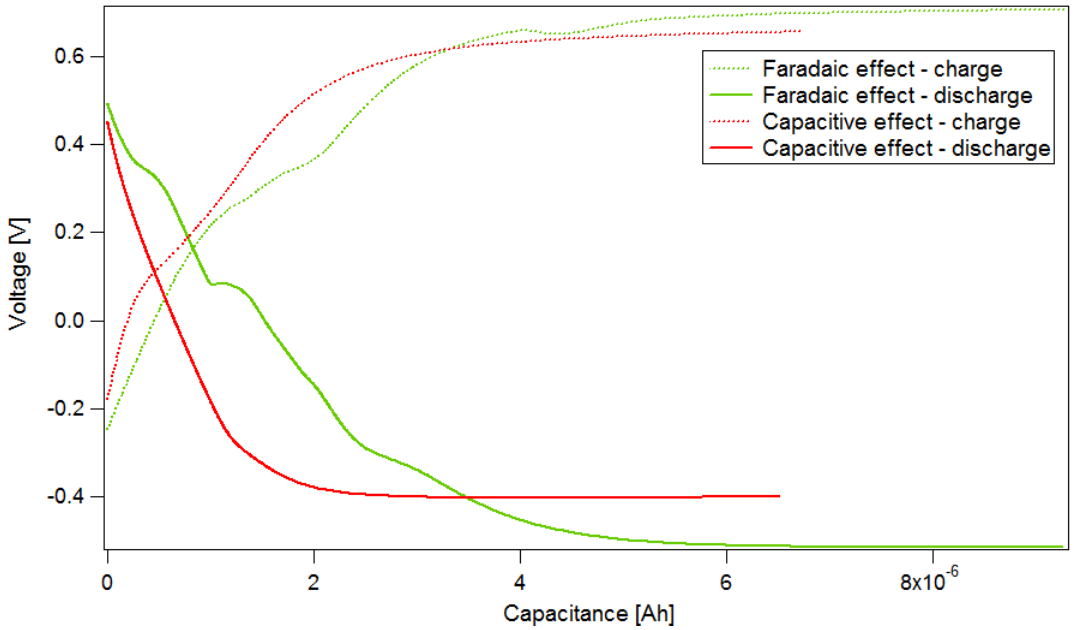

Figure 1.14. Voltage vs. capacitance graph example.
Source: Own elaboration

A plot voltage vs. time gives other type of information. An example is shown in Figure 1.15, where the graph in blue shows a higher current density than the graph in red. The stability of the electrode upon many cycles can be evaluated, with a drop on the voltage over time being characteristic of an unstable electrode. The stability of the electrode is a desirable characteristic, because it means a longer life time. On the other hand, the end of the charging gives information about the saturation achieved in that specific current density. If it turns flat, like the graph shown in blue, then there is a saturation; conversely, if it has a slope as shown in red, then the saturation is not reached at that specific current density. In the discharge part of the curve, the resistance to discharge is evaluated. If there is a smooth slope, then there is a resistance to discharge, but a sharp slope as shown below, indicates a rapid discharge, which is a desirable characteristic for an electrode. The change in the slope explained in Figure 1.14, can also be seen in this type of graphs. In this case, no change in slope is shown in the charge nor in the discharge, therefore, a capacitive effect is attributed [95].

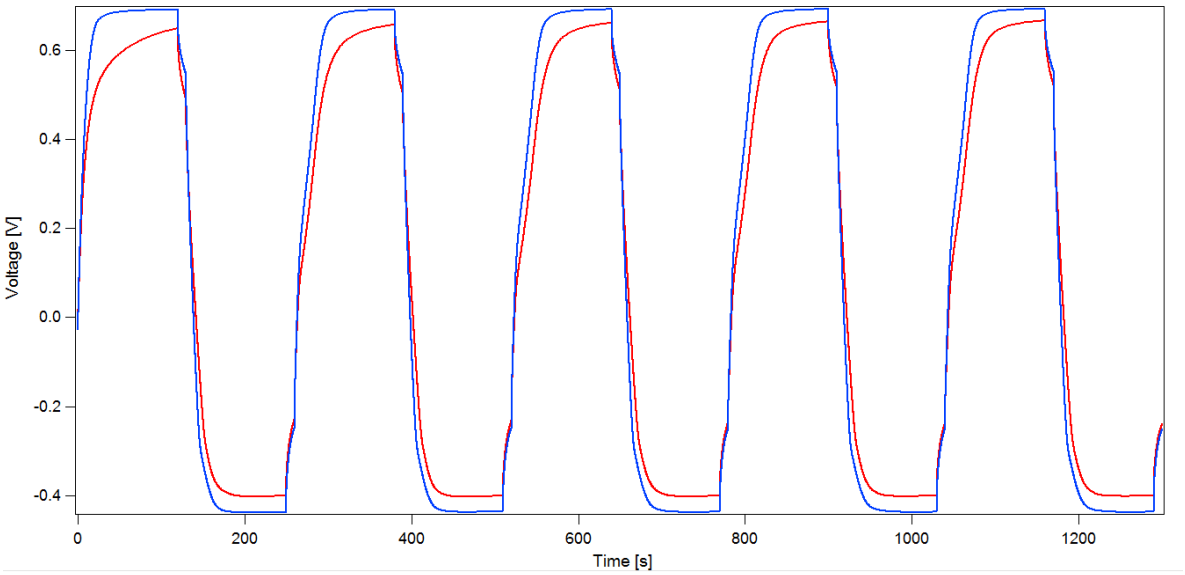

Figure 1.15. Voltage vs. time graph example.
Source: Own elaboration.

As can be seen, this test gives important information about the electrode. It determines which electrode acts as a battery electrode, and provides information about stability and resistance to discharge, informing therefore how efficient is a proposed electrode.

2 CHAPTER II
METHODOLOGY

2nd UNCONFERENCE RULE

"Whatever happens is the only thing that could have."

- Tim O'Reilly

Based on the information presented in the previous chapter, new materials for air cathodes for Zn-air batteries will be proposed, as well as a methodology for testing its performance. These materials are silver nanoparticles, impregnated over carbon nanotube (CNT) buckypaper (20 gsm C-grade CNT Buckypaper 12'' x 12'', NanoTechLabs, Inc., Yadkinville, NC, USA) through the ink evaporation method. The synthesis of silver nanoparticles employs sodium citrate as reducing agent and is based on the Frens method for synthesis of gold nanoparticles [19]. Another synthesis method using polyhydroxy fullerenes (PHF) as reducing agent is proposed, in order to form a nancomposite Ag-PHF. As reported in literature, PHF acts as stabilizer [74] and it is hypothesized to enhance the catalytic activity of the silver nanoparticles towards ORR and OER. The characterization methods considered by the author for silver nanoparticles are UV-vis and XPS, essential for the analysis and a comparison among them and the ones previously developed by the group.

After the synthesis, these materials must be impregnated onto the carbon buckypaper, which works as current collector in the Zn-air battery. The electrode is characterized by OCP, CV and galvanostatic charge-discharge test in neutral and alkaline media. The capacity, catalytic activity and stability of the different proposed electrodes must be evaluated for comparison and the establishment of the most suitable cathode for the battery. The data analysis was performed sing IgorPro (WaveMetrics, OR, USA). This methodology is summarized in and explained in detail in Figure 2.1 the following sections.

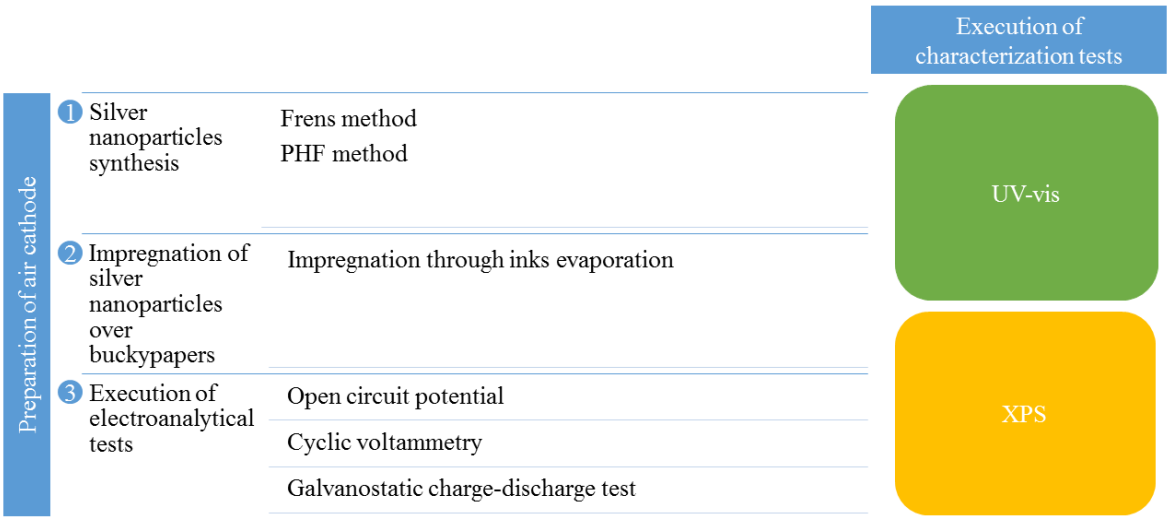

Figure 2.1. Methodology flow diagram.
Source: Own elaboration.

2.1 Preparation of the air cathode

The preparation of the air cathode was done under atmospheric conditions at UTEC facilities. The preparation process itself consists of two steps and a final characterization of the electrode. The two steps were: the synthesis of silver nanoparticles and their impregnation over CNT buckypapers. The characterization of the electrode was done using UV-vis and XPS, and its performance as air cathode was tested using three electroanalytical techniques: open circuit voltage, cyclic voltammetry and galvanostatic charge-discharge test. The detailed step-by-step procedure is explained in the following subsections.

2.1.1 Silver nanoparticles synthesis

2.1.1.1 Frens method

This procedure was presented by M. Gakiya Teruya, L. Palomino Marcelo and J.C. Rodriguez Reyes [19] and adapted for the following work at UTEC laboratories. This procedure uses sodium citrate as reducing agent for the silver nanoparticles formation. As explained in the previous section, an increase in temperature increases the reducing potential of the salt; therefore, the boiling point is reached in this method. On the other hand, sodium

citrate is injected in a short time in order to propitiate the fast formation of nuclei and the subsequent slow growth. This procedure is detailed in the following lines.

A solution of 50 mL of $AgNO_3$ (99.8%, J.A. Elmer, Lima, Peru) in distillated water at 1 mM is placed in an Erlenmeyer flask with a magnetic pill and totally covered with aluminum foil, in order to avoid exposure to light (as showed in Figure 2.3). The solution is heated until boiling point (100°C) and then a 500 µL solution of sodium citrate (at 99.9%, developed by Movilab, Lima, Peru) in distillated water at 0.189 M is added at once using a micropipette. The final solution is stirred for 20 minutes, obtaining a brownish color. Then, this solution is microcentrifugated (with an Eppendorf® Centrifuge 5415 C). This procedure is shown in Figure 2.2.

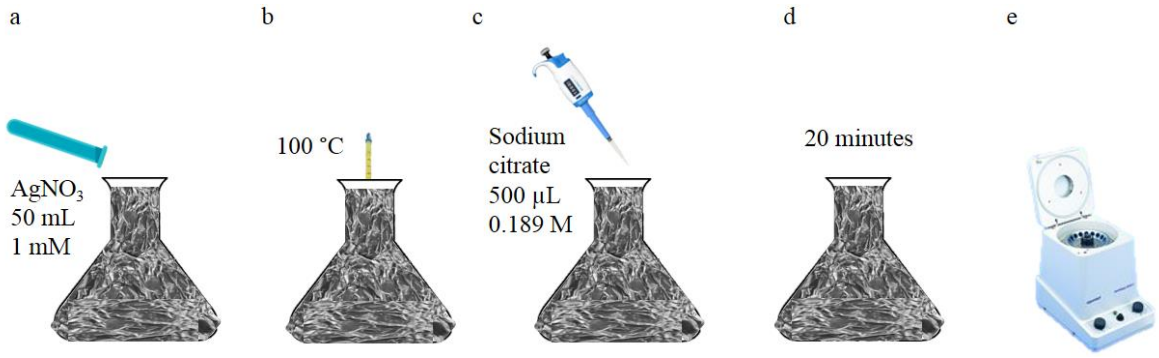

Figure 2.2. Schematic of the Frens method for silver nanoparticles synthesis. (a) Place of 50 mL of silver nitrate in Erlenmeyer flask covered with aluminum foil. (b) Heat the solution until boiling point. (c) Add 500 µL of sodium citrate. (d) Stir for 20 minutes. (e) Microcentrifugate to obtain the silver nanoparticles. Source: Own elaboration.

Figure 2.3. Erlenmeyer flask with a magnetic pill totally covered with aluminum foil being heated for the Frens method synthesis of silver nanoparticles.
Source: Own elaboration.

2.1.1.2 Method using PHF as reducing agent

The following procedure was developed by Juan Carlos Rodriguez-Reyes Research Group in collaboration with Cleveland Clinic and adapted for the following work at UTEC laboratories (work in preparation) PHF is used in the silver nanoparticle synthesis as surfactant to enhance the catalytic activity of this catalyst.

For the tests, 5 µL of a solution of $AgNO_3$ (99.8%, J.A. Elmer, Lima, Peru) at 1 M in distillated water, 500 µL of a solution of PHF at 1mg mL^{-1} in distillated water, and 495 µL of distillated water were added to a vial covered with aluminum foil to avoid exposure to light. Then, a shaker (Fisher VM-300) is used for stirring for 4 hours for a later centrifugation at 5712 relative centrifugal force (RCF) for 30 minutes at 25°C. After that, the supernatant is discarded and the pellet is resuspended in distillated water to achieve 1 mL.

2.1.2 Impregnation of silver nanoparticles over buckypapers through the ink evaporation method

The ink evaporation impregnation method is employed to deposit the silver nanoparticles and PHF over the CNT buckypapers. This method involved the formation of an ink of distillated water and isopropanol (IPA) with the silver nanoparticles and PHF for a further evaporation. The general schematics is presented in Figure 2.4.

In the case of the impregnation of electrodes with only silver nanopaticles, a resuspension of silver nanoparticles in 800 µL of distillated water and 200 µL of IPA (2-Propanol, developed by J.T. Baker, TM, Madrid, Spain) at 66mM of concentration was made. After that, the solution was sonicated using an DR-S20 Ultrasonic Cleaner 3L (Shenzhen Derui Ultrasonic Equipment Co., Shenzhen, China) for 30 minutes at 25°C. Then, 10 µL of the solution was added to the buckypaper. When the drop was beginning to evaporate, other 10 µL were added until 20 µL were deposited. After the 20 µL solution was deposited, the buckypaper was left under the infrared light for 15 minutes to favor the evaporation of the solvent. This is shown in Figure 2.5.

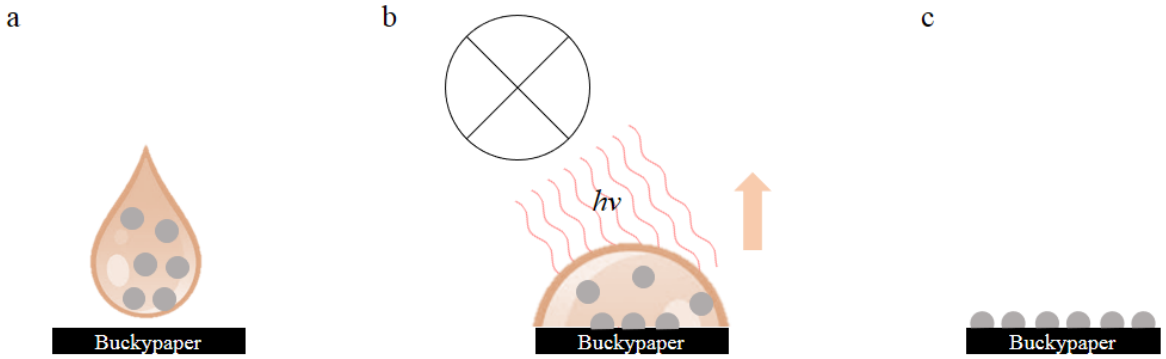

Figure 2.4. Schematic of silver nanoparticles impregnation through ink evaporation. (a) Deposition of colloids over the buckypaper. (b) Irradiation of light over the drop to dry the water and IPA. (c) Schematic of resultant electrode.
Source: Own elaboration.

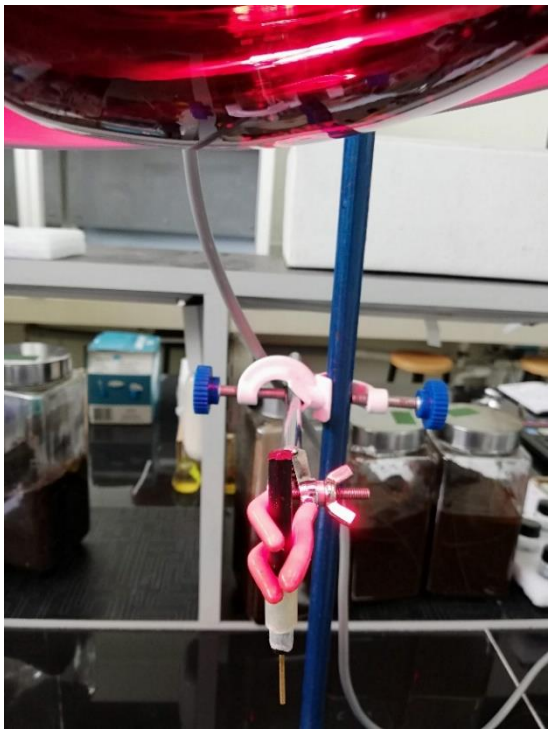

Figure 2.5. Silver nanoparticles ink drying by IR light over buckypaper pasted over glassy carbon work electrode
Source: Own elaboration

In the case of the impregnation of electrodes with silver nanoparticles synthesized with PHF as reducing agent, a solution of the colloid is done in 200 µL of DI and 50 µL of IPA. Each of these is stirred using he vortex. Then, 10 µL of the solution is added to the CNT buckypaper and irradiated with IR light, followed by another 10 µL until the 250 µL is impregnated. Stoichiometric calculation showed that we had comparable amounts of silver in both cases.

2.1.3 Execution of electroanalytical tests

The electroanalytical procedures are based on the procedures of the Research Group of Applied Electrochemistry at UNI, having in consideration the equipment available in their laboratories.

2.1.3.1 Open circuit potential

This is the first test performed to every electrode tested, to evaluate its potential and stability over time. It is especially important to define the starting voltage value for the CV test. The equipment used for this test is ZIVE SP2 potentiostat (WonATech Co., Ltd., Korea). This test is done using an amplitude of 5 mV, a start frequency of 10^{-6} Hz, a medium frequency of10^{-5} Hz and a final frequency of 10^{-3} Hz, the sample density is 50 point per decade with current range of 20 mA for 120 seconds.

2.1.3.2 Cyclic voltammetry

All the experiments will be done in a three electrode configuration and two electrolytes will be used for neutral and alkaline medium. In the case of the neutral medium, the electrodes used are silver/silver chloride at 3 M as reference electrode, platinum electrode as counter electrode, and vitreous/glassy carbon as work electrode. For the alkaline medium, the reference electrode was a mercury/mercury oxide electrode (E = 0.165 V vs. SHE) and the CNT Buckypaper acted as working electrode without support. All the electrodes were cleaned with ultrapure water before using them. The set-up used is shown in Figure 2.6**.**

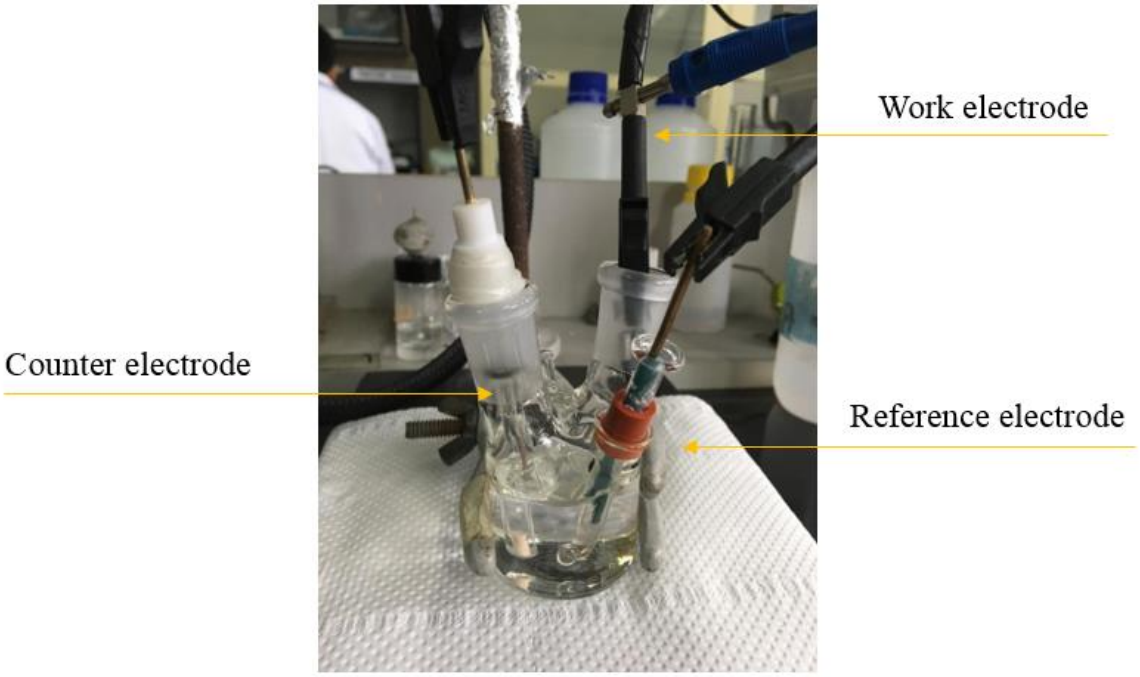

Figure 2.6. Set-up for the cyclic voltammetry.
Source: Own elaboration

The tests in neutral medium use sodium chloride (EMSURE ACS, ISO, Reag. PhEur) at 1M in ultrapure water as electrolyte and is performed as follows. The CNT buckypaper is put over the work electrode using a Nafion perfluorinated ion-exchange resin (developed by Sigma Aldrich, Darmstadt, Germany). To do it, 1 cm x 1 cm of buckypaper was cut, 10 µL of Nafion was put over the work electrode, and then the buckypaper over the Nafion. Finally, infrared light (IR) is used to dry the sample as shown in Figure 2.5.

Before each test, the electrode is cleaned as follows: slowly and in an 8-form, the electrode is sanded for 60 times. Then, the tip is cleaned using an ultrasonic bath for 15 minutes in distillated water and washed with ultrapure water (PURELAB Classic, ELGA LabWater, High Wycombe, UK). After that, an electrochemical cleaning using DY2100 Series Mini Potentiostat (Digi-Ivy, Inc., Austin, TX, USA), with a condition time of 180 seconds, a potential during condition time of -0.2V and a quiet time of 5 seconds is done. The general settings for the electrochemical cleaning are shown in Figure 2.7.

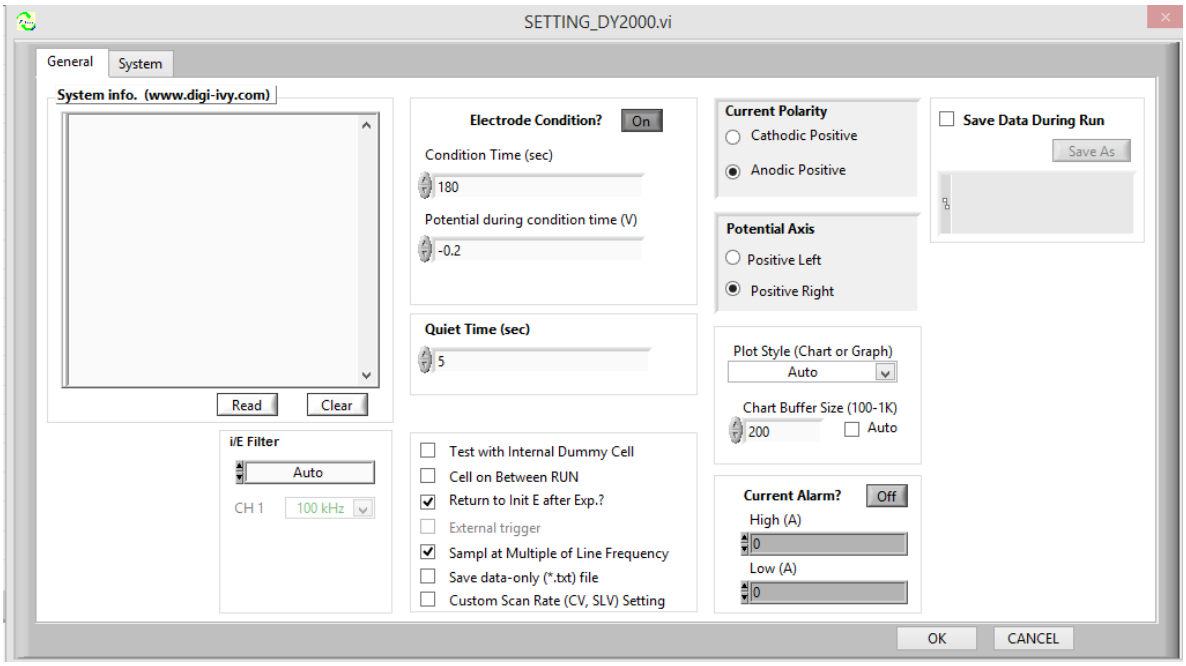

Figure 2.7. Settings for an electrochemical cleaning.
Source: Own elaboration.

The cleaning is followed by a blank experiment using glassy carbon cathode. The general settings for the cyclic voltammetry in neutral media are an anodic (positive) current, a quiet time of 5 seconds, a window from -1.2 V to 1.2 V at a scan rate of 0.05 V s^{-1} with a sensitivity of 1 x 10^{-3} for 5 cycles. These settings are shown in Figure 2.8. For the analysis of the data, the average of all the cycles done is used, excluding the first one because the first scan often involves conditions where the electrodes and the electrolyte are not stabilized yet.

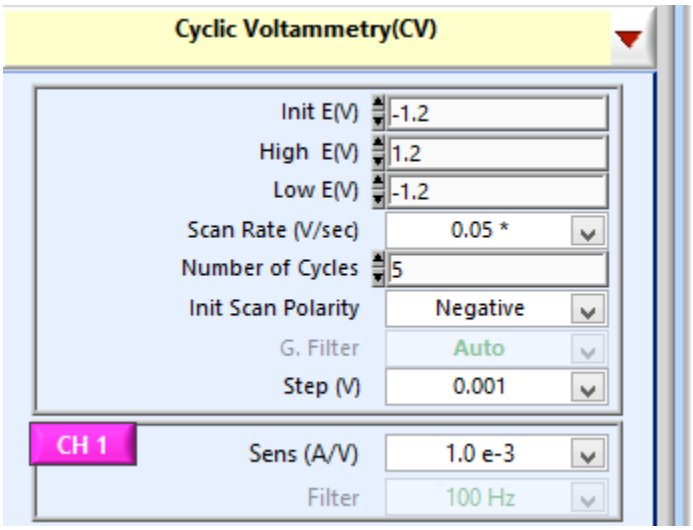

Figure 2.8. General settings for a cyclic voltammetry in neutral medium.
Source: Own elaboration.

The tests in alkaline medium use potassium hydroxide at 0.1 M as electrolyte and no work electrode; instead, the CNT buckypaper (0.5cm x 6cm approximately) with and without silver nanoparticles is connected directly through a female pin terminal (16-14 AWG). The CNT buckypaper is hydrophobic, therefore, it must be wet with Nafion perfluorinated ion-exchange resin before each test for it to be immerse in the electrolyte. At the beginning bubbles are formed around the CNT buckypaper, likely due to the evolution of trapped air. After 10 to 15 minutes, the bubbles disappeared and the measurements may start. For the calculations of current density, the only area considered is the one being immersed in the electrolyte. The equipment used for this test was ZIVE SP2 potentiostat (WonATech Co., Ltd., Korea).

The general settings for the cyclic voltammetry in alkaline medium are a quiet time of 5 seconds, a scan rate of 0.02 V s^{-1} with a sensitivity of 1 x 10^{-3} for 3 cycles, the initial potential must be determined using the OCP test and, due to the small differences among the carbon electrodes, all tests started at -0.1V in the first run. According to the IUPAC convention, the anodic current is represented as positive. A wide potential window is use to analyze the reactions occurring in the test, which goes from -0.5 V to 1 V. In addition, shorter windows having in consideration the resulting peaks are taken to confirm the reactions

occurring in the process. According to literature, these will be from -0.2 V to 0.6 V and from 0.2 V to 1 V. The results show the average of the cycles excluding the first one, except otherwise is specified. The graphs show current and not current density because the area of impregnation was constant in the samples.

2.1.3.3 Galvanostatic charge-discharge test

In order to evaluate the durability and stability of the cathodes throughout different cycles, a galvanostatic charge-discharge test is done. The set-up used was the same as in CV tests, using ZIVE SP2 potentiostat (WonATech Co., Ltd., Korea) with a three electrode configuration (silver/silver chloride at 3M as reference electrode and platinum as counter electrode) and sodium chloride at 0.1M as electrolyte. The general settings for this test were a charging and discharging time of 120 seconds and a rest time of 10 seconds for 5 cycles, a current range of 20 mA and a data acquisition rate of 1mV s^{-1} and 1mA. 0.16 mA, 0.2 mA, 0.24 mA, and 0.28 mA were applied to the electrode. After each test, the immersed area of the electrode in the electrolyte was measured to determine the current density.

2.2 Methods for characterization

2.2.1 Ultraviolet and visible spectroscopy

Spectroscopic measurements were conducted using a NanoDrop® ND-1000, Thermo Fisher Scientific INC (Waltham, MA, USA) spectrophotometer, with a xenon flash-lamp light source with a charge device attached for the refracted beam analysis For using the NanoDrop and analyzing the silver nanoparticles synthesized using the Frens method, the nanoparticles are resuspended in distillated water at 33 mM and 66 mM and for each measurement, 2 µL of sample is used. In the case of the silver nanoparticles synthesized using PHF as reducing agent, the resuspension is done for 5 mM of concentration.

The analysis was done in a window from 200 nm and 800 nm. The points are measured every 1 nm; however, when analyzed, the curve is smoothed and therefore the continuous line present points every 3 nm, which is the error the results will present. The absorbance at the maximum point is shown and the error presented corresponds to the biggest

difference between the absorbance measured and the absorbance in the next point. The full width at half maximum (FWHM) is calculated by measuring the difference in wavelength of the points which represent the half of the maximum absorbance value. Only one measurement was done per sample

2.2.2 X-ray photoelectron spectroscopy

The equipment used for this analysis is PerkinElmer 1500 XPS system (Hopkinton, MA, USA). As every XPS, ultra-high vacuum conditions must be achieved. For this purpose, two vacuum systems are used. The first one consists of a mechanical pump (need to find out brand and model), two turbomolecular pumps Turbo-V60 and Turbo-V70 (Varian, CA, USA) and finally an ion getter pump (Perkin Elmer XYZ).

The XPS is used for the analysis of the oxygen, carbon and silver states in the air electrodes before and after each procedure. In this sense, this characterization technique is used to analyze the CNT buckypapers, the impregnation of the silver nanoparticles synthesized by every method over them and the effect each electroanalytical method has over this samples.

The results presented will show the intensity in counts per second (CPS) and the binding energy in electron-volts (eV). First, a general scan of the whole spectrum is taken to identify the elements present in the sample, this scan is done in the range from 1100 to 0. After that, a high definition scan is done in the regions of interest, this values are shown in

Element	**Range [eV]**
Oxygen	542 to 522
Carbon	295 to 275
Silver	382 to 362
Fluorine	699 to 679

Figure 2.9. Range of high resolution scan of X-ray photoelectron spectroscopy for oxygen, carbon, silver and fluorine.

3 CHAPTER III
RESULTS AND DISCUSSION

3rd UNCONFERENCE RULE

"Whenever it starts is the right time."

- Tim O'Reilly

The results of this work show an improvement in the catalytic activity towards OER and ORR of a model air cathode is impregnated with Ag-PHF nanoparticles, as opposed to the same process with pure Ag nanoparticles, as shown in the CV tests. The XPS results show that the CNT structure helps avoiding the agglomeration of the nanoparticles when impregnated. Moreover, CV tests demonstrate a good stability and a faradaic behavior of the cathodes, which is suitable for battery applications. These results will be discussed in more detail in the following lines.

3.1 Preparation of the air cathode

The preparation of the air cathode consists of the synthesis of the catalyst selected, which is silver nanoparticles and silver nanoparticles with PHF, for their posterior impregnation over CNT buckypaper, which acts as current collector. The cathodes prepared with Ag nanoparticles showed good stability over the surface as showed by the XPS. Due to technical problems, which are explained in more detail during the chapter, XPS measurements were not done on the Ag PHF cathodes.

3.1.1 Silver nanoparticles synthesis

Nanoparticles were synthesized according to the methods specified in section Silver nanoparticles synthesis. They were characterized using visual inspection and UV-visible spectroscopy. Since these synthesis methods have been previously done in our group, a comparison between the data collected in this work and previous research was possible.

3.1.1.1 Frens method

At first sight, the solution of nanoparticles presented a yellowish-brownish color, which have been extendedly observed in the literature for silver nanoparticles (Ag NPs). This result is confirmed by the UV-vis spectrum results, which are shown in Figure 3.1 and a summary of spectrometric data is presented in Table 3.1.

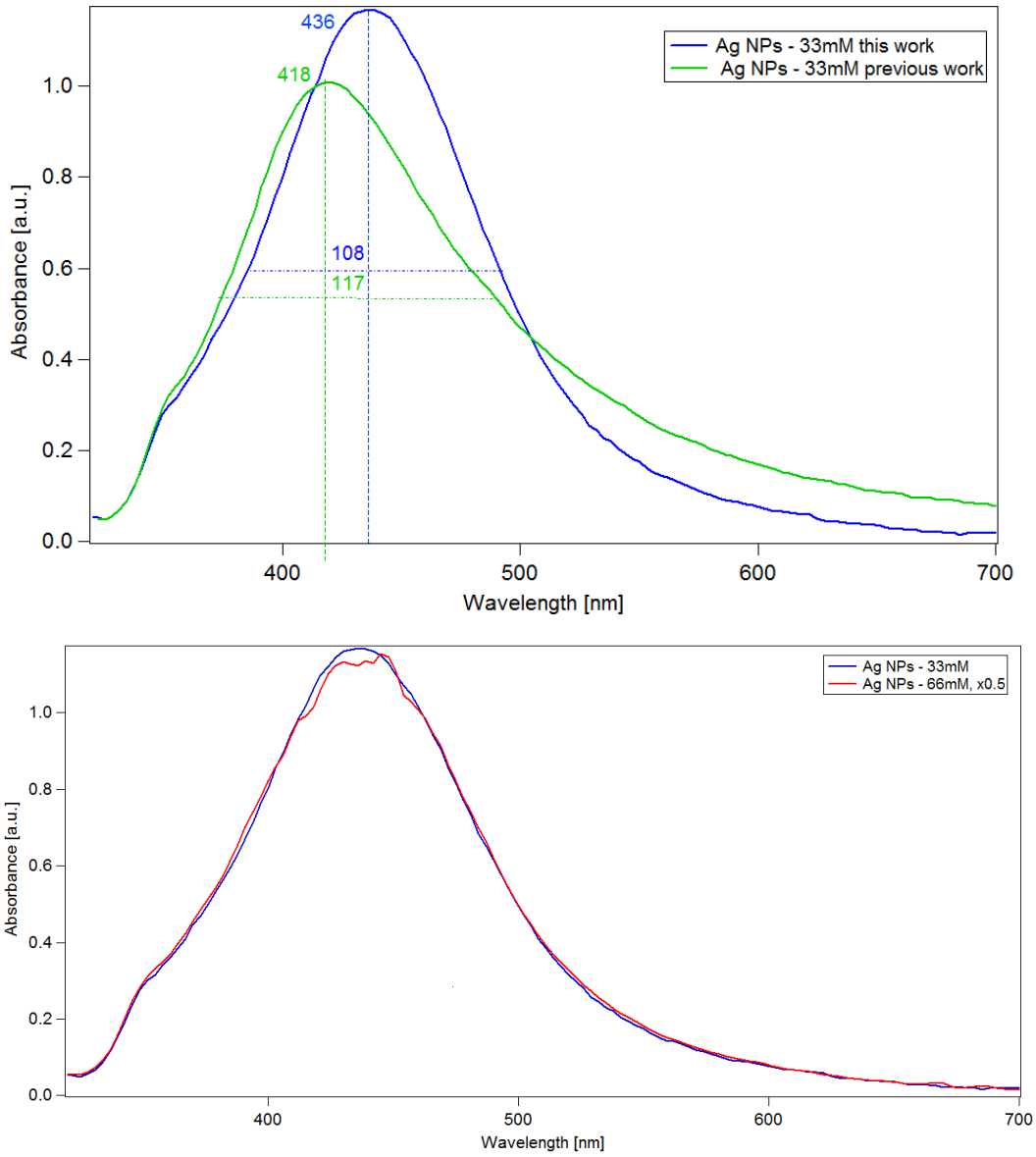

Figure 3.1. UV-vis spectrum of silver nanoparticles synthesized using Frens method. (a) shows the spectrum of a solutions from 33 mM of this work and previous work. (b) shows the spectrum of solutions from 33 mM and 66 mM multiplied by 0.5 for comparison.
Source: Own elaboration

Sample	Absorbance [u.a.]	Maximum λ [nm]	FWHM [nm]	Reference
Ag NPs at 33 mM	1.168 ± 0.005	436 ± 3	108 ± 6	This work
Ag NPs at 66 mM	1.1415 ± 0.023	442 ± 3	111 ± 6	This work
Ag NPs at 33 mM	0.95 ± 0.006	418 ± 3	117 ± 6	Previous work [66]

Table 3.1. UV-vis characterization of silver nanoparticles synthesized using Frens method.

As it can be seen in Figure 3.1 (a) and Table 3.1, silver nanoparticles at 33 mM synthesized in this work present a maximum wavelength of 436 nm, an absorbance of 1.168 u.a. and a FWHM of 108 nm. Compared to the nanoparticles previously prepared in our group [66], the nanoparticles prepared in this work show greater nanoparticles size, smaller particle size distribution and a greater intensity. The difference between both works are of 4.31% in the maximum wavelength, a 22.95% in the intensity at the maximum wavelength and 7.69% in the FWHM. Even though there is a change, this is small and thus a similar behavior between this and previous work is expected.

On the other hand, Figure 3.1 (b) shows the spectrum in two different concentrations, 33 mM and 66 mM, which were synthesized to test two different nanoparticle loadings on the carbon electrode. It will be shown that the solution 66 mM produce better electrodes, more effective for the results in CV and charge-discharge test. As it can be seen, samples resuspended at 33mM and 66 mM with distillated water present the same behavior. To help its visualization, the spectrum of 66 mM is plot multiplying the data by 0.5, since the concentration is the double of the one use for comparison with previous work. Finally, the stability of the silver nanoparticles in colloids of DI and IPA was tested with a measurement 5 days after the colloid was formed and are shown in Figure 3.2. It is important to mention that the impregnations were always done the same day in which the colloid in DI and IPA was prepared. A summary of spectrometric data is presented in Table 3.2.

Sample	Absorbance [u.a.]	Maximum λ [nm]	FWHM [nm]
Ag NPs at 33 mM in DI	1.1667 ± 0.0019	436 ± 3	108 ± 6
Ag NPs at 33 mM in DI with IPA	1.0105 ± 0.0035	445 ± 3	120 ± 6
Ag NPs at 66 mM in DI	2.2686 ± 0.0238	439 ± 3	114 ± 6
Ag NPs at 66 mM in DI with IPA	2.10933 ± 0.0161	445 ± 3	117 ± 6

Table 3.2. UV-vis characterization of silver nanoparticles synthesized using Frens method in colloids of distillated water and distillated water with isopropyl alcohol.

As it can be seen, the difference between the nanoparticles synthesized in both solvents is rather small. For the concentration of 66 mM the difference in the maximum wavelength is 6 nm, with a difference in intensity ofaround 0.16 a.u. In the case of the colloid at 33 mM, the difference in the maximum wavelength is 9 nm and the difference in the absorbance is around 0.15 a.u. This represents a small difference, and along with the results of the graphs of colloids at 66 mM, a good stability in IPA is concluded.

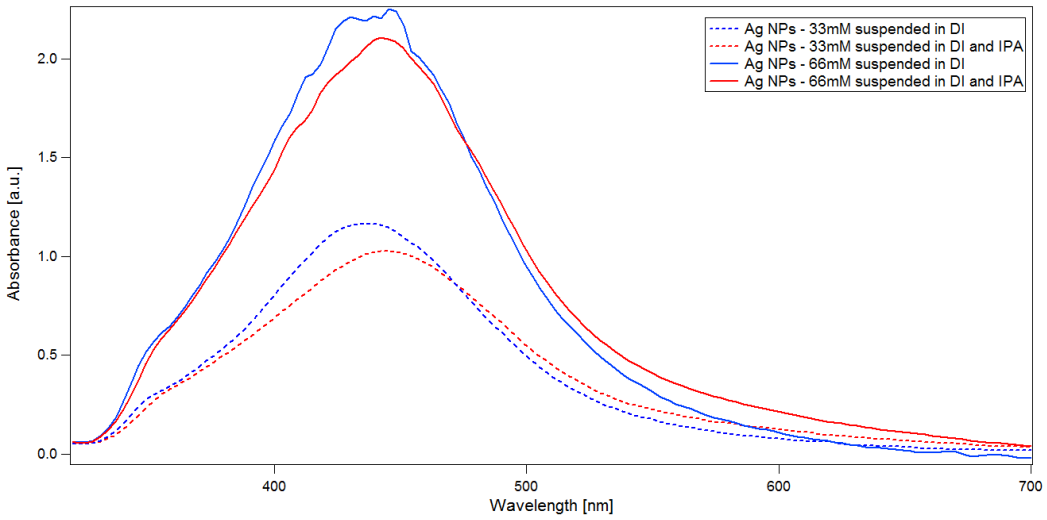

Figure 3.2. UV-vis spectrum of silver nanoparticles synthesized using Frens method in colloids of distillated water and distillated water with isopropyl alcohol
Source: Own elaboration

The silver nanoparticles capped with citrate have been previously studied, therefore, a reference on the size of the nanoparticles based on UV-vis has been previously reported [80]. That previous study is employed to determine the approximate size of the silver nanoparticles synthesized in the present study. The maximum wavelength for the sample at 33 mM is 436 nm, according to this reference, this size corresponds to a diameter of particle between 60 and 70 nm. In the case of the sample at 66 mM, the maximum wavelength is 442, which according to D. Paramelle, *et al.*, corresponds to the same range of diameter size. The referenced work has a diameter range of 40 nm to 50 nm.

Therefore, the success synthesis of silver nanoparticles using the Frens method previously done at UTEC laboratories was accomplished. These silver nanoparticles have a size range of 60 nm to 70 nm, which can be clearly seen using UV-vis, and are stable in IPA and DI solutions.

3.1.1.2 Synthetic method using PHF as reducing agent

The visual inspection shows a difference in the excess of PHF at the end of the centrifugation using DI. Since the PHF solution has a brownish color, it is assumed from Figure 3.3 that sample 3 has a higher excess of PHF, which resulted in the yellowish color of the solution; in contrast, sample 1 has a lower excess of PHF, which resulted in an almost colorless solution. As a result, the silver particles have different behaviors that will be discussed in the electroanalytical tests section. From now on, these three samples will be named as AgPHF3, AgPHF2, AgPHF1, in descending order or color intensity.

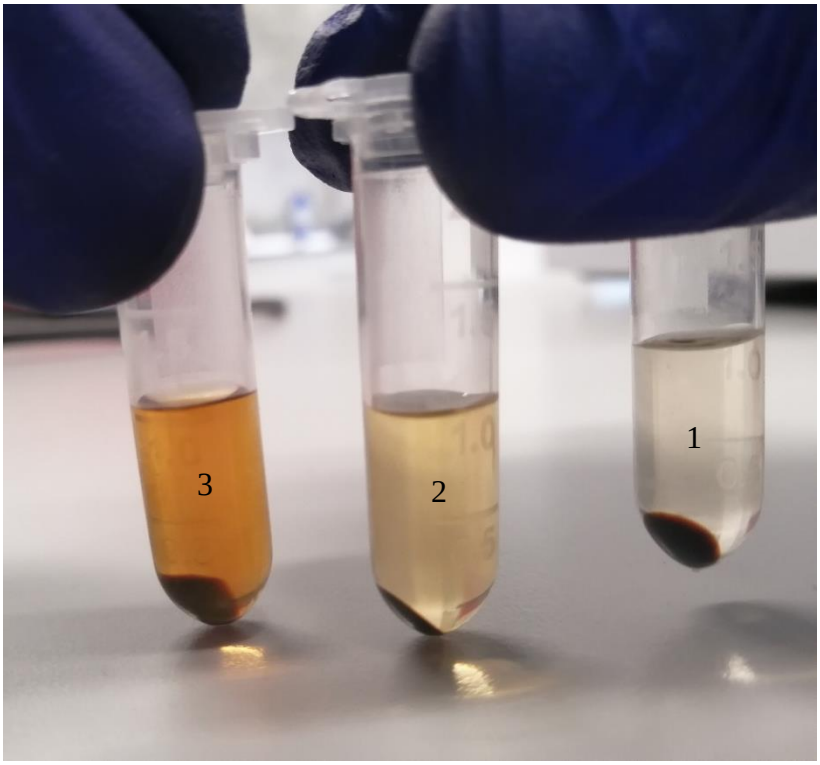

Figure 3.3. Silver particles with PHF after centrifugation using PI. 1, 2 and 3 were done with the same butch but tuned to have different colors because of the different fraction of PHF that was successfully capped the Ag nanoparticles, being 3 the one with less and 1 with less.
Source: Own elaboration

The Figure 3.4 shows the UV-vis spectrum of the synthesized particles, as can be seen, no particle in the nanoscale was observed. Since the PHF solution has a brownish color,

there cannot be a visual confirmation of the presence of Ag nanoparticles. Despite the coloration of the solution, there is no UV-vis confirmation of the presence of Ag nanoparticles, this could be due to an interference of the capped PHF. The presence of silver can be determined by the electroanalytical tests and its oxidation state, by XPS.

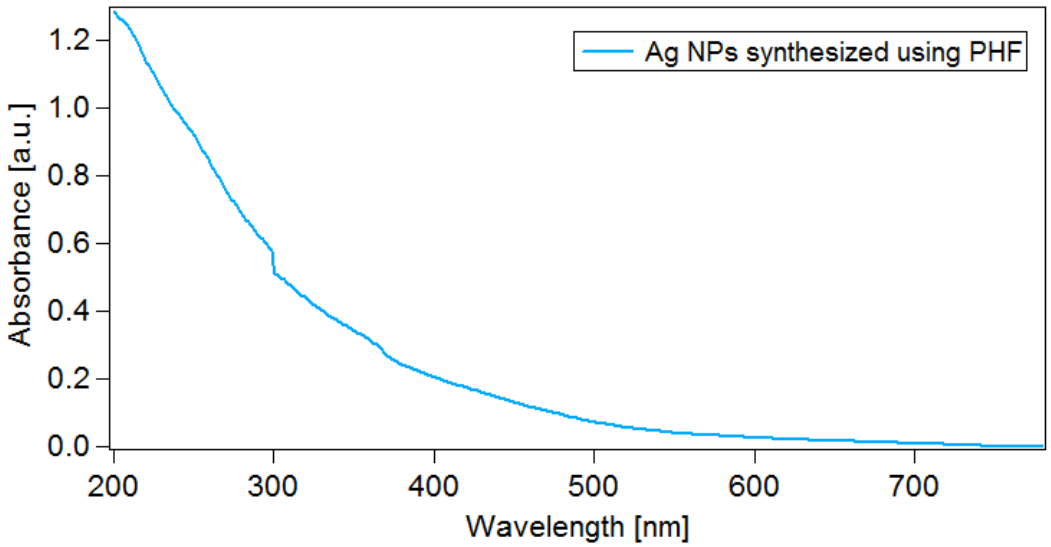

Figure 3.4. UV-vis spectrum of silver particles synthesized using PHF as reducing agent.
Source: Own elaboration

3.1.2 Impregnation of silver nanoparticles over buckypapers through ink evaporation

The success of the impregnation of silver nanoparticles over CNT buckypapers is evaluated using XPS, which shows the elements present on the surface and the oxidation states of each one of them. The analysis is done before impregnation, after washing and after electroanalytical tests are performed, to see the effectiveness of the different impregnation process and the effect of the electroanalytical tests performed. The results also include an estimation of the loading of silver per unit area.

The XPS spectra of the CNT buckypaper before and after Ag NPs impregnation show the presence of silver in the latter case (Figure 3.5.a). This means that there is a presence of silver in the CNT buckypaper after impregnated. Figure 3.5 (b) presents the spectrum in a short range to appreciate better the characteristics peaks of silver. The peak at 373.8 eV

corresponds to the binding energy of Ag $3d_{3/2}$ and the one at 367.8 eV, to Ag $3d_{5/2}$. These bindings energies are in accordance with previously reported values for bulk and big silver nanoparticles [84]. Higher binding energies would be expected in silver nanoparticles smaller than 10 nm [96], which is not the case of the ones synthesized in this study, as described in previous sections with the information provided by UV-vis. This impregnated CNT buckypaper was subjected to a washing process to test the resistance of the impregnation method upon the pressure of a fluid. As it can be seen in Figure 3.5 (b), the silver peak is not visible in the clean CNT sample and the peaks are almost the same before and after washing, which suggests that the impregnation is good.

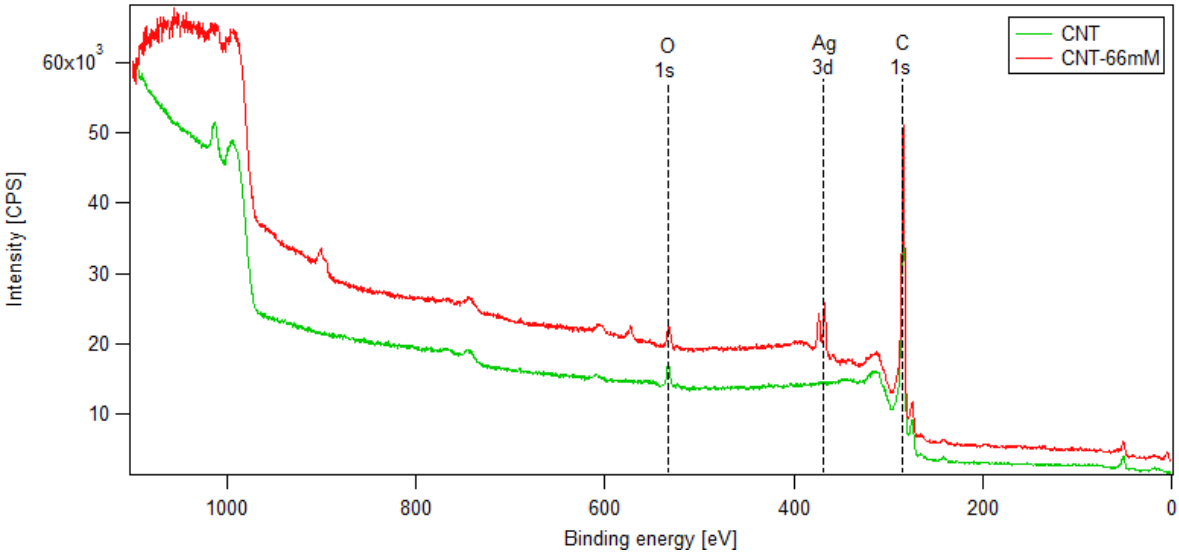

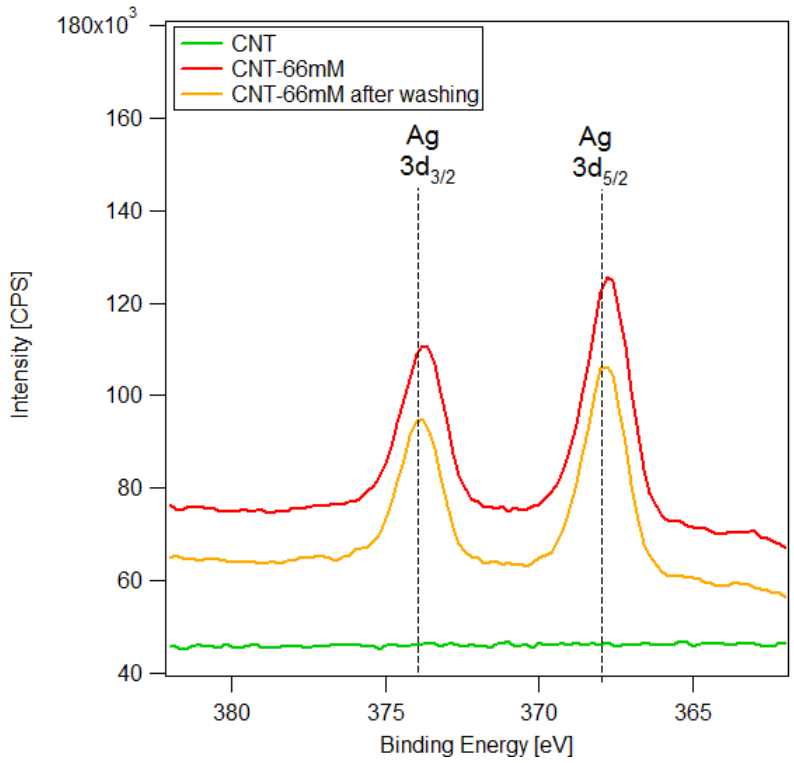

Figure 3.5. XPS spectrum from silver nanoparticles synthesized using the Frens method impregnated using ink evaporation method using a colloid at 66 mM. (a) Shows the whole spectrum of not impregnated and impregnated CNT buckypapers. (b) Shows a shorter range for the silver peak of silver nanoparticles after impregnation and after washing with distillated water.

Source: Own elaboration.

The results after the washing procedures demonstrate that the silver nanoparticles are not remove when the electrode is immersed in a liquid. XPS is also used after cyclic voltammetry procedures to see the effect of this test on the electrode. Figure 3.6 (a) shows the XPS spectrum of CNT buckypaper and CNT buckypapers impregnated with 66mM of silver nanoparticles before and after performing cyclic voltammetry test in alkaline medium. As reported before, the CNT buckypaper present peaks from oxygen and carbon. The CNT buckypaper submitted to cyclic voltammetry shows, in addition, a fluorine peak at 689.3 eV. The presence of fluorine is associated with the use of Nafion to immerse it in the electrolyte, as reported in literature [97], [98]. As can be seen, only the samples after cyclic voltammetry present this peak, because Nafion was only used on them according to the procedure presented in the previous section. The role of the fluorine in the performance of the air electrode has not been further investigated in the present study.

In addition to the CNT buckypaper peak, the spectrum of CNT buckypaper impregnated with 66mM of silver nanoparticles presents a silver peak. The difference in intensity of the silver peak before and after cyclic voltammetry test in alkaline medium is shown in Figure 3.6 (b). As can be seen, there is less amount of silver in the surface of the sample after CV test. Even though it could be hypothesized that it is caused by a loss of silver nanoparticles from the electrode, this result is not in accordance to the results presented in CV tests. Therefore, a diffusion of the silver nanoparticles into the porous structure of the carbon nanotubes could be the cause of the reduction in the intensity of this peak.

According to the explanation in the methodology section, the approximate loading of silver nanoparticles over the CNT buckypaper is of $1.36x10^{-6}$ mol of silver per 0.1 cm x 0.1 cm of CNT buckypaper.

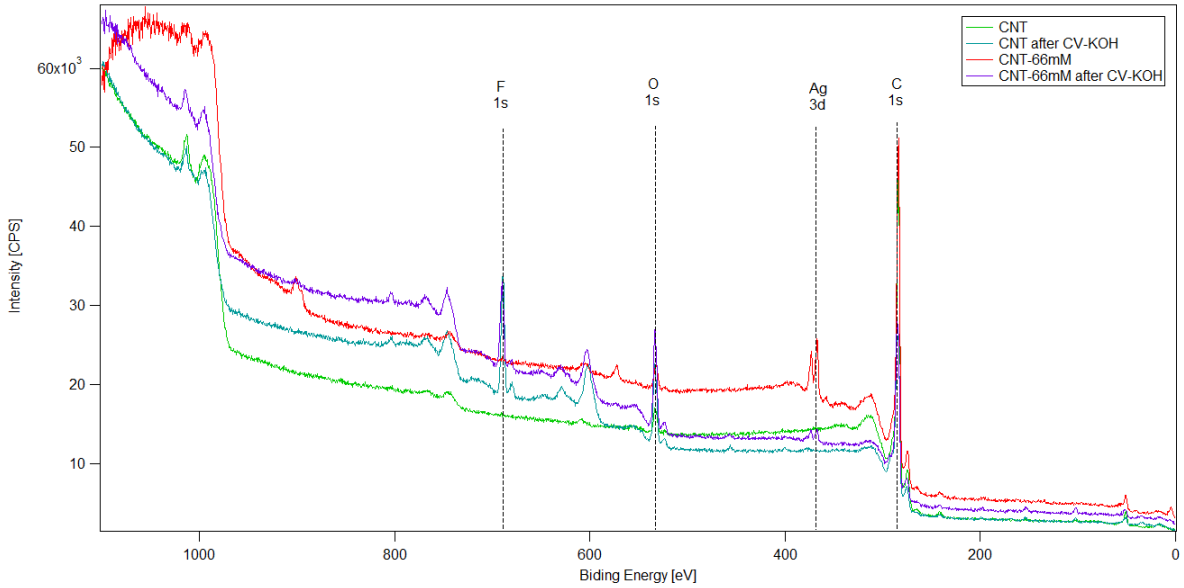

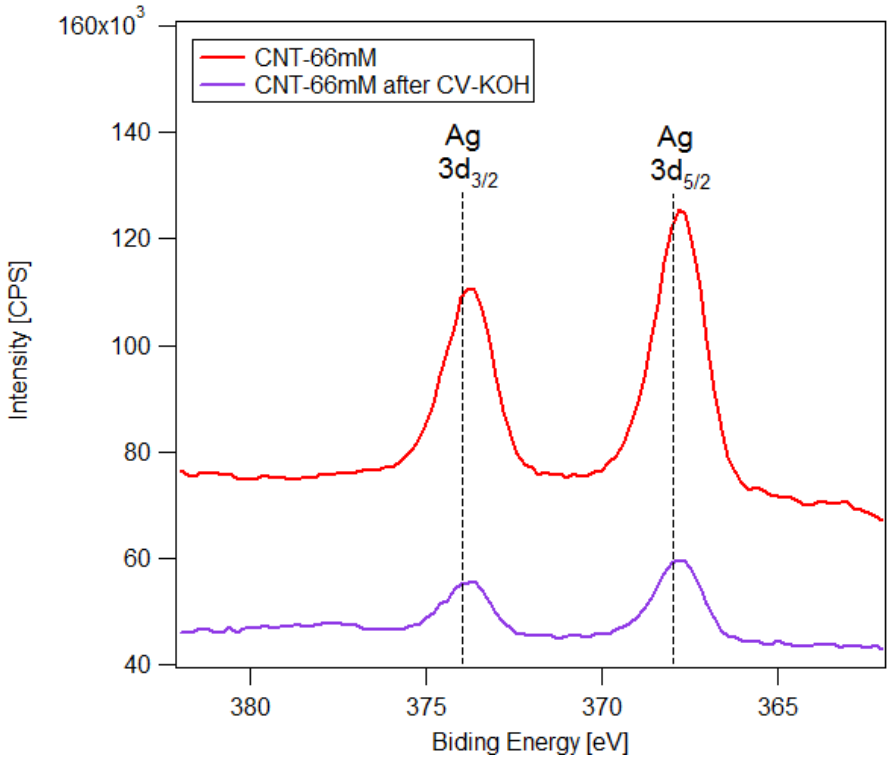

Figure 3.6. XPS spectrum from CNT buckypaper and silver nanoparticles synthesized using the Frens method impregnated over CNT buckypaper using ink evaporation method by a colloid at 66 mM before and after cyclic voltammetry in alkaline medium. (a) Shows the spectrum of CNT and CNT-66mM before and after cyclic voltammetry in alkaline medium. (b) Shows a shorter range for the lector to appreciate the silver peaks before and after cyclic voltammetry.
Source: Own elaboration.

After these results, it can be concluded that the impregnation of silver nanoparticles using the ink evaporation method was a success and that these nanoparticles are not removed by the electroanalytical tests; however, the PHF impregnation was not evaluated using this technique due to technical problems out of the control of the author. The performance of this test in CNT buckypapers is difficult because of the elimination of CNTs in ultra-high vacuum conditions and, as a result, it interfered with the electrical signal of the XPS components. The approximate loading of silver nanoparticles over the CNT buckypaper is of 1.36×10^{-6} mol of silver per 0.1 cm x 0.1 cm of CNT buckypaper.

3.2 Electroanalytical tests

The electrodes prepared are tested using cyclic voltammetry. This test allowed to determine the presence silver particles, its oxidation and reduction, as well as the reduction and evolution of oxygen. This test confirmed the presence of silver particles and, moreover, its maintenance after several cycles. Also, it confirmed the use of silver as catalyst for oxygen reduction and, in a smaller catalytic activity, for oxygen evolution. More importantly, it showed that the silver catalytic activity is enhanced with PHF. Finally, these tests determined the behavior of the electrode as a battery-like electrode and its stability over time.

3.2.1 Open circuit potential

As stated in the previous section, the OCP experiments were conducted for 120 seconds, and the initial and final value of the potential was taken to compare its variability in this time. It is better to have electrodes with stable potentials over time. The data shown in Table 3.3 indicates that the presence of silver increases the voltage of the electrode as it contributes with the conductivity. The CNT, CNT-Ag NPs, CNT-AgPHF2 electrodes are the most stable ones, since the variation is less than 1%. The CNT-AgPHF1 and CNT-AgPHF3 are not as stables as the others, but the variation in its voltage is still low. Therefore, we can conclude that the electrodes prepared are stable.

Sample	Initial potential [V]	Final potential [V]	Variation [%]
CNT	-0.0391	-0.0389	0.51%
CNT-Ag NPs	0.543	0.539	0.74%
CNT-AgPHF1	0.533	0.52	2.44%
CNT-AgPHF2	0.518	0.516	0.39%
CNT-AgPHF3	0.538	0.512	4.83%

Table 3.3. Open circuit potential results of all samples, variation shows the difference between the initial and final potential.

3.2.2 Cyclic voltammetry

First, tests were done in neutral medium and in atmospheric conditions. The results are shown in Figure 3.7. Glassy carbon represents the behavior of the work electrode and its

behavior is observed to be depreciable in comparison with the samples tested and its profile is in accordance to previous work done [99]. At first sight, they seem to have a battery-like behavior due to the sharp peaks observed in the CV, which are characteristic of a faradaic process. Capacitive behavior is also observed but is not dominant, as opposed to the behavior of a CNT buckypaper (CNT in the graph) [95], [100].

A small peak is seen near - 0.44 V, which is similar to the results previously reported [101], therefore, the presence of carbon nanotubes in a good state is confirmed. CNT-66 mM represents the results of the CNT buckypapers impregnated with silver nanoparticles synthesized by the Frens method through the ink impregnation method. The oxidation cycle presents the silver oxidation from Ag to Ag_2O, which is set at an onset potential of 0.06 V. Likewise, in the reduction peak, a reduction from Ag_2O to Ag is seen at -0.44 V with an early start at -0.03 V. This peaks and the amount of current measured is related to the amount of reactant elements. The larger peak at -0.44 V is attributed to the reduction of oxygen, which indicates that the silver nanoparticles are acting as ORR catalysts.

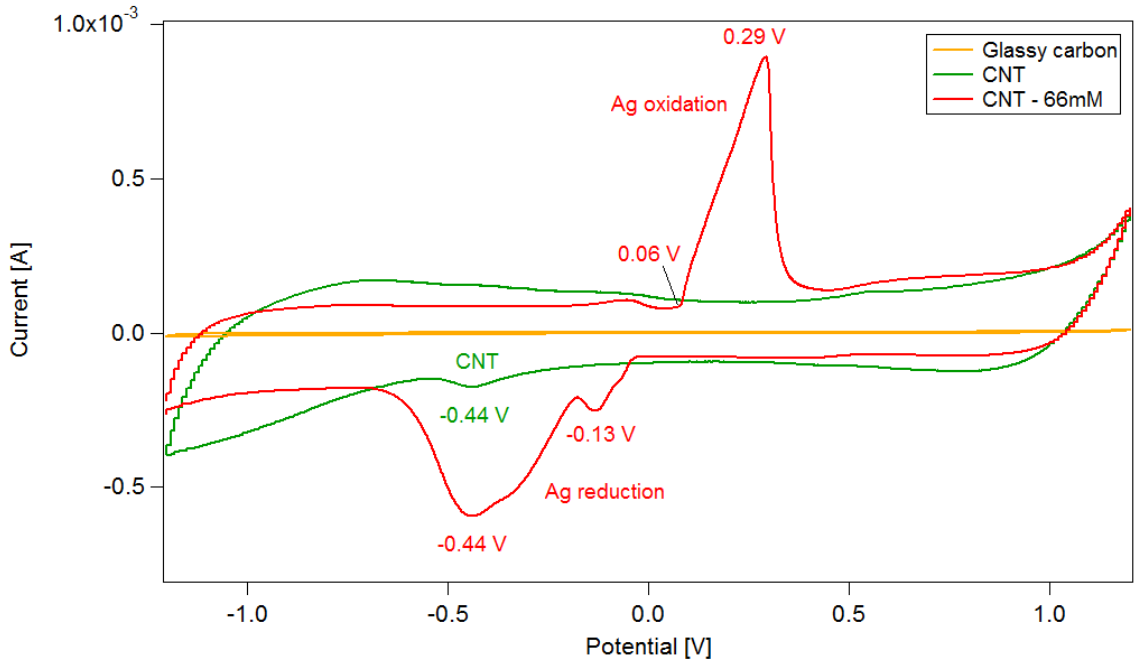

Figure 3.7. Cyclic voltammetry results in neutral medium for silver nanoparticles synthesized using the Frens method.
Source: Own elaboration.

As confirmed with the XPS results, there is a presence of metallic silver after the cyclic voltammetry tests and it is stable throughout the different cycles, as shown in Figure 3.8. The difference in the peaks between -0.45 V and -0.48 V are along the cycles are attributed to the difference in the amount of oxygen in the solution, which uncertainty may be eliminated by doing the test in O_2 saturated atmoshphere Then, it is concluded that this oxidation and reduction of the silver is a reversible reaction that might be useful as catalysts for ORR [61].

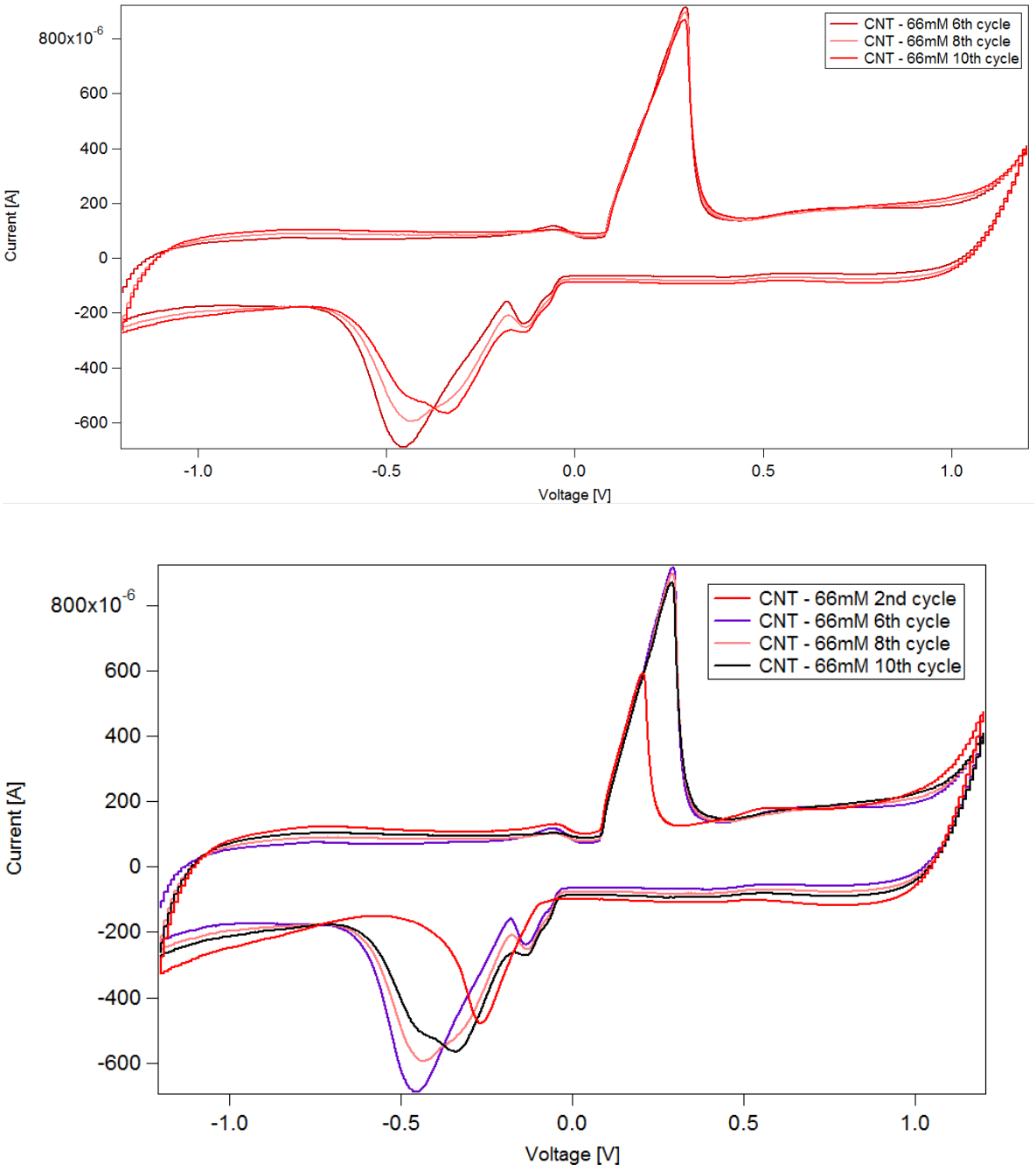

Figure 3.8. Cyclic voltammetry in neutral medium for silver nanoparticles along the different cycles.
Source: Own elaboration

The results of the cathode impregnated with silver nanoparticles are presented. Figure 3.9 (a) shows a comparison among the CNT buckypaper and the CNT buckypaper

impregnated with silver nanoparticles. As shown in neutral medium, the CNT buckypaper electrode shows a capacitive effect, while the one impregnated with silver nanoparticles shows peaks corresponding to silver reactions and oxygen reactions that where analyzed in more detail by changing the window of the cyclic voltammetry.

The first scan range starts at - 0.2 V and ends at 0.6 V, allowing an analysis on the silver peaks shown as A and B in Figure 3.9 (b). These peaks are at 0.139 V and 0.451 V using Hg/HgO as reference electrode. The first peak is attributed the reduction of Ag_2O into metallic silver, while the peak in the oxidation current is attributed to the oxidation of Ag into Ag_2O [61]. As these reactions have been widely studied, a comparison among the results presented in this work and others done before is shown in Table 3.4. As can be seen, the values presented at the table are comparable, indicating that these peaks can be attributed to the silver reactions. Moreover, as both can be seen in this short window, indicates they are the reduction and oxidation of the same element, making it a reversible cycle. These results are in accordance with the XPS results, because they indicate that the silver nanoparticles were successfully impregnated over the CNT buckypaper and their maintenance over the cycles.

A scan range between 0.2 V and 0.9 V was used to analyze the ORR and OER reactions, shown as C and D in Figure 3.9 (c). These peaks are at 0.427 V and 0.761 V using Hg/HgO as reference electrode. The first peak is attributed to the reduction of oxygen, as their potential value is comparable with other five works shown in Table 3.5. It can be concluded that the peak at 0.761 is caused by the evolution of oxygen because of its presence in this short window, indicating that it is the oxidation of the element which was reduced in the peak C. In this sense, when the scan range was decreased below 0.7 V, neither peak appeared. As a summary, the absence of peak C in Figure 3.9 (b) and of peak B in Figure 3.9 (c) indicate that signals C/D and A/B correspond to two independent reduction/oxidation pairs. The C/D peaks correspond to OER and ORR and A/B peaks correspond to silver reactions.

a)

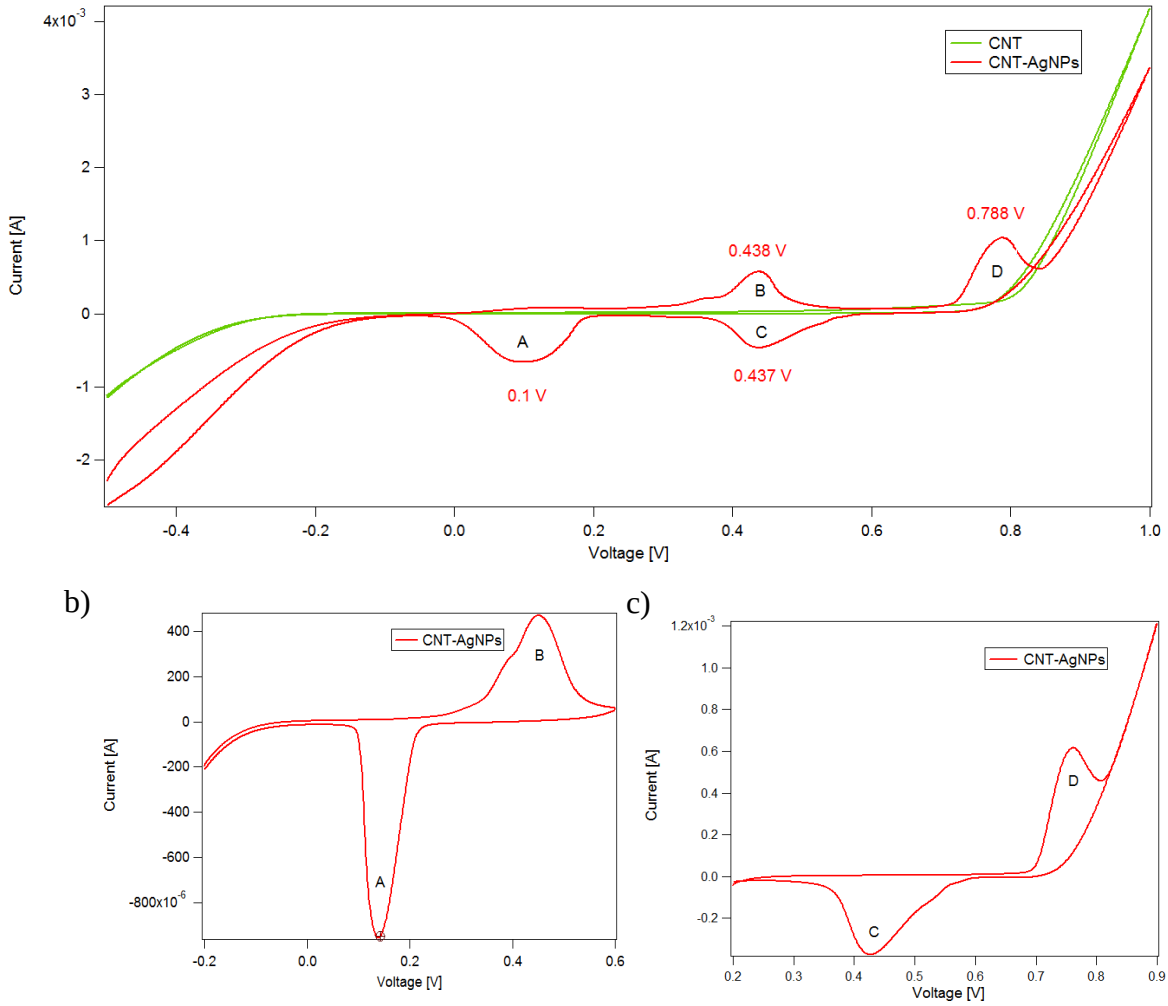

Figure 3.9. Cyclic voltammetry results in alkaline medium for (a) CNT buckypaper and silver nanoparticles synthesized using the Frens method at a width window, (b) CNT buckypaper impregnated with silver nanoparticles showing Ag peaks, and (c) CNT buckypaper impregnated with silver nanoparticles showing OER and ORR peaks. The absence of peak C in (b) and of peak B in (c) indicate that signals C/D and A/B correspond to two independent reduction/oxidation pairs.
Source: Own elaboration.

Peak	**This work**	**Ref** [62]	**Ref** [61]	**Ref** [102]	**Ref** [103]	**Ref** [104]
Ag reduction (A)	0.304 V	0.265 V	0.288 V	-0.364 V	0.490 V	0.218 V
Ag oxidation (B)	0.616 V	0.375 V	0.588 V	0.456 V	0.590 V	0.428 V

Table 3.4. Peaks attributed to silver reactions in this work and other references using as reference SHE.

Peak	**This work**	**Ref** [105]	**Ref** [106]	**Ref** [107]	**Ref** [108]
O_2 reduction (C)	0.592 V	0.75 V	0.82 V	0.333 V	0.75 V

Table 3.5. Peaks attributed to oxygen reduction reaction in this work and other references using as reference the standard hydrogen electrode.

Peak	**This work**	**Ref** [109]	**Ref** [110]	**Ref** [111]	**Ref** [112]
O_2 evolution (D)	0.761 V	0.848 V	1.715 V	1.453 V	0.915 V

Table 3.6. Peaks attributed to oxygen evolution reaction in this work and other references using as reference the standard hydrogen electrode.

As it was discussed in previous sections, the synthesis of silver nanoparticles using PHF resulted in different concentrations of PHF caping the silver particles. As a result, their electrochemical behavior is different, as can be seen in Figure 3.10. CNT-AgPHF1 and CNT-AgPHF2 presented higher currents than the CNT-AgPHF3. Also, CNT-AgPHF1 and CNT - AgPHF3, presented a well-defined peak for OER. Moreover, CNT-AgPHF1 and CNT - AgPHF2 presented two peaks instead of one between 0.2 V and 0.4 V, this could be attributed to an early reduction of oxygen, or a change in the mechanism of reaction (two reactions of two-electron pathway). It can be concluded that the sample with the best performance among the three of them is CNT-AgPHF1; which is the one with less PHF excess in the solution after centrifugation, which means is the one with more PHF caping the silver particles. This could mean that with more PHF, the silver particles are more stable.

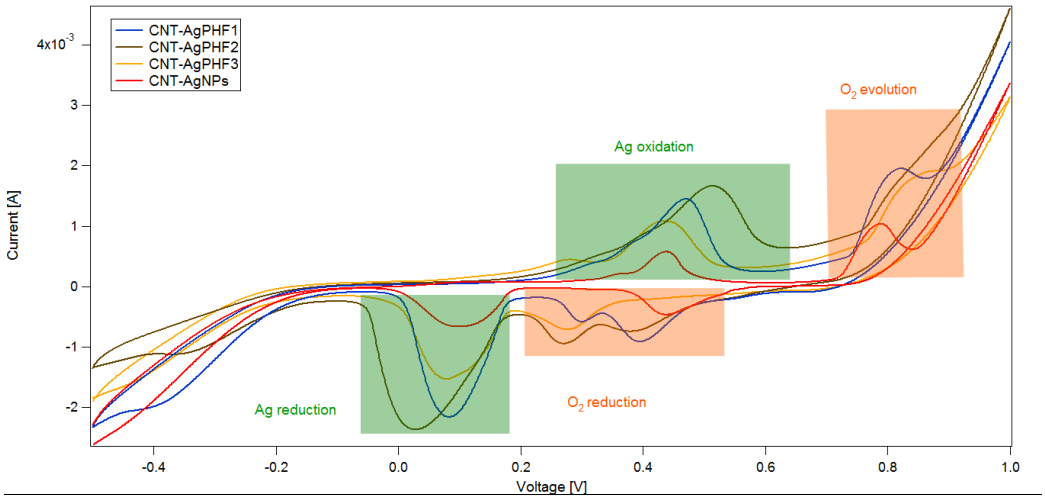

Figure 3.10. Cyclic voltammetry results in alkaline medium for the three different samples of silver particles synthesized using PHF as reducing agent. The difference between the three is the amount of capped PHF on the silver nanoparticle, as can be seen from the difference in catalytic activity.
Source: Own elaboration

To analyze the effect of PHF in the catalytic activity of silver particles towards ORR and OER, the cyclic voltammetry signals of CNT-AgNPs and CNT-AgPHF1 are compared. This sample was the one selected as was the one which presented the best performance for the cathodes with silver and PHF. As can be seen in Figure 3.11 (a), the cyclic voltammetry peaks of the cathode CNT-AgPHF1 presents higher currents for silver and oxygen peaks than CNT-AgNPs, this means that the presence of PHF increases the amount of reduced and evolved oxygen. Moreover, as can be seen in Figure 3.11 (b), the PHF by itself cannot act as catalyst for OER and ORR, therefore, it is concluded that it enhance the catalytic activity of silver, and is not a catalyst by itself. The main difference among the CNT cathode and CNT-PHF cathode is the width of the signal, the CNT-PHF cathode presents a higher current, which is attributed to the presence of the OH group in the PHF. This group has short and reversible reactions causing a quasi-capacitive effect, rather than a faradaic effect.

a)

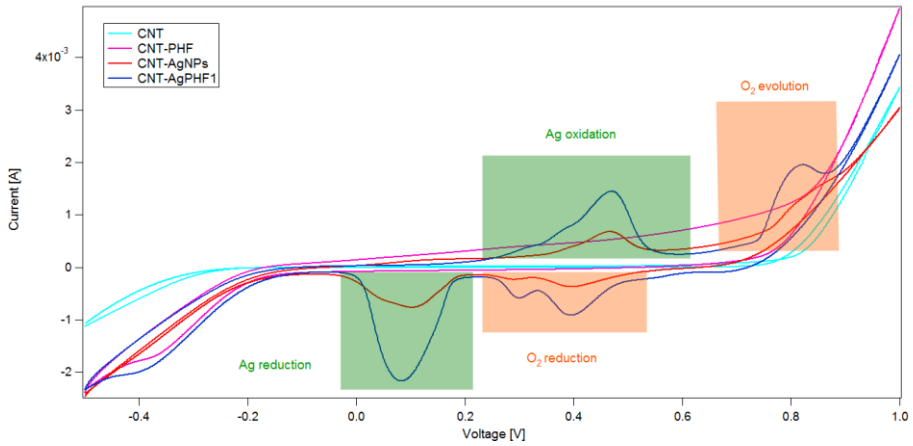

b)

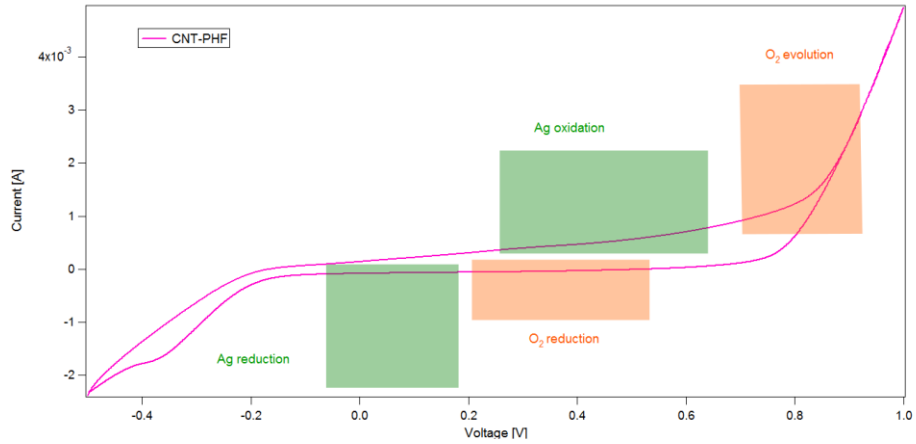

Figure 3.11. Cyclic voltammetry results in alkaline medium for (a) CNT cathode, CNT buckypaper impregnated with silver nanoparticles synthesized by Frens method, silver particles synthesized using PHF as reducing agent, and only PHF; and (b) CNT impregnated with only PHF.
Source: Own elaboration

Overall, the cyclic voltammetry showed a predominant faradaic effect of the air electrodes, which makes the Ag-PHF decorated electrodes good candidates for electrodes in batteries. Moreover, silver nanoparticles showed a good catalytic activity for OER and ORR that was enhanced by PHF because it allowed more oxygen to react. However, the stability of the CNT-AgPHF cathodes must be further evaluated, since the OCP showed a lower stability (as shown in Table 3.3) and, during the cyclic voltammetry tests, a coloration of the electrolyte was observed. The bifunctionality towards OER and ORR makes this electrode

promising for Zn-air batteries, in accordance to discussion in other investigations on the topic [113].

The onset potential is employed to compare the catalytic activity of the presented catalysts and others found in literature. In the case of ORR, the onset potential of the AgPHF catalyst is more positive than that of the silver nanoparticles. This further confirms that PHF enhanced the catalytic activity of silver nanoparticles. In comparison with other values in literature, as shown in Table 3.7, they defer by around 0.1 V, so there is more place for improvement in terms of oxygen reduction reaction. However, this synthesis methods are more complicated and require more steps than the one presented in this work.

Catalyst	**ORR onset potential [V]**	**Ref.**
Ag nanoparticles	0.69	This work
AgPHF	0.81	This work
Hierarchical nanostructured $NiCo_2O_4$	0.93	[114]
Co_3O_4 nanosheets/N- rGO	0.92	[115]
Co-N-SWCNTN	0.97	[106]

Table 3.7. Comparison among the onset potentials for oxygen reduction reaction in cyclic voltammetry in volts against standard hydrogen electrode.

In the case of OER, the onset potential of the AgPHF catalyst is lower than that of the silver nanoparticles. This further confirms previous our previous observations. On the other hand, the presented onset potentials are much lower than the ones find in literature, this could be caused by different systems used when measuring, but also by a higher catalytic activity of AgPHF.

Catalyst	OER onset potential [V]	Ref.
Ag NPs	0.57	This work
Ag PHF	0.53	This work
$PrBa_{0.5}Sr_{0.5}Co_{2-x}Fex\text{-}O_{5+d}$ Nanofibers	1.52	[116]
Fe_3C/Co(Fe)Ox@NCNT	1.5	[117]

Table 3.8. Comparison among the onset potentials for oxygen evolution reaction in cyclic voltammetry in volts against standard hydrogen electrode.

3.2.3 Galvanostatic charge-discharge test

The galvanostatic charge-discharge test was used to study the stability of the electrode throughout cycles, as well as its resistance to discharge and its behavior (capacitive or faradaic). Four different currents were applied and the area was measured afterwards as explained in the previous chapter.

Figure 3.12 shows the second cycle of the charge-discharge cycles for the three tested samples. This cycle was chosen for comparison because of the poor stability of the sample with PHF. As it can be seen, the profile of the CNT buckypaper shows that a capacitive effect is predominant, in accordance to the results from cyclic voltammetry (section Cyclic voltammetry). In the case of CNT – 66mM - PHF, due to the loss of PHF and silver nanoparticles, the graph shows the behavior of the bare CNT, and does not show the true behavior of this electrode. The graph of the electrode impregnated only with silver nanoparticles shows, first, a capacitive behavior due to the CNT and the double layer; then, there is a change in the slope which is typical of the faradaic effect, which is in accordance with the CV graphs.

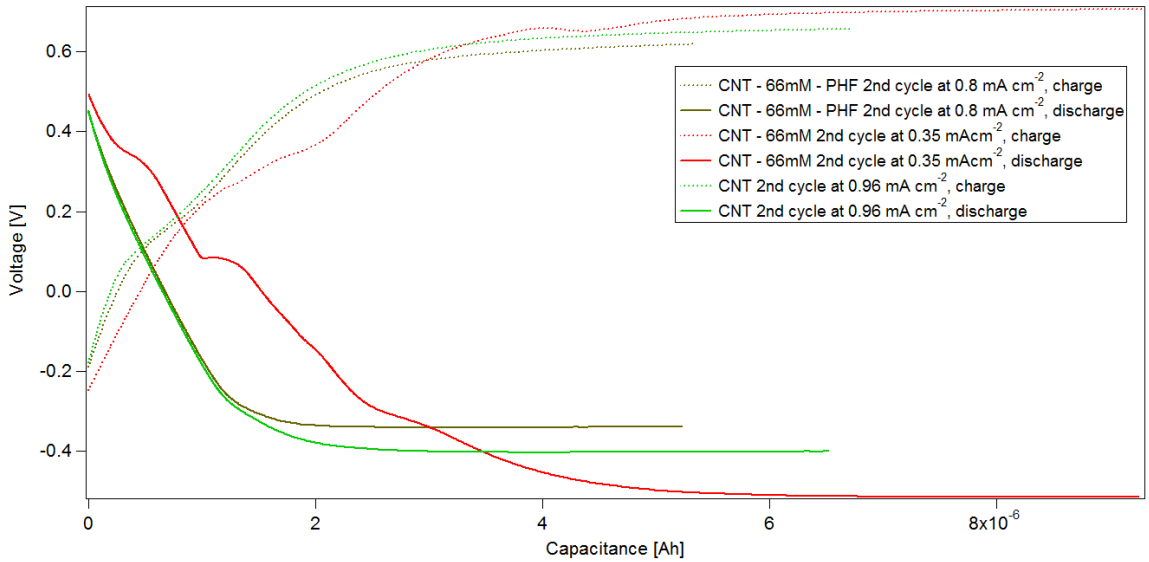

Figure 3.12. Second cycle of the galvanostatic charge-discharge test for CNT, CNT with silver nanoparticles and CNT with PHF.
Source: Own elaboration.

Figure 3.13 shows the five cycles of the charge-discharge test for CNT buckypaper and overall, a good stability is seen, especially when redox reactions are involved.. As can be seen, the voltage is being maintained through the five cycles. The tests at 0.64 mA cm^{-2} and 0.8 mA cm^{-2} show a smooth curve towards the saturation of charging; on the other hand, the test at 0.96 mA cm^{-2} and 1.12 mA cm^{-2} presents a square form which shows the saturation current of the electrode. The capacitance is shown to increase with an increase in current density. There is no resistance to discharge shown.

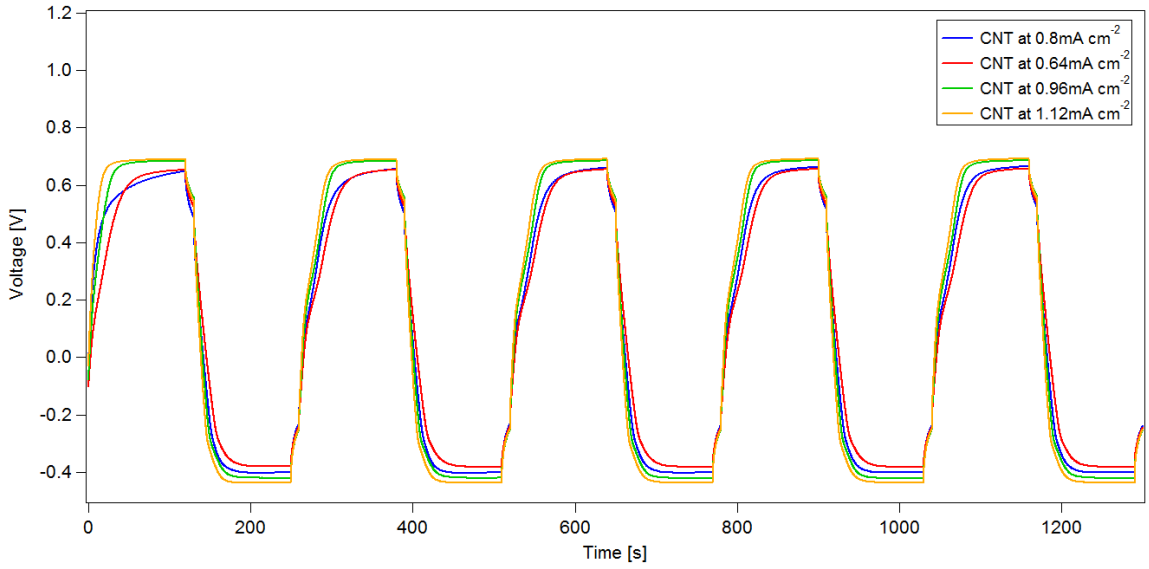

Figure 3.13. Galvanostatic charge-discharge test of CNT at 0.64 mA cm^{-2}, 0.8 mA cm^{-2}, 0.96 mA cm^{-2} and 1.12 mA cm^{-2}.
Source: Own elaboration.

In the case of the cathode with silver nanoparticles a faradaic effect is shown in the charge and discharge profiles, as can be seen in the change of slope in Figure 3.14. The saturation current was not achieved in these current densities. A deeper voltage discharge is achieved at higher current densities. Moreover, it can be seen from the lack of change in the profiles at the start of the discharge with increasing current, that there is no resistance to discharge. Overall, a good stability is seen in the five cycles.

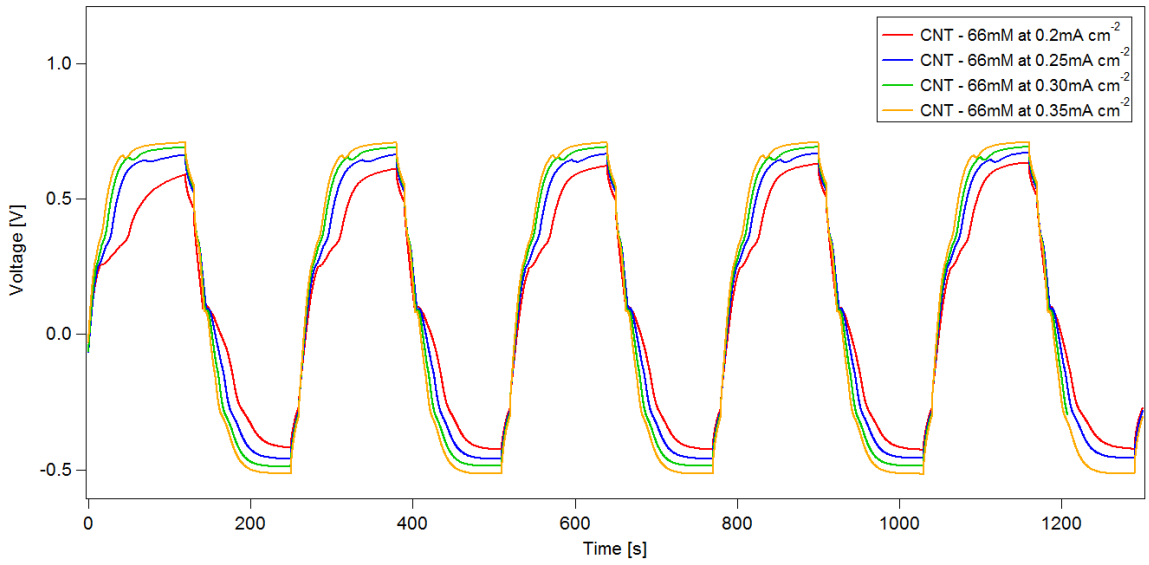

Figure 3.14. Galvanostatic charge-discharge test of CNT and silver nanoparticles synthesized using Frens method at 0.2 mA cm^{-2}, 0.25 mA cm^{-2}, 0.30 mA cm^{-2} and 0.35 mA cm^{-2}.
Source: Own elaboration.

In the case of the electrodes impregnated with silver nanoparticles and PHF, the stability of the electrode did not tolerate the five cycles, for which only the first two cycles are shown. As can be seen in Figure 3.15, there is a little faradaic effect seen, probably due to the presence of silver particles which were not removed with the PHF loss. The saturation current was almost achieved, compared to the graph of CNT, it is concluded that this cathode stores more charge. Even though the low stability was evident, there was no resistance to discharge shown during the first cycles, as can be seen from the lack of change in the profile at the start of the discharge with increasing current.

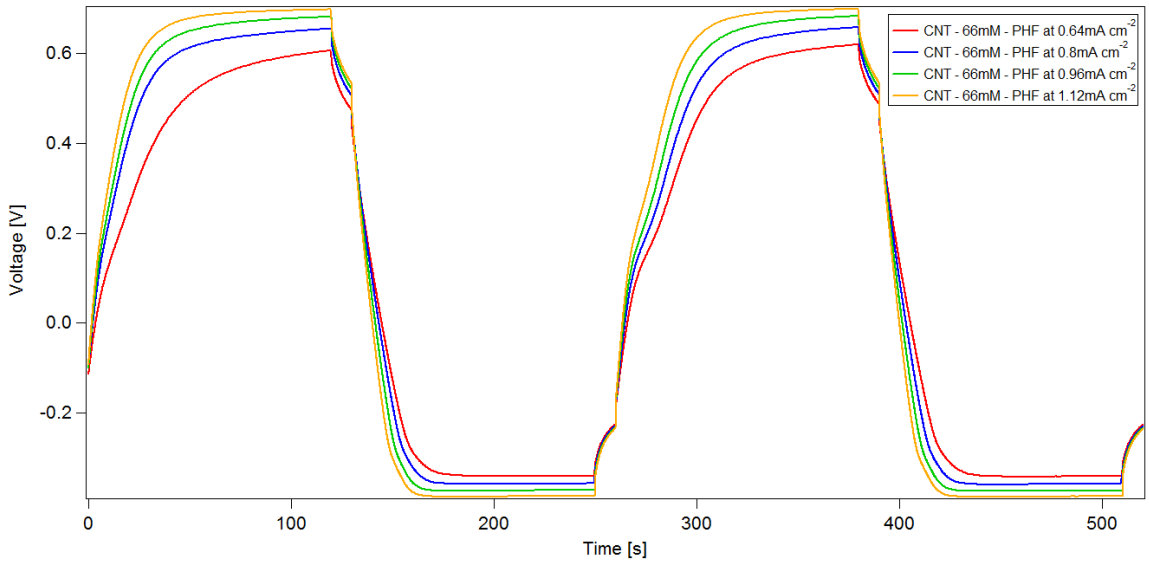

Figure 3.15. Galvanostatic charge-discharge test of CNT impregnated with silver nanoparticles synthesized using Frens method and PHF at 0.64 mA cm^{-2}, 0.8 mA cm^{-2}, 0.96 mA cm^{-2} and 0.1.12 mA cm^{-2}.
Source: Own elaboration.

Figure 3.16 shows a comparison among three electrodes at different currents. CNT-AgNPs shows a clear faradaic effect, as discussed previously, which differs from the profile of CNT. In the case of CNT-AgPHF1, the faradaic effect is not clearly seen. This could be caused by the instability of the silver nanoparticles over the electrode. At 240 µA, CNT achieves the saturation current, in contrast to the electrodes with Ag and AgPHF nanoparticles. Therefore, it is concluded that the electrodes with silver nanoparticles can store more charge than only CNT.

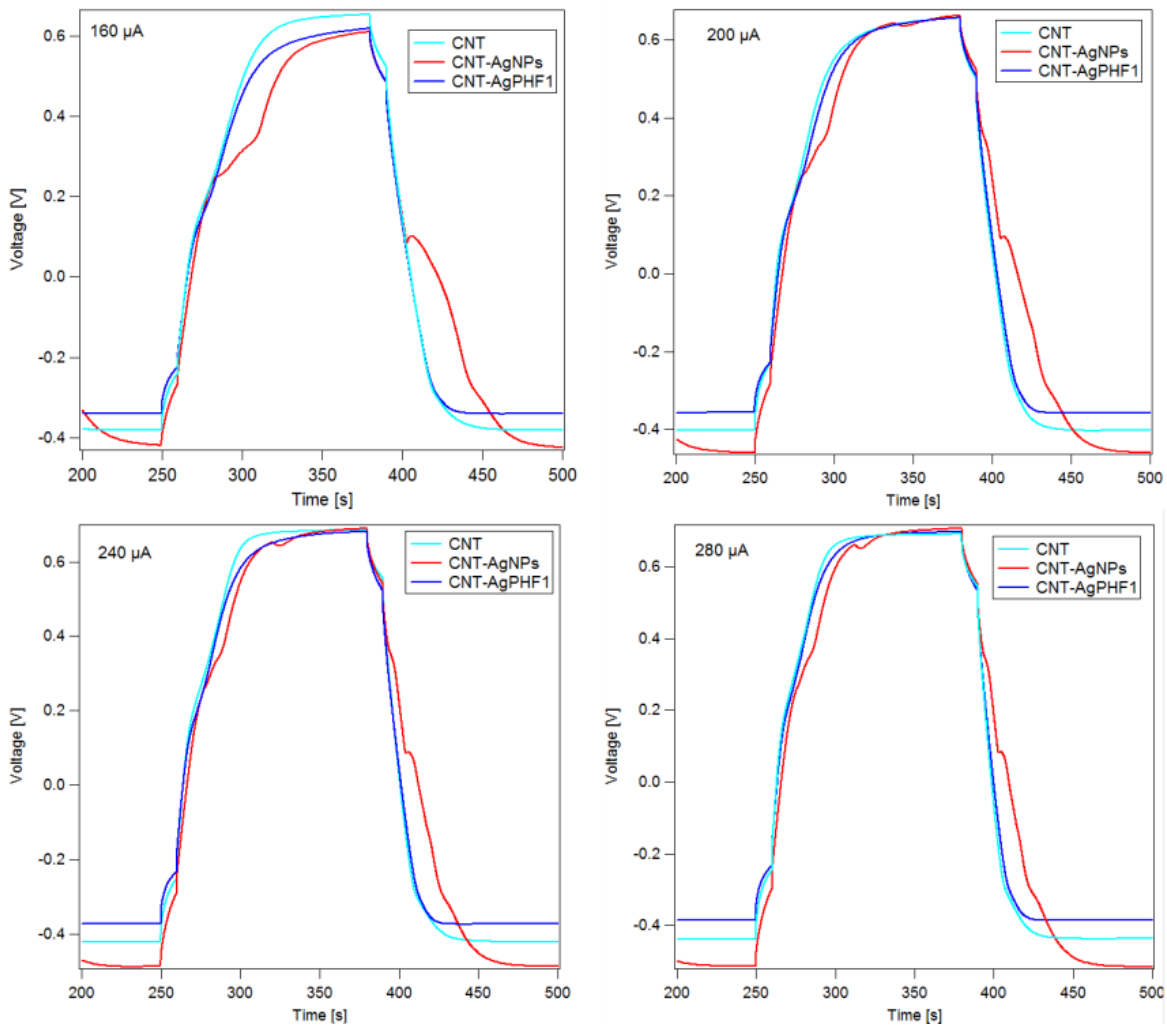

Figure 3.16. 2nd cycle of galvanostatic charge-discharge test three of CNT, CNT impregnated with silver and silver with PHF nanoparticles at .160 µA, 200 µA, 240 µA, 280 µA.
Source: Own elaboration.

The results of charge-discharge test were in accordance with the ones presented in cyclic voltammetry, the cathode presents a predominant faradaic effect, which makes this cathode appropriate for batteries and not for capacitors. Moreover, this test showed a lack of resistance to discharge from the electrodes, which means that, in a battery, the cathode will complete the charge and discharge cycle without resistance. Furthermore, the CNT electrode achieve the saturation current before the other electrodes. This means that the electrodes with silver nanoparticles are able to store more charge. However, it is shown that the cathode with

silver nanoparticles and PHF was not stable over time. This means, that the impregnation method was not suitable and further improvement is needed.

As a summary, the electroanalytical tests showed that the behavior of the cathode is appropriate for Zn-air batteries, since they have a faradaic effect and does not present resistance to discharge. Moreover, it is shown by the galvanostatic charge-discharge test that the silver nanoparticles enable the electrode to store more charge. Furthermore, the cyclic voltammetry tests demonstrated that PHF enhanced the catalytic activity of silver nanoparticles towards ORR and OER. However, the AgPHF cathode was not stable over time, therefore, another impregnation method which is suitable for the application is sought.

3.3 Flexibility test

There are many tension, torsion and compression tests which demonstrated the flexibility of different materials. Even though the evaluation of the mechanical properties is out of the scope of the present work, the flexibility of the CNT buckypaper was tested empirically. This is shown in Figure 3.17, where the CNT buckypaper was fold into half without breaking apart.

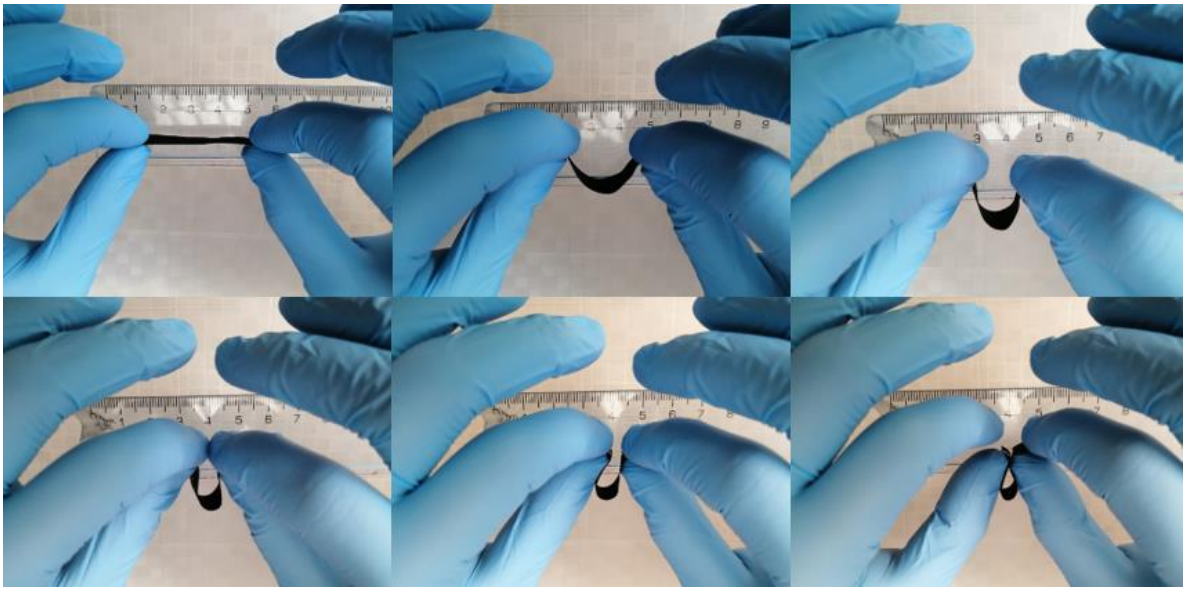

Figure 3.17. Folding of CNT buckypaper without breaking.
Source: Own elaboration.

CONCLUSIONS

"The Road goes ever on and on,
Down from the door where it began.
Now far ahead the Road has gone,
And I must follow, if I can,
Pursuing it with eager feet,
Until it joins some larger way
Where many paths and errands meet.
And whither then? I cannot say."

- *J.R.R. Tolkien*

This study developed cathodes proposed to be used in flexible Zn-air batteries, based on CNT buckypapers impregnated with silver nanoparticles and silver particles with PHF. Overall, the silver nanoparticles impregnated over the buckypapers showed to be a good catalyst for OER and ORR, as shown first in CV, and the electrode proved to be stable and did not showed resistance to discharge in galvanoststic charge-discharge tests. Moreover, the PHF enhanced the catalytic activity of the silver particles for OER and ORR. However, it was not well impregnated over the CNT buckypaper, therefore this electrode was not stable over time. These results demonstrate the good synergy between PHF and silver particles for ORR and OER, but there is a need to improve the impregnation method of PHF to the buckypaper. This bifunctionality makes these electrodes suitable for Zn-air batteries, as has been proven in other studies [13], [46], [94], [113]. In addition, the flexibility of the CNT buckypapers confers the electrode with this same property. In summary, this study contributes to the worldwide efforts of the scientific community to develop flexible, small and light batteries and may be a starting point in the use of PHF for this application by enhancing the catalytic activity of silver nanoparticles towards OER and ORR.

1. The synthesis of silver nanoparticles in the range of 60 nm to 70 nm using the Frens method with sodium citrate as reducing agent was successfully done. The silver nanoparticles sizes were determined using UV-vis.
2. The CNT buckypaper was successfully impregnated with silver particles through ink evaporation, as shown by the XPS peaks of Ag $3d_{3/2}$ and $3d_{5/2}$ before and after the washing test. The loading was done at 1.36×10^{-6} mols per 0.01 cm^2. The structure of CNT buckypapers prevents the agglomeration of silver nanoparticles.
3. Moreover, the silver nanoparticles were stable over the CNT buckypapers even after several electroanalytical tests, as all the CV results after ten cycles were the same and the five cycles of the charge-discharge tests at different current density achieved the same voltage. However, in the XPS spectrum a less amount of silver nanoparticles was found, which is assumed to be due to a diffusion phenomenon towards the porous CNT structure rather than the loss of silver nanoparticles. More tests are suggested to confirm this hypothesis.
4. The PHF and silver particles electrode was not stable over time, according to the results of OCP; CV and galvanostatic charge-discharge tests, other test like XPS need to be done to confirm this results. Furthermore, an improvement in the stability of this electrode will be done in a future work.
5. CV results showed oxidation and reduction peaks of silver, which meant not only the presence of the metal in the sample, but also the reversibility of this reaction and, therefore, its stability over several cycles. Also, OER and ORR peaks were observed. Overall, the electrode presented a faradaic behavior with a small component of capacitive behavior, typical of battery electrodes, and saturation at current densities higher than 0.96 mA cm^{-2}. More tests in O_2 and N_2 saturated atmosphere are suggested to confirm these results.
6. The presence of PHF enhanced the catalytic activity of silver particles, as shown in the higher current achieved in the CV with this cathode. Further tests should be done with a stable electrode.

7. The effect of the fluorine due to the Nafion presence on the electrodes for the electrochemical measurements, as shown in the XPS spectrum, was not evaluated, but will be done in a future work.

BIBLIOGRAPHY

[1] Statista, "Wearables sales worldwide by region 2015-2021," 2018. [Online]. Available: https://www.statista.com/statistics/490231/wearable-devices-worldwide-by-region/. [Accessed: 12-Sep-2018].

[2] J. Fu, Z. P. Cano, M. G. Park, A. Yu, M. Fowler, and Z. Chen, "Electrically Rechargeable Zinc-Air Batteries: Progress, Challenges, and Perspectives," *Adv. Mater.*, vol. 29, no. 7, p. 1604685, Feb. 2017.

[3] Q. Liu, Z. Chang, Z. Li, and X. Zhang, "Flexible Metal-Air Batteries: Progress, Challenges, and Perspectives," *Small Methods*, vol. 2, no. 2, p. 1700231, Feb. 2018.

[4] J. Chira Fernández, C. Ríos Moreno, G. Trelles Vásquez, and E. Villarreal Jaramillo, "Estimación del potencial minero metálico del Perú y su contribución económica al Estado, acumulado al 2050," Lima, 2018.

[5] U.S. Department of the Interior, "Historical Statistics for Mineral Commodities in the United States," 2017. [Online]. Available: https://minerals.usgs.gov/minerals/pubs/historical-statistics/. [Accessed: 22-Sep-2018].

[6] M. L. Söderman, D. Kushnir, and B. Sandén, "Will metal scarcity limit the use of electric vehicles?," *Syst. Perspect. Electromobility 2013*, pp. 76–89, 2013.

[7] J.-S. Lee *et al.*, "Metal-Air Batteries with High Energy Density: Li-Air versus Zn-Air," *Adv. Energy Mater.*, vol. 1, no. 1, pp. 34–50, Jan. 2011.

[8] J. Pan, Y. Y. Xu, H. Yang, Z. Dong, H. Liu, and B. Y. Xia, "Advanced Architectures and Relatives of Air Electrodes in Zn-Air Batteries," *Adv. Sci.*, vol. 5, no. 4, p. 1700691, Apr. 2018.

[9] S. Suren and S. Kheawhom, "Development of a High Energy Density Flexible Zinc-Air Battery," *J. Electrochem. Soc.*, vol. 163, no. 6, pp. 846–850, 2016.

[10] A. Sumboja, M. Lübke, Y. Wang, T. An, Y. Zong, and Z. Liu, "All-Solid-State, Foldable, and Rechargeable Zn-Air Batteries Based on Manganese Oxide Grown on Graphene-Coated Carbon Cloth Air Cathode," *Adv. Energy Mater.*, vol. 7, no. 20, p. 1700927, Oct. 2017.

[11] J. Fu *et al.*, "Flexible Rechargeable Zinc-Air Batteries through Morphological Emulation of Human Hair Array," *Adv. Mater.*, vol. 28, no. 30, pp. 6421–6428, Aug. 2016.

[12] D. U. Lee, J. Y. Choi, K. Feng, H. W. Park, and Z. Chen, "Advanced extremely durable 3D bifunctional air electrodes for rechargeable zinc-air batteries," *Adv. Energy Mater.*, vol. 4, no. 6, Apr. 2014.

[13] J. Pan *et al.*, "Recent Progress on Transition Metal Oxides as Bifunctional Catalysts for Lithium-Air and Zinc-Air Batteries," *Batter. Supercaps*, vol. 2, no. 4, pp. 336–347, Apr. 2019.

[14] X. Wu, F. Chen, Y. Jin, N. Zhang, and R. L. Johnston, "Silver–Copper Nanoalloy Catalyst Layer for Bifunctional Air Electrodes in Alkaline Media," *ACS Appl. Mater.*

Interfaces, vol. 7, no. 32, pp. 17782–17791, Aug. 2015.
[15] J. Guo, A. Hsu, D. Chu, and R. Chen, "Improving oxygen reduction reaction activities on carbon-supported Ag nanoparticles in alkaline solutions," *J. Phys. Chem. C*, vol. 114, no. 10, pp. 4324–4330, Mar. 2010.
[16] J. Guo, H. Li, H. He, D. Chu, and R. Chen, "CoPc- and CoPcF16-modified ag nanoparticles as novel catalysts with tunable oxygen reduction activity in alkaline media," *J. Phys. Chem. C*, vol. 115, no. 17, pp. 8494–8502, May 2011.
[17] Y. Jin, F. Chen, Y. Lei, and X. Wu, "A Silver-Copper Alloy as an Oxygen Reduction Electrocatalyst for an Advanced Zinc-Air Battery," *ChemCatChem*, vol. 7, no. 15, pp. 2377–2383, Aug. 2015.
[18] A. Pinedo, B. Alcázar, J. C. Rodriguez-Reyes, A. Pinedo-Flores, and B. Alcázar°, "Protocol for the synthesis of silver nanoparticles using sodium citrate and sodium borohydride as reducing agents," 2018.
[19] M. Gakiya-Teruya, L. Palomino-Marcelo, and J. C. Rodriguez-Reyes, "Synthesis of Highly Concentrated Suspensions of Silver Nanoparticles by Two Versions of the Chemical Reduction Method," *Methods Protoc.*, vol. 2, no. 1, p. 3, Dec. 2018.
[20] R. Das, "Three Hot Trends in Printed and Flexible Electronics," 2017.
[21] H. C. Koydemir and A. Ozcan, "Wearable and Implantable Sensors for Biomedical Applications," *Annu. Rev. Anal. Chem.*, vol. 11, no. 1, pp. 127–146, Jun. 2018.
[22] Y. Khan, A. E. Ostfeld, C. M. Lochner, A. Pierre, and A. C. Arias, "Monitoring of Vital Signs with Flexible and Wearable Medical Devices," *Adv. Mater.*, vol. 28, no. 22, pp. 4373–4395, Jun. 2016.
[23] H. Zhu, Y. Shen, Y. Li, and J. Tang, "Recent advances in flexible and wearable organic optoelectronic devices," *J. Semicond.*, vol. 39, no. 1, p. 011011, Jan. 2018.
[24] D. Ross, M. P. Nemitz, and A. A. Stokes, "Controlling and Simulating Soft Robotic Systems: Insights from a Thermodynamic Perspective."
[25] R. Van Noorden, "The rechargeable revolution: A better battery," *Nature*, vol. 507, no. 7490, pp. 26–28, 2014.
[26] J. W. Choi and D. Aurbach, "Promise and reality of post-lithium-ion batteries with high energy densities," *Nature Reviews Materials*, vol. 1, no. 4. Nature Publishing Group, pp. 1–16, 31-Mar-2016.
[27] F. Rojas, V. Garay, and J. Cantallopts, "Mercado internacional del litio y su potencial en Chile," 2018.
[28] D. Desormeaux, "Litio: Mercado y Regulación en Chile Daniela Desormeaux-Socia y Gerente General-signumBOX Inteligencia de Mercados EXPOMIN," 2018.
[29] N. J. Tro, *Chemistry : a molecular approach*, 3rd ed. Pearson, 2013.
[30] C. M. A. Brett, "Standard Electrode Potentials and Application to Characterization of Corrosion Phenomena," in *Encyclopedia of Interfacial Chemistry*, Elsevier, 2018, pp. 511–516.
[31] T. L. Brown, H. E. Lemay, B. E. Bursten, C. J. Murphy, and P. M. Woodward, *Chemistry-The-Central-Science-in-SI-Units-global-edition-14th-ed-*. 2017.
[32] V. S. Bagotsky and A. N. Frumkin, *Fundamentals of Electrochemistry*. 2006.
[33] OpenStax, "Chemistry." .
[34] T. Stoebe, "Classification of Cells or Batteries," *University of Washington*, 2000. [Online]. Available:

https://depts.washington.edu/matseed/batteries/MSE/classification.html. [Accessed: 27-Nov-2018].
[35] Battery Association of Japan, "BAJ Website | Monthly battery sales statistics," 2018. [Online]. Available: http://www.baj.or.jp/e/statistics/02.php. [Accessed: 27-Nov-2018].
[36] EPEC, "Primary and Rechargeable Battery Chemistries with Energy Density," 2018. [Online]. Available: https://www.epectec.com/batteries/chemistry/. [Accessed: 28-Nov-2018].
[37] T. B. Reddy and D. Linden, *Linden's handbook of batteries*. McGraw-Hill, 2011.
[38] FuelCellsEtc, "Commercial Fuel Cell Components Gas Diffusion Layer (GDL)," 2017.
[39] L. Li, Z. Chang, and X.-B. Zhang, "Recent Progress on the Development of Metal-Air Batteries," *Adv. Sustain. Syst.*, vol. 1, no. 10, p. 1700036, Oct. 2017.
[40] K. Wongrujipairoj, L. Poolnapol, A. Arpornwichanop, S. Suren, and S. Kheawhom, "Suppression of zinc anode corrosion for printed flexible zinc-air battery," *Phys. status solidi*, vol. 254, no. 2, p. 1600442, Feb. 2017.
[41] R. Putt, N. Naimer, B. Koretz, and T. Atwater, "Advanced Zinc-Air Primary Batteries," in *39th Power Sources Conference*, 2000.
[42] M. G. Park, D. U. Lee, M. H. Seo, Z. P. Cano, and Z. Chen, "3D Ordered Mesoporous Bifunctional Oxygen Catalyst for Electrically Rechargeable Zinc-Air Batteries," *Small*, vol. 12, no. 20, pp. 2707–2714, May 2016.
[43] D. U. Lee, M. G. Park, H. W. Park, M. H. Seo, X. Wang, and Z. Chen, "Highly Active and Durable Nanocrystal-Decorated Bifunctional Electrocatalyst for Rechargeable Zinc-Air Batteries," *ChemSusChem*, vol. 8, no. 18, pp. 3129–3138, Sep. 2015.
[44] W. E. Org, W. Hong, H. Li, and B. Wang, "ELECTROCHEMICAL SCIENCE A Horizontal Three-Electrode Structure for Zinc-Air Batteries with Long-Term Cycle Life and High Performance," *Int. J. Electrochem. Sci*, vol. 11, pp. 3843–3851, 2016.
[45] J. Fu *et al.*, "Defect Engineering of Chalcogen-Tailored Oxygen Electrocatalysts for Rechargeable Quasi-Solid-State Zinc-Air Batteries," *Adv. Mater.*, vol. 29, no. 35, p. 1702526, Sep. 2017.
[46] Q. Liu, Y. Wang, L. Dai, and J. Yao, "Scalable Fabrication of Nanoporous Carbon Fiber Films as Bifunctional Catalytic Electrodes for Flexible Zn-Air Batteries," *Adv. Mater.*, vol. 28, no. 15, pp. 3000–3006, Apr. 2016.
[47] S. Li, Z. P. Guo, C. Y. Wang, G. G. Wallace, and H. K. Liu, "Flexible cellulose based polypyrrole–multiwalled carbon nanotube films for bio-compatible zinc batteries activated by simulated body fluids," *J. Mater. Chem. A*, vol. 1, no. 45, p. 14300, Oct. 2013.
[48] J. Park, M. Park, G. Nam, J. Lee, and J. Cho, "All-Solid-State Cable-Type Flexible Zinc-Air Battery," *Adv. Mater.*, vol. 27, no. 8, pp. 1396–1401, Feb. 2015.
[49] C. C. Yang and S. J. Lin, "Improvement of high-rate capability of alkaline Zn-MnO2 battery," *J. Power Sources*, vol. 112, no. 1, pp. 174–183, Oct. 2002.
[50] H. Ma, C. Li, Y. Su, and J. Chen, "Studies on the vapour-transport synthesis and electrochemical properties of zinc micro-, meso- and nanoscale structures," *J. Mater. Chem.*, vol. 17, no. 7, pp. 684–691, Feb. 2007.
[51] L. F. Urry, "Zinc anode for an electochemical cell," 2000.

[52] N. C. Tang, "ELECTRODE FOR AN ELECTROCHEMICAL CELL INCLUDING RIBBONS," 2001.
[53] X. G. Zhang, "Fibrous zinc anodes for high power batteries," *J. Power Sources*, vol. 163, no. 1 SPEC. ISS., pp. 591–597, Dec. 2006.
[54] J.-F. Drillet *et al.*, " Development of a Novel Zinc/Air Fuel Cell with a Zn Foam Anode, a PVA/KOH Membrane and a MnO 2 /SiOC-Based Air Cathode ," *ECS Trans.*, vol. 28, no. 32, pp. 13–24, Dec. 2019.
[55] Y. Li and H. Dai, "Recent advances in zinc–air batteries," *Chem. Soc. Rev.*, vol. 43, no. 15, pp. 5257–5275, Jul. 2014.
[56] K. Wang *et al.*, "Dendrite growth in the recharging process of zinc–air batteries," *J. Mater. Chem. A*, vol. 3, no. 45, pp. 22648–22655, Nov. 2015.
[57] H. Yang, H. Zhang, X. Wang, J. Wang, X. Meng, and Z. Zhou, "Calcium Zincate Synthesized by Ballmilling as a Negative Material for Secondary Alkaline Batteries," *J. Electrochem. Soc.*, vol. 151, no. 12, p. A2126, Dec. 2004.
[58] J. Huang, Z. Yang, R. Wang, Z. Zhang, Z. Feng, and X. Xie, "Zn–Al layered double oxides as high-performance anode materials for zinc-based secondary battery," *J. Mater. Chem. A*, vol. 3, no. 14, pp. 7429–7436, Mar. 2015.
[59] D. U. Lee, J. Fu, M. G. Park, H. Liu, A. Ghorbani Kashkooli, and Z. Chen, "Self-Assembled NiO/Ni(OH) 2 Nanoflakes as Active Material for High-Power and High-Energy Hybrid Rechargeable Battery," *Nano Lett.*, vol. 16, no. 3, pp. 1794–1802, Mar. 2016.
[60] Z. Ma *et al.*, "Degradation characteristics of air cathode in zinc air fuel cells," *J. Power Sources*, vol. 274, pp. 56–64, Jan. 2015.
[61] C. Lai, P. Kolla, Y. Zhao, H. Fong, and A. L. Smirnova, "Lignin-derived electrospun carbon nanofiber mats with supercritically deposited Ag nanoparticles for oxygen reduction reaction in alkaline fuel cells," *Electrochim. Acta*, vol. 130, pp. 431–438, Jun. 2014.
[62] H. Erikson, A. Sarapuu, and K. Tammeveski, "Oxygen Reduction Reaction on Silver Catalysts in Alkaline Media: a Minireview," *ChemElectroChem*, vol. 6, no. 1, pp. 73–86, Jan. 2019.
[63] T. M. D. Dang, T. T. T. Le, E. Fribourg-Blanc, and M. C. Dang, "Influence of surfactant on the preparation of silver nanoparticles by polyol method," *Adv. Nat. Sci. Nanosci. Nanotechnol.*, vol. 3, no. 3, Sep. 2012.
[64] E. M. Egorova, A. A. Kubatiev, and V. I. Schvets, *Biological effects of metal nanoparticles*. Springer International Publishing, 2016.
[65] Y. Wang and Y. Xia, "Bottom-up and top-down approaches to the synthesis of monodispersed spherical colloids of low melting-point metals," *Nano Lett.*, vol. 4, no. 10, pp. 2047–2050, Oct. 2004.
[66] P. M. Luis Alberto, "Evaluación de la interacción de nanopartículas de plata con factor de crecimiento epidermal para su uso potencial en sistemas que mejoren la regeneración de tejidos epiteliales," Universidad Nacional Mayor de San Marcos, 2019.
[67] Z. Khan, S. A. Al-Thabaiti, A. Y. Obaid, and A. O. Al-Youbi, "Preparation and characterization of silver nanoparticles by chemical reduction method," *Colloids Surfaces B Biointerfaces*, vol. 82, no. 2, pp. 513–517, Feb. 2011.

[68] N. G. Bastús, F. Merkoçi, J. Piella, and V. Puntes, “Synthesis of Highly Monodisperse Citrate-Stabilized Silver Nanoparticles of up to 200 nm: Kinetic Control and Catalytic Properties,” *Chem. Mater.*, vol. 26, no. 9, pp. 2836–2846, May 2014.
[69] K. Mavani, “Synthesis of Silver Nanoparticles by using Sodium Borohydride as a Reducing Agent.”
[70] L. Kvítek *et al.*, “Effect of surfactants and polymers on stability and antibacterial activity of silver nanoparticles (NPs),” *J. Phys. Chem. C*, vol. 112, no. 15, pp. 5825–5834, Apr. 2008.
[71] T. A. Skipa and V. K. Koltover, “Fullerene Trend in Biomedicine: Expectations and Reality.” 2019.
[72] J. Gao *et al.*, “Polyhydroxy fullerenes (fullerols or fullerenols): beneficial effects on growth and lifespan in diverse biological models.,” *PLoS One*, vol. 6, no. 5, p. e19976, 2011.
[73] V. Krishna *et al.*, “Contaminant-Activated Visible Light Photocatalysis,” *Sci. Rep.*, vol. 8, no. 1, Dec. 2018.
[74] K. Kokubo, M. K. E. Cabbello, N. Sato, Y. Uetake, and H. Sakurai, “Gold Nanoparticles Stabilized by Molecular Fullerenols,” *ChemNanoMat*, p. cnma.201900778, Feb. 2020.
[75] R. Ciganda *et al.*, “Gold nanoparticles as electron reservoir redox catalysts for 4-nitrophenol reduction: A strong stereoelectronic ligand influence,” *Chem. Commun.*, vol. 50, no. 70, pp. 10126–10129, Sep. 2014.
[76] M. T. Islam *et al.*, “Fullerene stabilized gold nanoparticles supported on titanium dioxide for enhanced photocatalytic degradation of methyl orange and catalytic reduction of 4-nitrophenol,” *J. Environ. Chem. Eng.*, vol. 6, no. 4, pp. 3827–3836, Aug. 2018.
[77] D. A. Skoog, D. M. West, F. J. Holler, and S. R. Crouch, *Fundamentals of analytical chemistry*. .
[78] C. De Caro, “UV / VIS Spectrophotometry,” *Mettler-Toledo Int.*, no. September 2015, pp. 4–14, 2015.
[79] R. Desai, V. Mankad, S. K. Gupta, and P. K. Jha, “Size distribution of silver nanoparticles: UV-visible spectroscopic assessment,” *Nanosci. Nanotechnol. Lett.*, vol. 4, no. 1, pp. 30–34, 2012.
[80] D. Paramelle, A. Sadovoy, S. Gorelik, P. Free, J. Hobley, and D. G. Fernig, “A rapid method to estimate the concentration of citrate capped silver nanoparticles from UV-visible light spectra,” *Analyst*, vol. 139, no. 19, pp. 4855–4861, Aug. 2014.
[81] A. W. Czanderna and D. M. Hercules, Eds., *Ion Spectroscopies for Surface Analysis*. Boston, MA: Springer US, 1991.
[82] J. C. Zamarripa Rodríguez, “La constante de Planck.”
[83] J. W. Niemantsverdriet, *Spectroscopy in catalysis : an introduction*. VCH, 1995.
[84] M. Gakiya-Teruya, L. Palomino-Marcelo, S. Pierce, A. M. Angeles-Boza, V. Krishna, and J. C. F. Rodriguez-Reyes, “Enhanced antimicrobial activity of silver nanoparticles conjugated with synthetic peptide by click chemistry,” *J. Nanoparticle Res.*, vol. 22, no. 4, pp. 1–11, Apr. 2020.
[85] C. Cushman, S. Chatterjee, G. H. Major, N. J. Smith, A. J. Roberts, and M. R. Linford, “Trends in Advanced XPS Instrumentation. 1. Overview of the Technique,

Automation, High Sensitivity, Imaging, Snapshot Spectroscopy, Gas Cluster Ion Beams, and Multiple Analytical Techniques on the Instrument." p. 8, 2016.
[86] P. W. (Peter W. Atkins and J. De Paula, *Physical chemistry*. W.H. Freeman and Co, 2010.
[87] N. N. Elgrishi, K. J. Rountree, B. D. Mccarthy, E. S. Rountree, T. T. Eisenhart, and J. L. Dempsey, "A Practical Beginner's Guide to Cyclic Voltammetry," 2017.
[88] V. Knap *et al.*, "Reference Performance Test Methodology for Degradation Assessment of Lithium-Sulfur Batteries," *J. Electrochem. Soc.*, vol. 165, no. 9, pp. A1601–A1609, Jan. 2018.
[89] KEITHLEY, "Rechargeable Battery Charge/Discharge Cycling Using the Keithley Model 2450 SourceMeter ® SMU Instrument," 2013.
[90] MIT Electric Vehicle Team, "A Guide to Understanding Battery Specifications," 2008.
[91] C. J. Zhong, N. T. Woods, G. B. Dawson, and M. D. Porter, "Formation of thiol-based monolayers on gold: Implications from open circuit potential measurements," *Electrochem. commun.*, vol. 1, no. 1, pp. 17–21, Jan. 1999.
[92] M. J. Avena, O. R. Cámara, and C. P. De Pauli, "Open circuit potential measurements with Ti/TiO2 electrodes," *Colloids and Surfaces*, vol. 69, no. 4, pp. 217–228, Jan. 1993.
[93] Y. Liang *et al.*, "Co3O4 nanocrystals on graphene as a synergistic catalyst for oxygen reduction reaction," *Nat. Mater.*, vol. 10, no. 10, pp. 780–786, 2011.
[94] D. Yang, H. Tan, X. Rui, and Y. Yu, "Electrode Materials for Rechargeable Zinc-Ion and Zinc-Air Batteries: Current Status and Future Perspectives," *Electrochem. Energy Rev.*, pp. 1–33, May 2019.
[95] Y. Wang, Y. Song, and Y. Xia, "Electrochemical capacitors: Mechanism, materials, systems, characterization and applications," *Chemical Society Reviews*, vol. 45, no. 21. Royal Society of Chemistry, pp. 5925–5950, 07-Nov-2016.
[96] P. Prieto, V. Nistor, K. Nouneh, M. Oyama, M. Abd-Lefdil, and R. Díaz, "XPS study of silver, nickel and bimetallic silver-nickel nanoparticles prepared by seed-mediated growth," *Appl. Surf. Sci.*, vol. 258, no. 22, pp. 8807–8813, Sep. 2012.
[97] C. Chen, G. Levitin, D. W. Hess, and T. F. Fuller, "XPS investigation of Nafion® membrane degradation," *J. Power Sources*, vol. 169, no. 2, pp. 288–295, Jun. 2007.
[98] M. Schulze, M. Lorenz, N. Wagner, and E. Gülzow, "XPS analysis of the degradation of Nafion," *Fresenius. J. Anal. Chem.*, vol. 365, no. 1–3, pp. 106–113, 1999.
[99] M. B. Hernández, R. H. Díaz, and R. Vásquez, "Determinación de capacitancias específicas y áreas superficiales específicas de diversos materiales carbonosos mediante distintas técnicas electroquímicas," Lima, 2018.
[100] Y. Gogotsi and R. M. Penner, "Energy Storage in Nanomaterials – Capacitive, Pseudocapacitive, or Battery-like?," *ACS Nano*, vol. 12, no. 3, pp. 2081–2083, Mar. 2018.
[101] J. N. Barisci, G. G. Wallace, and R. H. Baughman, "Electrochemical studies of single-wall carbon nanotubes in aqueous solutions," *J. Electroanal. Chem.*, vol. 488, no. 2, pp. 92–98, Jul. 2000.
[102] J. Judith Vijaya *et al.*, "Bioreduction potentials of dried root of Zingiber officinale for a simple green synthesis of silver nanoparticles: Antibacterial studies," *J. Photochem.*

Photobiol. B Biol., vol. 177, pp. 62–68, Dec. 2017.
[103] M. Baccarin *et al.*, "Direct electrochemistry of hemoglobin and biosensing for hydrogen peroxide using a film containing silver nanoparticles and poly(amidoamine) dendrimer," *Mater. Sci. Eng. C*, vol. 58, pp. 97–102, Jan. 2016.
[104] L. A. Goulart, R. Gonçalves, A. A. Correa, E. C. Pereira, and L. H. Mascaro, "Synergic effect of silver nanoparticles and carbon nanotubes on the simultaneous voltammetric determination of hydroquinone, catechol, bisphenol A and phenol," *Microchim. Acta*, vol. 185, no. 1, pp. 1–9, Jan. 2018.
[105] L. Osmieri, R. Escudero-Cid, A. H. A. Monteverde Videla, P. Ocón, and S. Specchia, "Application of a non-noble Fe-N-C catalyst for oxygen reduction reaction in an alkaline direct ethanol fuel cell," *Renew. Energy*, vol. 115, pp. 226–237, Jan. 2018.
[106] Q. Yu, C. Wu, J. Xu, Y. Zhao, J. Zhang, and L. Guan, "Nest-like assembly of the doped single-walled carbon nanotubes with unique mesopores as ultrastable catalysts for high power density Zn-air battery," *Carbon N. Y.*, vol. 128, pp. 46–53, Mar. 2018.
[107] M. A. Costa de Oliveira *et al.*, "Graphene oxide nanoplatforms to enhance catalytic performance of iron phthalocyanine for oxygen reduction reaction in bioelectrochemical systems," *J. Power Sources*, vol. 356, pp. 381–388, Jul. 2017.
[108] N. Jia *et al.*, "N-doped carbon nanocages: Bifunctional electrocatalysts for the oxygen reduction and evolution reactions," *Nano Res.*, vol. 11, no. 4, pp. 1905–1916, Apr. 2018.
[109] B. Lu, D. Cao, P. Wang, G. Wang, and Y. Gao, "Oxygen evolution reaction on Ni-substituted Co3O4 nanowire array electrodes," *Int. J. Hydrogen Energy*, vol. 36, no. 1, pp. 72–78, Jan. 2011.
[110] Y. Deng, A. D. Handoko, Y. Du, S. Xi, and B. S. Yeo, "In Situ Raman Spectroscopy of Copper and Copper Oxide Surfaces during Electrochemical Oxygen Evolution Reaction: Identification of CuIII Oxides as Catalytically Active Species," *ACS Catal.*, vol. 6, no. 4, pp. 2473–2481, Apr. 2016.
[111] R. Kötz, S. Stucki, D. Scherson, and D. M. Kolb, "In-situ identification of RuO4 as the corrosion product during oxygen evolution on ruthenium in acid media," *J. Electroanal. Chem.*, vol. 172, no. 1–2, pp. 211–219, Aug. 1984.
[112] R. L. Doyle and M. E. G. Lyons, "Kinetics and Mechanistic Aspects of the Oxygen Evolution Reaction at Hydrous Iron Oxide Films in Base," *J. Electrochem. Soc.*, vol. 160, no. 2, pp. H142–H154, Jan. 2013.
[113] Y. Zhang *et al.*, "Multiwall carbon nanotube encapsulated Co grown on vertically oriented graphene modified carbon cloth as bifunctional electrocatalysts for solid-state Zn-air battery," *Carbon N. Y.*, vol. 144, pp. 370–381, Apr. 2019.
[114] M. Prabu, K. Ketpang, and S. Shanmugam, "Hierarchical nanostructured NiCo2O4 as an efficient bifunctional non-precious metal catalyst for rechargeable zinc-air batteries," *Nanoscale*, vol. 6, no. 6, pp. 3173–3181, Mar. 2014.
[115] Y. Li *et al.*, "Atomically Thin Mesoporous Co 3 O 4 Layers Strongly Coupled with N-rGO Nanosheets as High-Performance Bifunctional Catalysts for 1D Knittable Zinc-Air Batteries," *Adv. Mater.*, vol. 30, no. 4, p. 1703657, Jan. 2018.
[116] Y. Bu *et al.*, "A Highly Efficient and Robust Cation Ordered Perovskite Oxide as a Bifunctional Catalyst for Rechargeable Zinc-Air Batteries," *ACS Nano*, vol. 11, no. 11, pp. 11594–11601, Nov. 2017.

[117] M. Wang, T. Qian, S. Liu, J. Zhou, and C. Yan, "Unprecedented Activity of Bifunctional Electrocatalyst for High Power Density Aqueous Zinc-Air Batteries," *ACS Appl. Mater. Interfaces*, vol. 9, no. 25, pp. 21216–21224, Jun. 2017.
[118] Y. Jin and F. Chen, "Facile preparation of Ag-Cu bifunctional electrocatalysts for zinc-air batteries," *Electrochim. Acta*, vol. 158, pp. 437–445, Mar. 2015.
[119] J. Hu, Z. Shi, X. Wang, H. Qiao, and H. Huang, "Silver-modified porous 3D nitrogen-doped graphene aerogel: Highly efficient oxygen reduction electrocatalyst for Zn−Air battery," *Electrochim. Acta*, vol. 302, pp. 216–224, Apr. 2019.
[120] Q. Wang, H. Miao, S. Sun, Y. Xue, and Z. Liu, "One-Pot Synthesis of Co3O4/Ag Nanoparticles Supported on N-Doped Graphene as Efficient Bifunctional Oxygen Catalysts for Flexible Rechargeable Zinc–Air Batteries," *Chem. - A Eur. J.*, vol. 24, no. 55, pp. 14816–14823, Oct. 2018.
[121] F. W. T. Goh, Z. Liu, X. Ge, Y. Zong, G. Du, and T. S. A. Hor, "Ag nanoparticle-modified MnO 2 nanorods catalyst for use as an air electrode in zinc-air battery," *Electrochim. Acta*, vol. 114, pp. 598–604, 2013.

ANNEXES

ANNEX 1: Zn-air batteries with Ag-based catalysts

Bifunctional air electrode	Synthesis method	Cell components	Performance	Ref.
AgCu on Ni foam	Electrochemical deposition	Zn/6M KOH + 0.2M $Zn(OAc)_2$	86.5 mW cm^{-2} @ 100 mA cm^{-2}, round efficiency of 56.4% @ 20 mA cm^{-2}	[17]
AgCu on Ni foam	Galvanic displacement on Ni-foam	Zn plate/6M KOH + 0.2M Zinc acetate	85.8 mW cm^{-2} @ 100 mA cm^{-2}, 572 mAh g^{-1} normalized by Zn anode consumed, 53.08% after 100 cycles	[118]
Ag on 3D N-doped graphene	One-step hydrothermal method	Zn plate/KOH	29.8 mW cm^{-2} @ 100 mA cm^{-2}	[119]
Co_3O_4/Ag on N-reduced graphene	One-pot solvothermal method	Zn foil/polyacrylic acid-based gel-electrolyte	108 mW cm^{-2} @ ~175 mA cm^{-2}, charge-discharge gap after 100 cycles are 0.77 V	[120]
$Ag_{50}Cu_{50}$ on Ni foam	Pulsed layer deposition	Zn plate/6M KOH + 0.1M $Zn(CH_3COO)_2$	45.1 mW cm-2 @ 100 mA cm^{-2}, ~50% efficiency @ 20 mA cm^{-2}	[14]
Ag-αMnO_2	Microwave-assisted polyol method	Zn plate/6M KOH	Battery voltage sustained after 270 cycles	[121]

Table 0.1. Zn-air batteries with Ag-based catalysts and their performances.